Table of Contents

RÉSUMÉ IV

ABSTRACT VII

FOREWORD IX

ACKNOWLEDGEMENT X

LIST OF FIGURES XI

LIST OF TABLES XV

ACRONYMS XVI

NOMENCLATURES XVII

SECTION A 1

CHAPTER 1 2

INTRODUCTION 2

1.1 CONTEXT 2

1.2 OBJECTIVE OF THE THESIS 5

1.3 STRUCTURE OF THE THESIS 6

REFERENCES 7

CHAPTER 2 11

ADSORPTIVE HYDROGEN STORAGE SYSTEM MODEL DEVELOPMENT AND ITS VALIDATION 11

2.1 Basics of adsorption *11*

2.2 Development of adsorptive system model for predicting the multiphysics performance of a hydrogen storage system *15*

2.3 Validation of model with experimental data obtained from the test bench using MOF-5 as an adsorbent material *19*

2.4 Validation of the model with experimental data obtained from the test bench using Maxsorb™ activated carbon as an adsorbent material 31

2.5 Conclusion 36

References 36

CHAPTER 3 ..... **40**

EFFECTS OF FLOWTHROUGH COOLING AND *PARA-ORTHO* CONVERSION ON THE PERFORMANCE OF A SUBSCALE-PROTOTYPE HYDROGEN STORAGE TANK FILLED WITH MOF-5 40

3.1 Background 40

3.2 Effect of flowthrough cooling on the performance of a subscale-prototype tank filled with MOF-5 44

3.3 Effect of para-ortho conversion heat on the performance of a subscale-prototype storage system filled with MOF-5 48

3.4 Conclusion 56

References 57

CHAPTER 4 ..... **60**

MULTIPHYSICS PERFORMANCE OF A BULK CRYO-ADSORPTIVE HYDROGEN STORAGE RESERVOIR FILLED WITH MOF-5 60

4.1 Thermal and storage performance of the bulk tank 61

4.2 Effect of flowthrough cooling together with para-ortho conversion on the storage tank performance 69

4.3 Effect of the mass flow rate on the cooling time reduction during the flowthrough cooling stage 71

4.4 Performance of the bulk tank during the dormancy stage 72

4.5 Conclusion 74

Reference 75

CHAPTER 5 ..... **76**

SUMMARY OF THE THESIS AND FUTURE WORK 76

5.1 Adsorptive storage system model development and its validation 76

5.2 Effects of flowthrough cooling and para-ortho conversion on the performance of a subscale-prototype hydrogen storage tank filled with MOF-5 77

5.3 Multiphysics performance of a cryo-adsorptive bulk hydrogen storage reservoir filled with MOF-5 79

5.4 Future work 80

References 81

SECTION B **82**

ARTICLES 82

Article – 1 83

Article – 2 94

Article – 3 107

SECTION C **117**

ANNEXURE 117

Résumé

Cette thèse présente l'évaluation multiphysique du comportement thermique et de la capacité de stockage d'un réservoir d'hydrogène fonctionnant par cryo-sorption de grand volume rempli d'un matériel adsorbant de type métallo-organique, le MOF-5, pour les applications stationnaires qui requièrent un grand volume d'hydrogène et pour des systèmes de distribution d'hydrogène. Dans un premier temps, un modèle général du système de stockage d'adsorption basé sur la mécanique des fluides numérique (MFN) est développé et implémenté dans la plateforme MFN du logiciel multiphysique COMSOL. Afin de valider le modèle développé, des expériences de stockage de l'hydrogène sont menées : de l'hydrogène gazeux à 77 K est chargé dans prototype de stockage à petite échelle (2,5 L) rempli de MOF-5 jusqu'à ce que la pression atteigne 9 MPa. La température et la pression mesurées expérimentalement sont comparées avec la température et la pression simulées, et nous observons un bon accord entre les résultats de simulation et les résultats expérimentaux. La vérification de la cohérence du modèle de stockage d'adsorption est également réalisée en comparant les températures obtenues lors de la simulation avec ceux obtenus à partir des mesures de banc d'essai à l'aide du charbon activé AX-21™ comme adsorbant.

Le modèle est ensuite adapté à l'étude des effets du refroidissement par circulation continue sur les performances thermiques et la capacité de stockage du réservoir prototype à petite échelle rempli de MOF-5. Les résultats de simulation montrent une fois de plus un bon accord avec les résultats expérimentaux. Dans le processus de refroidissement par circulation continue, une partie de l'hydrogène rempli est adsorbée et le reste passe au travers le milieu

poreux et est récupéré. Les résultats expérimentaux et les simulations montrent que la chaleur générée pendant le temps de charge est transportée hors du réservoir pendant le refroidissement par circulation continue, ce qui entraîne une diminution de la température du système de stockage. Le modèle est ensuite utilisé pour étudier l'effet de la conversion endothermique *para-ortho* de l'hydrogène sur le comportement thermique et la capacité de stockage du réservoir prototype à petite échelle. Les résultats montrent que la conversion endothermique permet de réduire la température du système et augmente ainsi la capacité de stockage nette.

Le modèle CFD qui est utilisé pour simuler le refroidissement par circulation continue et la conversion *para-ortho* est étendu afin d'étudier la performance multiphysique d'un réservoir de stockage d'hydrogène de grande capacité (20 m^3) rempli de MOF-5. La pression maximale du réservoir est réglée à 4 MPa. Dans un premier temps, la simulation est effectuée pour réduire la température initiale du réservoir de 300 K à 80 K. La réduction de la température initiale est obtenue par des cycles de charge-décharge. Une fois que la température du réservoir atteint 80 K, le réservoir est rempli d'hydrogène à 77 K jusqu'à ce que la pression maximale de 4 MPa soit atteinte. Après, on utilise le refroidissement par circulation continue pour maintenir la température autour de 80 K. Après ~5.5 heures de refroidissement en circulation continue, un seuil de viabilité de l'approche est atteint lorsque la masse totale d'hydrogène stocké dans le réservoir (~275 kg) devient égale à celle stockée dans un réservoir cryo-comprimé similaire avec de l'hydrogène maintenu à 77 K et 4 MPa. Après 5.5 heures, le réservoir rempli de MOF-5 utilisant le refroidissement par circulation continue contient nettement plus d'hydrogène qu'un réservoir cryo-comprimé. La température du gaz

d'échappement d'hydrogène pendant le temps de refroidissement de recirculation est également simulée; le résultat montre que l'énergie nécessaire pour refroidir l'*hydrogène* qui sort du système peut être réduite lorsque le refroidissement par recirculation est en cours. En plus, on a étudié l'effet de la conversion *para-ortho* ensemble avec le refroidissement par recirculation et l'effet du débit massique sur la réduction du temps de refroidissement pendant l'étape de refroidissement de recirculation. Enfin, la perte de la masse d'hydrogène dans la phase de dormance de 10 jours est calculée. Le résultat montre que pour chaque jour, ~2.4 kg d'hydrogène doivent être retirés du réservoir pour éviter une pression excessive à l'intérieur du réservoir.

Abstract

This thesis presents multiphysics performances such as thermal and storage performance of a bulk cryo-adsorptive hydrogen storage reservoir filled with a metal-organic framework adsorbent material, MOF-5, for bulk storage and distribution applications. At first, a general adsorptive storage system computational fluid dynamics (CFD) model is developed and it is implemented in the CFD software COMSOL Multiphysics® platform. In order to validate the developed model, hydrogen storage experiments are conducted: hydrogen gas at 77 K is charged into a subscale-prototype (2.5 L) storage tank filled with MOF-5 until a pressure of 9 MPa is reached. The measured temperature and pressure are compared with simulated temperature and pressure, and we observe good agreement between simulation and experimental results. The consistency checking of the adsorptive storage system model is also carried out by comparing temperatures obtained from the simulation with those obtained from the bench test measurements using activated carbon (AX-21™) as an adsorbent. After that, the model is extended to study the effect of flowthrough cooling on the performance of a subscale-prototype storage system filled with MOF-5. The simulation results show once again good agreement with experimental results. The flowthrough simulation/experimental results show that the heat generated during the charging time is transported out of the tank during the flowthrough cooling stage, subsequently the temperature of the storage system is decreased. In the next stage, the model is applied to investigate the effect of endothermic *para-ortho* hydrogen conversion on the performance of a subscale-prototype storage tank. The results show that the endothermic conversion reduces the system temperature that helps to fill more amount of hydrogen gas in the reservoir.

The CFD model that is used to simulate the flowthrough cooling and *para-ortho* conversion is further extended to investigate the multiphysics performance of a bulk (20 m^3) hydrogen storage reservoir filled with MOF-5. The maximum pressure of the reservoir is set to be 4 MPa. Here, at first, simulation is performed for reducing the initial temperature of the reservoir to 80 K from 300 K. This initial temperature reduction is achieved through charging-discharging cycles. Once the temperature of the whole tank reaches 80 K, hydrogen at 77 K is filled in the reservoir until the maximum pressure of 4 MPa is reached. After this, the model is set to flowthrough cooling. In ~5.5 hours of flowthrough cooling, the temperature of the system is reduced significantly. While this time the reservoir stored ~275 kg of hydrogen, this storage amount is equal to the net storage amount in a similar cryo-compressed tank with hydrogen maintained at 77 K and 4 MPa. Above 5.5 hours, flowthrough cooled cryo-adsorptive MOF-5 tank stores significantly more hydrogen than a cryo-compressed storage tank. The temperature of the exhaust hydrogen gas during the flowthrough cooling time is also simulated; the result shows that the required energy for cooling the exhaust hydrogen can be reduced when the flowthrough cooling is on progresses. Further, the effect of *para-ortho* conversion together with the flowthrough cooling and the effect of mass flow rate on cooling time reduction during the flowthrough cooling stage are investigated. Finally, the hydrogen mass loss during the 10 days of dormancy stage is calculated. The result shows that, each day ~2.4 kilogram of hydrogen needs to be removed from the reservoir for avoiding the risks arising due to excess pressure inside the tank.

Foreword

The present thesis has been carried out as part of collaboration with Air Liquide Company. The prime objective is to develop a CFD adsorptive storage system model that is capable of predicting the multiphysics performance of the MOF-5 filled bulk tank. Hence, we developed a CFD model and validated it with experimental data obtained from subscale-prototype MOF-5 filled tank. The validated model subsequently applied to the same volume tank and tested the cooling performance of the storage system. Finally, CFD model is extended to study the thermal and storage performance of the bulk tank. We hope that the thesis will stimulate the possibility of using MOF-5 in a large storage system for bulk storage applications to replace the actual storage reservoirs in which hydrogen is stored conventionally as compressed gas (CGH_2) or cryogenic liquid (LH_2). The reservoirs presently used in hydrogen refuelling and dispensing stations suffers from technical limitations such as low net volumetric energy density, high capital cost (for CGH_2) and fuel-loss due to the boiling off of liquid hydrogen (for LH_2).

Acknowledgement

At the outset, I would like to express my deepest gratitude to my advisor, Professor Richard Chahine, for his guidance, patience, and for providing me with an ideal atmosphere for pursuing my research. I express my sincere gratitude to my co-director, Professor Pierre Bénard, for his valuable support and insightful suggestions. I would like to thank Professor Renju Zacharia and Professor Jinsheng Xiao for extending their valuable help and for nourishing me with constructive discussions throughout my PhD work. I would also like to thank Professor Jacques Goyette, for his valuable suggestions and timely corrections which improved my articles and thesis. I would like to thank Dr. Maha Bhouri, who helped me in the beginning for acquiring the basics of CFD modeling which proved to be crucial in this thesis. My thanks to Dr. Marc-Andre Richard and Dr. Ege Dundar for providing me useful discussions regarding to adsorption models. I also thank to Mr. Follivi Kloutse for supplying the data regarding specific heat capacity and isosteric heat of MOF-5. I wish to thank Eng. Daniel Cossement, Francis Lafontaine, Marie-eve Marchand and Dr. Ahmed Hourri, those who helped me to get the experimental data for validating my CFD model. I would like to acknowledge the administrative support of Lucie Bellemare and Diane Robert. I cherish the friendships and good humour of all the people in IRH. Finally, my heartfelt thanks to my parents and brothers who had always supported me and encouraged me to pursue my work with great zeal.

List of Figures

Figure 2.1: Difference between absolute adsorption (n_a) and excess adsorption (n_{ex}).....12

Figure 2.2: Schematic representation of storage/flowthrough experimental test bench.....19

Figure 2.3: Fitted modified D-A parameters using experimental data for MOF-5. 23

Figure 2.4: Isosteric heat as a function of absolute adsorption. 24

Figure 2.5: Geometry of the tank with monitoring points. 25

Figure 2.6: Excess adsorption of hydrogen on MOF-5 measured at 77 K using the test bench compared with the lab-scale measurements and data reported previously. 26

Figure 2.7: Temperature evolution during model validation with experiment in which 77 K hydrogen is charged into a 2.5 L cryo-sorptive MOF-5 tank. Model calculations are performed using experimentally measured temperature-dependent specific heats and isosteric heat.....28

Figure 2.8: Pressure and mass evolution when 77 K hydrogen is charged into a 2.5 L cryo-sorptive MOF-5 tank. 29

Figure 2.9: Heat source contributions and their influence on bed temperature evolutions as 77 K hydrogen is charged at a rate of 15 SLPM into 2.5 L cryo-sorptive tank filled with MOF-5. Arrows point toward the axis corresponding to the data. 30

Figure 2.10: P&ID of the test bench and the monitoring points of the tank. 31

Figure 2.11: Comparison between the temperatures at points T_1, T_2 and T_4 of experimental validation and simulations at room temperature. An entire charging/discharging cycle is shown here.....33

Figure 2.12: Comparison between the temperatures at points T_1, T_2, T_3 and T_6 of experimental validation and simulations at cryogenic temperature. Only the charging stage is shown here.....34

Figure 2.13: Experimental and simulation results for the pressure in the tank at room temperature.....35

Figure 2.14: Experimental and simulation results for the pressure in the tank at cryogenic temperature.....35

Figure 3.1: Comparison of the experimental pressure with that obtained from the simulation during a flowthrough run.....45

Figure 3.2: Comparison of the experimental temperature with that obtained from the simulation during a flowthrough run.....46

Figure 3.3: Comparison of the average bed temperatures obtained from flowthrough simulations with those obtained when only a LN_2 cooling bath was used.....47

Figure 3.4: The amount of hydrogen stored in the system obtained from flowthrough simulations with those obtained when only a LN_2 cooling bath was used. The amount of hydrogen stored during flowthrough experiments are also compared with that obtained from simulation.....48

Figure 3.5: Equilibrium fraction of *para* hydrogen as function of temperature and enthalpy of *para-ortho* hydrogen conversion.....50

Figure 3.6: Temperature profiles at T_4 in the tank with (dashed lines) and without (solid lines) taking into account the *para-ortho* conversion at 4 inlet temperatures. 53

Figure 3.7: Pressure profiles at T_4 in the tank with (dashed lines) and without (solid lines) taking into account the *ortho-para* conversion at 4 inlet temperatures. 53

Figure 3.8: Heat sources profiles in the system at the point T_4. 54

Figure 3.9: Temperature profiles at the point T_4 when different heat source terms are considered separately. 55

Figure 3.10: Hydrogen mass balance in the system with and without conversion. 56

Figure 4.1: Storage reservoir and its 2d-axisysmmetrical representation. 60

Figure 4.2: Pressure of the tank during the charging/discharging cycles. 62

Figure 4.3: Temperature of the tank during the charging/discharging cycles. 63

Figure 4.4: Pictorial representation of tank's temperature profile during the charging/discharging cycles. 64

Figure 4.5: Average bed temperature, pressure and outlet temperature during the whole charging/flowthrough stage. 65

Figure 4.6: Evolution of the temperature inside the 20 m^3 bulk storage tank containing MOF-5. (a) at the onset of charging, (b) after charging hydrogen at a rate of 10000 SLPM, (c) during flowthrough for 30 hours and (d) during idling for 30 hours (without flowthrough) 66

Figure 4.7: Stored mass of hydrogen during the whole charging/flowthrough stage. 68

Figure 4.8: Average temperature and pressure in the system when *para-ortho* conversion together with flowthrough cooling and flowthrough cooling alone scenario.....70

Figure 4.9: Effect of the mass flow rate on the temperature reduction during the flowthrough stage.....71

Figure 4.10: Hydrogen loss during the dormancy stage.....73

Figure 4.11: Temperature history during the 10 days dormancy stage.....73

List of Tables

Table 2.1: Volume calibration of different parts of storage/flowthrough test bench.....21

Table 2.2: Modified D-A model parameters of MOF-5.....23

Table 2.3: Densities and porosities of MOF-5. 24

Table 2.4: Modified D-A model parameters of AX-21™.....32

Table 2.5: Material properties of AX-21™.....32

Table 2.6: Boundary conditions of charge-discharge cycle of AX-21™ system.....33

Acronyms

BET	:	Brunauer–Emmett–Teller
BPR	:	Back Pressure Regulator
BPV	:	Back Pressure Valve
CFD	:	Computational Fluid Dynamics
DOE	:	Department of Energy of United States of America
D-A	:	Dubinin-Astakhov
D-R	:	Dubinin-Radushkevich
EOS	:	Equation of State
LN_2	:	Liquid Nitrogen
MFC	:	Mass Flow Controller
MOF	:	Metal Organic Framework
NI	:	National Instruments
NIST	:	National institute for Standard and Technology
PT	:	Pressure Transducer
SLPM	:	Standards Litre per Minute
TMFC	:	Thermal Mass Flow Controller
TMFR	:	Thermal Mass Flow Reader

Nomenclatures

C_{pg}	:	Specific heat capacity of hydrogen gas, J $kg^{-1}K^{-1}$
C_{ps}	:	Specific heat capacity of adsorbent, J $kg^{-1}K^{-1}$
D_P	:	Particle diameter, mm
H, h	:	Enthalpy, kJ kg^{-1}
h_w	:	Heat transfer coefficient of water, W m^{-2} K^{-1}
k	:	Permeability, m^2
k_{eq}	:	Equivalent thermal conductivity, W $m^{-1}K^{-1}$
k_s	:	Thermal conductivity of adsorbent, W m^{-1} K^{-1}
k_g	:	Thermal conductivity of hydrogen gas, W $m^{-1}K^{-1}$
M_{H2}	:	Molecular mass of hydrogen, kg mol^{-1}
m_a	:	Mass of adsorbed hydrogen, kg
m_g	:	Mass of gas phase hydrogen, kg
m_t	:	Total mass, kg
n_a	:	Absolute adsorption amount/unit mass of adsorbent, mol kg^{-1}
n_{max}	:	Limiting adsorption (per unit mass of adsorbent), corresponding to the maximum filling of the entire volume of adsorption space, mol kg^{-1}
P	:	Pressure, Pa
P_0	:	Pseudo-saturation pressure, Pa
T_f	:	Fluid temperature, K
Q	:	Heat source term, W m^{-3}
Q_a	:	Adsorption heat source, W m^{-3}
Q_p	:	Heat source due to pressure-volume work, W m^{-3}
Q_c	:	Heat source due to endothermic *para-ortho* H_2 conversion, W m^{-3}

q_{st}	:	Isosteric heat of adsorption, J mol^{-1}
R	:	Universal gas constant, J $mol^{-1}K^{-1}$
S_m	:	Mass source term, kg m^{-3} s^{-1}
T	:	Temperature, K
U	:	Darcy velocity, m s^{-1}
α	:	Enthalpic factor, J mol^{-1}
β	:	Entropic factor, J mol^{-1} K^{-1}
γ	:	Ratio of specific heat capacities
μ	:	Dynamic viscosity, Pa s
ρ_b	:	Bulk density, kg m^{-3}
ρ_g	:	Density of hydrogen gas, kg m^{-3}
ρ_s	:	Skeleton density of adsorbent, kg m^{-3}
ε_b	:	Bed porosity
ε_t	:	Total porosity
ε_{mi}	:	Micro porosity

Section A

Chapter 1

Introduction

1.1 Context

Energy is a pre-requisite for economic development. Every sector of economy, namely agriculture, industry, transport, commercial, and domestic, needs inputs of energy. The growing consumption of energy has turned this world increasingly dependent on fossil fuels such as coal, oil and gas. Increased use of fossil fuels contributes to various environmental problems [1-3]. Hydrogen has been identified as a potential energy carrier for the future mainly due to the possibility of producing it from renewable sources and its non-polluting nature [4-6]. However, there are many technical challenges that remain to be solved before hydrogen can be introduced in a significant way into our energy system [7, 8]. Among them, hydrogen storage is a key challenge in developing a resilient hydrogen economy. Compressed hydrogen storage is one of the few commercially available hydrogen storage technologies. It is relatively simple and the filling of a tank can be completed in a short period of time [9]. However, low volumetric and gravimetric densities are the major disadvantages of the compressed storage method. Hydrogen is stored in the form of liquid hydrogen (LH_2) is another commercially available hydrogen storage technology [10, 11]. Due to its higher density, liquid hydrogen requires much lesser volume for the same quantity of hydrogen than in the compressed storage method. However, the high energy consumption associated with liquefaction processes and continuous boil-off during storage are the major disadvantages of the liquid hydrogen storage method [12]. To overcome these storage issues, many alternative storage methods are being extensively researched. Among the various approaches for hydrogen

storage, hydrogen storage via physisorption on porous materials has attracted great attention due to the fast kinetics of the sorbent materials at low temperatures and moderate pressure, large surface area, complete reversibility of the storage process, etc. [13-15]. Among these porous materials, the microporous material MOF-5 has been enticed as one of the promising materials for adsorptive hydrogen storage due to its large surface area, high gravimetric hydrogen capacity at low temperature and affordable material cost [16-18]. Hydrogen molecules interact with the MOF-5 via the weak Van der Waals force which results in low isosteric heat of adsorption in the range of 4-7 kJ mol^{-1} at room temperature. Because of the weakness of the gas-surface interactions, hydrogen uptake in MOF-5 is relatively low (~1 wt %) at room temperature [15, 16]. Therefore, in order to achieve the desired hydrogen uptake in MOF-5, it is necessary to use cryogenic temperatures [19].

Even though MOF-5 can meet the storage density necessary for vehicular hydrogen storage applications purely on the basis of its adsorption capacity, it is not evident that any realistic hydrogen storage system built using the MOF-5 can readily meet all required system performance targets [20]. This is because the overall performance of a storage system depends not only on MOF-5's hydrogen storage density but also on the storage and thermal behavior of the entire storage system. Since thermal effects in a cryo-adsorptive storage system play a predominant role in designing an efficient adsorption based system, proper thermal management throughout the charging-discharging process is necessary [21]. During the hydrogen charging process, the heat generated due to adsorption and pressure work must be removed from the storage system to maintain the cryogenic condition of the MOF-5 filled system [22]. However, the heat removal

from powdered MOF-5 filled storage system is difficult due to the poor thermal conductivity of powdered MOF-5 [23, 24]. To enhance the heat removal from the MOF-5 bed, approaches such as the addition of expanded natural graphite material to the MOF-5 and inclusion of conducting material in storage system have been previously studied[23, 24, 25]. Either way, the net volumetric hydrogen density of the storage system is reduced due to the addition of non-adsorbing heat transfer materials. Alternative heat removal methods are the implementation of the flowthrough cooling and the charge-discharge cycles in the storage system. Flowthrough cooling is the circulation of cold hydrogen through the adsorbent bed, where the adsorptive heat from the bed is removed convectively by continuous flowing of cold hydrogen gas [26]. A flowthrough system consists of a loop of hydrogen gas through which the cold gas is introduced into the storage system and any non-adsorbed hot gas is recirculated back into a refrigeration unit, where the hot gas is cooled and reintroduced into the storage vessel. Since hydrogen desorption from the adsorbent bed is an endothermic process, charge-discharge cycles or adsorption-desorption cycles can be considered as a cooling option for cooling the storage system. On the other hand, a hydrogen storage system can experience the cooling effect if the *para* hydrogen to *ortho* hydrogen conversion takes place in the storage system. Molecular hydrogen has two phases of nuclear spin orientation: *para* hydrogen (nuclear spin is anti-parallel, triplet state) and *ortho* hydrogen (nuclear spin is parallel, singlet state). At room temperature, normal hydrogen is at thermodynamic equilibrium, which has 75 % *ortho* and 25 % *para* fractions. Below the room temperature, the composition of *para-ortho* fraction present in the hydrogen is defined as equilibrium hydrogen. The composition of these isomers is known to evolve to 100 % *para* form as the

temperature decreases to 20 K. The conversion of *para* to *ortho* and *ortho to para* are endothermic and exothermic reactions, respectively [27]. Currently, the method for storage system filling uses either pre-cooled hydrogen at liquid nitrogen temperature or cryo-compressed supercritical hydrogen [28]. In such cases, if the cryogenic hydrogen is not already at equilibrium *ortho-para* composition, depending upon the temperature increment owing to the heat leak in the tank, a significant amount of hydrogen would be lost during the storage time due to heat release during the conversion. A method to avoid this storage loss is to naturally or catalytically convert normal hydrogen to the *para* form after the cooling. If *para* hydrogen enters the storage tank, the temperature of the tank will be reduced due to the endothermic *para* to *ortho* conversion. Although hydrogen storage research focuses mainly on the vehicular storage tanks, research on the larger bulk counterparts, which are used at central hydrogen production facilities, transport terminals and end-use locations are gaining attention. However, unlike the vehicular tanks, the pilot-scale design and experimentation of bulk-hydrogen storage tank filled with MOF-5 to evaluation of its multiphysics performance is cumbersome, expensive and practically difficult. A convenient approach is therefore to predict such bulk tank's thermal and storage performance using a numerical model that couples heat and mass transfer with the adsorption kinetics.

1.2 Objective of the thesis

The objective of the work presented in this thesis is to understand the thermal and storage performance of a bulk (20 m^3) hydrogen storage reservoir filled with MOF-5. In order to investigate the performance of the storage reservoir using a multiphysics approach, initially, a general computational fluid dynamics (CFD) model is developed. The CFD model is validated with the experimental data

obtained from the test bench equipped with a subscale-prototype (2.5 L) cryo-adsorptive tank filled with MOF-5. The validated model is extended by applying the flowthrough cooling to study its effects on the multiphysics performance of the storage system. In order to compare flowthrough simulation results with bench test results, a series of flowthrough experiments are performed. The original validated model is then extended to study the effect of *para-ortho* conversion on the performance of the storage system. Here, we assume that MOF-5 has enough catalytic activities for causing rapid *para-ortho* conversion. Finally, the CFD model that accounts for flowthrough cooling, *para-ortho* conversion and charge-discharge cycle is scaled to study the performance of the bulk storage reservoir. For all CFD simulations in this thesis, COMSOL Multiphysics® is used as a platform to implement the model.

1.3 Structure of the thesis

The thesis is divided into three sections. Section A consists of five chapters including introduction, three working chapters and a general summary followed by future outlook. Context, objective and structure of the thesis are presented in chapter 1. Chapter 2 covers the basics of adsorption, development of adsorptive storage system computational fluid dynamics model and model validation using subscale-prototype storage tank filled with MOF-5. Chapter 3 deals with the results from the effect of flowthrough cooling and *para-ortho* conversion on the thermal and storage performance of the subscale-prototype tank filled with MOF-5. Chapter 4 discusses the multiphysics performance of the bulk hydrogen storage reservoir filled with MOF-5. The general summary of the thesis and future outlook is presented in chapter 5. The published articles are

presented in the section B of the thesis. Section C of the thesis presents the method of the model implementation in COMSOL Multiphysics® platform.

References

[1] Chiari L, Zecca A. Constraints of fossil fuels depletion on global warming projections. Energy Policy 2011; 39:5026–5034.

[2] Ward JD, Nel WP. Comment on fossil-fuel constraints on global warming by A. Zecca and L. Chiari [Energy Policy 38 (2010) 1–3]. Energy Policy 2011; 39:7464–7466.

[3] Abbasi T, Abbasi SA. Decarbonization of fossil fuels as a strategy to control global warming. Renew sust energ rev 2011; 15:1828–1834.

[4] Dutta S. A review on production, storage of hydrogen and its utilization as an energy resource. J Ind Eng Chem 2014; 20:1148–1156.

[5] Nicoletti G. The hydrogen option for energy: a review of technical, environmental and economic aspects. Int J Hydrogen Energy 1995; 20:759-765.

[6] Satyapal S, Petrovic J, Read C, Thomas G, Ordaz G. The U.S. department of energy's national hydrogen storage project: Progress towards meeting hydrogen-powered vehicle requirements. Catal Today 2007; 120:246–256.

[7] Ehteshami SMM, Chan SH. The role of hydrogen and fuel cells to store renewable energy in the future energy network–potentials and challenges. Energy Policy 2014; 73:103–109.

[8] Mazloomi K, Gomes C. Hydrogen as an energy carrier: Prospects and challenges. Renew sust energ rev 2012; 16:3024–3033.

[9] Zhang J, Fisher TS, Ramachandran PV, Gore JP, Mudawar I. A review of heat transfer issues in hydrogen storage technologies. J Heat Transfer 2005, 127: 1391-1399.

[10] Klell M, Kindermann H, Jogl C. Thermodynamics of gaseous and liquid hydrogen storage. Proceedings international hydrogen energy congress and exhibition IHEC; July 13-15, 2007, Istanbul, Turkey.

[11] Zhou L. Progress and problems in hydrogen storage methods. Renew sust energ rev 2005; 9:395-408.

[12] Jena P. Materials for hydrogen storage: past, present, and future. J Phys Chem Lett 2011; 2:206–211.

[13] Zhao D, Yuan D, Zhou H-C. The current status of hydrogen storage in metal–organic frameworks, Energy Environ Sci 2008; 1:222–235.

[14] Sillar K, Hofmann A, Sauer J. Ab initio study of hydrogen adsorption in MOF-5. J Am Chem Soc 2009; 131: 4143–4150.

[15] Yang J. Hydrogen storage in metal organic frameworks, Thesis, Technische Universiteit Delft; 2012, Netherlands.

[16] Serhiy Luzan. Materials for hydrogen storage and synthesis of new materials by hydrogenation, Thesis, Umeå University; 2012, Sweden.

[17] Kaye SS, Dailly A, Yaghi OM, Long JR. Impact of preparation and handling on the hydrogen storage properties of Zn_4O (1, 4-benzenedicarboxylate)$_3$ (MOF-5). J Am Chem Soc 2007; 129:14176-14177.

[18] Li J, Cheng S, Zhao Q, Long P, Dong J. Synthesis and hydrogen-storage behaviour of metal–organic framework MOF-5. Int J hydrogen energy 2009; 34:1377–1382.

[19] Rosi NL, Eckert J, Eddaoudi M, Vodak DT, Kim J, O'Keeffe M, Yaghi OM. Hydrogen storage in microporous metal-organic frameworks. Science 2003; 300:1127-1129.

[20] Schmitz B, U Müller, Trukhan N, Schubert M, Férey G, Hirscher M. Heat of adsorption for hydrogen in microporous high-surface-area materials. Chem Phys Chem 2008; 9:2181–2184.

[21] Collins DJ, Zhou HC. Hydrogen storage in metal–organic frameworks. J Mater Chem 2007; 17:3154–3160.

[22] Hardy BJ, Anton DL. Hierarchical methodology for modeling hydrogen storage systems. Part II: Detailed models. Int J Hydrogen energy 2009; 34: 2992–3004.

[23] Chakraborty A, Kumar S. Thermal management and desorption modeling of a cryo-adsorbent hydrogen storage system. Int J Hydrogen Energy 2013; 38:3973-3986.

[24] Purewal J, Liu D, Sudik A, Veenstra M, Yang J, Maurer S, Müller U, Siegel DJ. Improved hydrogen storage and thermal conductivity in high-density MOF-5 Composites. J Phys Chem C 2012; 116:20199–20212.

[25] Liu D, Purewal JJ, Yang J, Sudik A, Maurer S, Mueller U, Ni J, Siegel DJ. MOF-5 composites exhibiting improved thermal conductivity. Int J Hydrogen energy 2012; 37: 6109-6117.

[26] Schuetz W, Michl F, Polifke W, Paggiaro R. Storage system for storing a medium and method for loading a storage system with a storage medium and emptying the same therefrom. US patent. US 2008/0020250 A1, Jan. 24, 2008.

[27] Ahluwalia RK, Hua TQ, Peng JK, Papadias D, Kumar R. System level analysis of hydrogen storage options. Presentation, DOE Hydrogen Program Review; May 9-13, 2011, Washington DC, USA.

[28] Ahluwalia RK, Peng JK. Automotive hydrogen storage system using cryo-adsorption on activated carbon. Int J Hydrogen Energy 2009; 34:5476–5487.

Chapter 2

Adsorptive hydrogen storage system model development and its validation

This chapter discusses the basics of adsorption, the development of computational fluid dynamics (CFD) adsorptive hydrogen storage system model and the model validation with experimental results.

2.1 Basics of adsorption

Adsorption is the preferential adhesion of a chemical species from a gas, liquid or dissolved solid to a solid surface. This results in increased concentration of chemical species close to the surface of the solid relative to the bulk of the solid [1]. The solid surface that adsorbing the chemical species is called an adsorbent, while the adsorbed chemical species are referred to as the adsorbate. On the basis of the forces of attraction between adsorbent and adsorbate, adsorption is classified as physisorption or chemisorption. Physisorption occurs mainly due to the weak Van der Waals force of attraction between the adsorbent and the adsorbate, while chemisorption occurs when the adsorbate is held on an adsorbent surface by stronger chemical forces that are specific for each adsorbent and adsorbate.

2.1.1 Absolute and Excess adsorption

The absolute amount adsorbed, n_a is defined as the quantity of adsorbate contained in the adsorption volume, V_a the space where the density of the adsorbate is higher than that of the bulk gas. It is given by [2]:

$$n_a = \frac{n_{tot}}{ms} - \rho_g\left(V_{v,sys} - V_a\right) \tag{2.1}$$

where, n_{tot} is the total amount of adsorbate introduced into the measuring system containing the adsorbent, m_s is the mass of adsorbent, ρ_g is the density of the bulk gas, and $V_{v,sys}$ is the total void volume of the adsorption system (including the pore volume of the adsorbent, the interstitial space, and any additional empty space). The total void volume can be measured by helium probing. However, V_a cannot be measured separately. Consequently, the absolute adsorption cannot be measured directly. However, the excess adsorption which is the additional amount of adsorbate present in the adsorption volume can be measured directly:

$$n_{ex} = \frac{n_{tot}}{m_s} - \rho_g V_{v,sys} \tag{2.2}$$

In terms of absolute adsorption variables, the excess adsorption is thus given by:

$$n_{ex} = n_a - \rho_g V_a = n_a \left[1 - \frac{\rho_g}{\rho_a}\right] \tag{2.3}$$

The measured excess adsorption data can be converted into absolute adsorption by fitting the experimental excess data to an adsorption model isotherm.

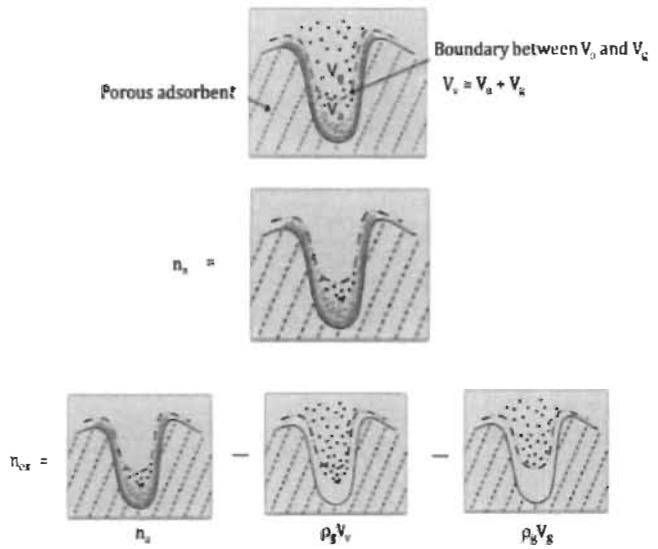

Figure 2.1: Difference between absolute adsorption (n_a) and excess adsorption (n_{ex}) [3].

Figure 2.1 shows the pictorial representation of the difference between absolute adsorption (n_a) and excess adsorption (n_{ex}). It shows that the absolute adsorption

is calculated by subtracting the amount of gas phase hydrogen present in the gas phase volume from the total amount of hydrogen present in the adsorptive storage system whereas the excess adsorption is estimated by subtracting the amount of gas phase hydrogen present in the adsorption volume from absolute adsorption.

2.1.2 Adsorption models

The adsorption isotherm is a curve which shows the variation of adsorption with pressure at a given constant temperature. The adsorption model is a mathematical representation of excess or absolute adsorption isotherms and it is required for predicting the thermal and storage performance of the adsorptive hydrogen storage system. A series of adsorption models such as Langmuir, Freundlich, Brunauer–Emmett–Teller (BET), Toth, MPTA, Ono-Kondo, Dubinin–Radushkevich (D-R), Dubinin–Astakhov (D-A), modified Dubinin–Astakhov, etc. have been suggested and studied [4-6]. Among these, the modified Dubinin–Astakhov (D-A) model is one of the most widely used adsorption models for adsorptive hydrogen storage system model [7-9].

2.1.2.1 Modified Dubinin and Astakhov (D-A) model

The theory of volume filling micropores (TVFM) for analyzing the gas adsorption isotherms on microporous materials has been proposed by Dubinin-Radushkevich (D-R) [10]. On the basis of TVFM theory, Dubinin and Radushkevich derived a temperature invariant adsorption isotherm model. It is given by:

$$n_a = n_{max} exp\left[\left(\frac{-A}{\varepsilon}\right)^2\right] \tag{2.4}$$

where, n_a and n_{max} represents the amount of gas adsorbed per unit mass of adsorbent and the limiting adsorption, respectively. The terms A and ε denote adsorption potential and characteristic free energy of adsorption, respectively.

The adsorption potential, A, is given by:

$$A = RTln\left(\frac{P_0}{P}\right) \tag{2.5}$$

where, R is the gas constant, P is the equilibrium pressure at temperature T, and Po is the saturation vapour pressure in subcritical adsorption (for supercritical adsorption Po is termed as pseudo-saturation pressure). After combined the equations (2.4) and (2.5), the obtained linear form of the D-R equation is widely used for linearizing the gas adsorption isotherm, and the micropore volume can be obtained from the intercept of the D-R plot. However, some isotherms may give rise to curved D-R plots due to the presence of wider micropores and broad pore size that leads to inaccuracies in the determination of micropore volume [11]. Dubinin-Astakhov (D-A) equation which is similar in form to the D-R equation, can linearize the adsorption data more effectively due to an additional parameter, k, in the equation [11]. The isotherm is given by:

$$n_a = n_{max}exp\left[\left(\frac{-A}{\varepsilon}\right)^k\right] \tag{2.6}$$

The parameter k is generally close to a small integer. The assumption of temperature invariance in the D-R and D-A models leads to a temperature independent characteristic free energy of adsorption, ε. However, the assumption of temperature invariance may not be valid for very large temperature and pressure ranges. It was found that ε could vary linearly with temperature [12]. Therefore, Richard et *al* proposed the following form of the characteristic free energy of adsorption [2].

$$\varepsilon = \alpha + \beta T \tag{2.7}$$

the terms α and β in reference [2] are interpreted as the enthalpic and entropic factors of the characteristic free energy.

By combining Eq. (2.4), (2.5), (2.6) and (2.7), the excess adsorption is given by:

$$n_{ex} = n_{max} exp\left[-\left(\frac{RT}{\alpha+\beta T}\right)^k \ln^k\left(\frac{P_0}{P}\right)\right] - \rho_g V_a \quad (2.8)$$

The modified Dubinin–Astakhov model has been successfully adapted to describe supercritical hydrogen adsorption in activated carbons and zeolites [2]. Recently, this model has also been used to predict the hydrogen adsorption isotherm of MOF-5 [7, 9]. The main disadvantage of the modified D-A model is that, at low pressure, it does not reduce to Henry's law and at high temperature (above 200 K), the model results negative excess adsorption data. Other than the expression for the excess adsorption, the modified D-A model also provided an analytical expression for the isosteric heat (q_{st}) of adsorption [2].

$$q_{st} = \alpha\sqrt{-\ln\frac{n_a}{n_{max}}} \quad (2.9)$$

2.2 Development of adsorptive system model for predicting the multiphysics performance of a hydrogen storage system

General heat and mass transfer equations together with the modified D-A model is needed for developing the computational fluid dynamics model of the hydrogen adsorptive storage system.

2.2.1 Mass and momentum balance equations

The Darcy's equation together with the continuity equation is used for solving the mass and the momentum balance equations in the adsorptive storage system model. The Darcy's equation is based on Darcy's law, which states that the velocity field is determined by the pressure gradient, the fluid viscosity and the structure of the porous medium. Darcy's equation is given by:

$$\vec{u} = -\frac{k}{\mu}\nabla p \quad (2.10)$$

where, $\vec{u}$ is the velocity of the fluid, k is the permeability of the porous medium, μ is the dynamic viscosity of the fluid and ∇p is the pressure gradient. The combined form of Darcy's equation and the continuity equation is given by:

$$\frac{\partial}{\partial t}(\rho\varepsilon_b) + \nabla \cdot \left(\rho\left(-\frac{k}{\mu}\nabla p\right)\right) = S_m \tag{2.11}$$

In Eq. (2.11), ρ and ε_b are the density of the hydrogen gas flowing through the adsorbent bed and bed porosity, respectively. The bed porosity, ε_b is the fraction of the porous bed where hydrogen is present in the gaseous state. The bed porosity is calculated by using the total porosity, ε_t and the micro porosity, ε_{mi} of the porous bed [13]. In the porous bed, total porosity is the fraction of the bed where hydrogen is present in the gas/adsorbed phases and micro porosity is the fraction of the bed where hydrogen is present in the adsorbed phase. The following correlations are used to deduce the total, micro and bed porosities of the adsorbent bed in the tank.

$$\text{Total porosity, } \varepsilon_t = 1 - \frac{\rho_b}{\rho_s} \tag{2.12}$$

$$\text{Micro porosity, } \varepsilon_{mi} = \frac{V_a \times M_{adsorbent}}{V_{bed}} \tag{2.13}$$

$$\text{Bed porosity, } \varepsilon_b = \varepsilon_t - \varepsilon_{mi} \tag{2.14}$$

where, ρ_b, ρ_s, V_a, $M_{adsorbent}$ and V_{bed} are bed density, skeleton density, adsorption volume obtained from the modified D-A model, the mass of the adsorbent and the volume of the adsorbent bed, respectively. The dynamic viscosity, μ of the hydrogen gas is obtained from NIST standard reference database [14]. The permeability, k of the Eq. (2.11) is determined from the diameter of the adsorbent particles, D_p and bed porosity, ε_b using the relation [15].

$$K = \frac{1}{150}\frac{{D_p}^2{\varepsilon_b}^3}{(1-\varepsilon_b)^2} \tag{2.15}$$

In Eq. (2.11), S_m is the mass source term or the term which refers to the mass generation rate per unit volume of the adsorbent that includes only the micropore volume of the adsorbent.

$$S_m = -\rho_b M_{H2} \frac{\partial n_a}{\partial t} \tag{2.16}$$

where, ρ_b, M_{H2} and n_a are the adsorbent bed density, molar mass of hydrogen gas and absolute adsorption, respectively. The negative sign of the S_m implies that desorption increases the amount of gaseous hydrogen. In Eq. (2.16), n_a is the absolute adsorption obtained using the modified Dubinin-Astakhov (D-A) adsorption model. In this model, the absolute adsorption is related to the state variables, temperature T and pressure P using Eq. (2.16) [2].

$$n_a = n_{max} exp\left[-\left(\frac{RT}{\alpha+\beta T}\right)^m ln^m\left(\frac{p_0}{p}\right)\right] \tag{2.17}$$

where, R is the universal gas constant. The term m is the heterogeneity parameter of the adsorbent material. The quantity, n_{max} represents the limiting absolute adsorption corresponding to the limit $p \rightarrow p_0$, where p_0 is the pseudo-saturation pressure. The terms α and β are enthalpy and entropic contributions to the free energy of adsorption.

2.2.2 Energy conservation equation

To describe the energy conservation of the storage system, we use the standard energy balance equation for hydrogen gas flowing through the adsorbent bed [7]:

$$(\rho C_p)_{eq} \frac{\partial T}{\partial t} + \rho C_p \vec{u} \cdot \nabla T = \nabla \cdot \left(k_{eq} \nabla T\right) + Q \tag{2.18}$$

the first and second term in the left hand side of the Eq. (2.18) represent enthalpy and convection, respectively. The first and second terms of the right hand side represent the conduction and the heat sources, respectively.

In Eq. (2.18), the equivalent volumetric heat capacity of the adsorbent-gas system is given by:

$$(\rho C_p)_{eq} = \varepsilon_b \rho_g C_{pg} + n_a M_{H2} \rho_b C_{pa} + \rho_b C_{ps} \quad (2.19)$$

where, ρ_g and ρb are the densities of the hydrogen gas and the adsorbent material, C_{pg}, C_{pa} and C_{ps} are specific heat capacities of the hydrogen gas, the adsorbent-gas mixture and the porous material, respectively. The heat capacity of the adsorbent-gas system is written as a volumetric average of the gas and the solid phases; the solid phase includes the contribution of the adsorbed phase of hydrogen. In the model, the specific heat capacity of adsorbed gas is assumed to be the same as that for the adsorbed phase. i.e., $C_{pa} \approx C_{pg}$. The equivalent conductivity of the adsorbent-gas system in Eq. (2.18) is the net conductivity of the medium including that of the adsorbent k_s and of the gas k_g, weighed using the effective porosity. The equivalent thermal conductivity is obtained using the mixing rule [16]:

$$k_{eq} = \varepsilon_b k_g + (1 - \varepsilon_b) k_s \quad (2.20)$$

The heat source term Q in Eq. (2.18) is the sum of the contributions from the adsorption heat Q_a, and heat produced by pressure-volume work Q_p. The heat of adsorption Q_a, is given by [8]:

$$Q_a = \rho_b \frac{dn_a}{dt} q_{st} \quad (2.21)$$

where, q_{st} is the isosteric heat of adsorption, which is given by the modified D-A model as [2]:

$$q_{st} = \alpha \sqrt{-\ln \frac{n_a}{n_{max}}} \quad (2.22)$$

The heat generated due to pressure-volume work is given by the following expression [8]:

$$Q_p = \varepsilon_b \frac{\partial p}{\partial t} + u_r \frac{\partial p}{\partial r} + u_z \frac{\partial p}{\partial z} \quad (2.23)$$

where, u_r and u_z are the components of velocity field along the radial and axial direction.

2.3 Validation of model with experimental data obtained from the test bench using MOF-5 as an adsorbent material

A detailed description of the test bench, the experimentation, the parameters used for simulation, the geometry and monitoring points, the initial and boundary conditions, and the results and discussions are presented in this section.

2.3.1 Test bench

The schematic of the bench-scale test system used to probe hydrogen charging and flowthrough is shown in the Figure 2.2.

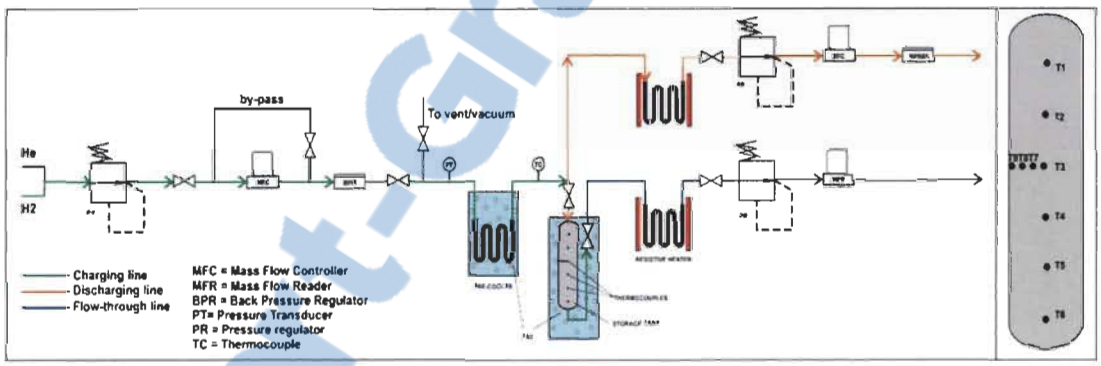

Figure 2.2: Schematic representation of storage/flowthrough experimental test bench.

The test bench consists of a charging manifold, a discharging manifold and a flowthrough manifold all tethered to a subscale-prototype (2.5 L) stainless steel tank filled with MOF-5 adsorbent. For charging experiments, pressure regulator is adjusted and then hydrogen gas (99.999 %, Praxair) is admitted into the tank by means of a thermal mass flow controller (TMFC, Brooks 0–100 SLPM) and a back pressure regulator (BPR, TESCOM) installed on the charging manifold. A bypass manifold and a manual valve connected across the TMFC help to maintain the required 50 psia pressure difference between the inlet and outlet of the TMFC

at the start of flow control. Once admitted into the tank, the pressure of the hydrogen gas is monitored using a pressure transducer, PT (Dresser DXD, 0–3000 psia). For cryogenic charging tests, hydrogen gas is pre-cooled to ~77 K before it enters the storage tank by means of a helical cooling loop immersed inside a liquid nitrogen (LN_2)-filled 40 L cryogenic vessel, while the storage tank is vertically immersed in a 125 L cryogenic vessel (CryoFAB) filled with LN_2. Nine k-type thermocouples are attached along the axial (T_1–T_6 along axial from top to bottom) and radial (T_7–T_9 along radial from axis to tank wall) directions within the tank to monitor the spatial distribution of tank temperature, while a single k-type thermocouple inserted at the entrance of storage tank monitors the inlet hydrogen temperature. To isolate the hydrogen manifolds from the storage tank, two all-metal valves (Swagelok) are attached at the entrance and exit of the tank. To measure the flow of the gas during discharging and flowthrough, two thermal mass flow meters are used (TMFR, Brooks 0-30 SLPM, Bronkhorst TMFC (0-150 SLPM). A rotary vane pump is attached to the charging manifold to evacuate the whole system prior to all experiments. The data acquisition and control of valves, mass flow controllers and temperature sensors are made possible using National Instruments Compact Field Point communication system which is interfaced to a PC using NI LabVIEW professional development software suite. Pressure data are acquired by interfacing the transducer to PC using RS-232 Serial communication protocol

2.3.2 Sample loading and void volume measurement

The MOF-5 sample required in our tests is obtained from BASF. Since this adsorbent is sensitive to moisture and air, it was stored and handled within a dry argon-filled glove box workstation. After embedding the thermocouples in the

storage tank, the tank is transferred into the glove box and 358 g of MOF-5 is added into it. After filling, all-metal valves on both sides of the tank are closed until it is re-inserted back into the test bench setup. Once attached, the argon gas is out-gassed by means of the mechanical pump. The empty tank volume, the manifold volume (the volume between MFC and the all-metal valve at the tank inlet) and the void volume of MOF-5 tank are estimated by admitting known amounts of ultrapure helium (99.999 %, Praxair) into the system. Void volume measurements with MOF-5 are carried out at room temperature and at a final equilibrium pressures of less than 2 MPa, so as to minimize any potential *He* adsorption.

Table 2.1: Volume calibration of different parts of the storage/flowthrough test bench.

Part	Volume (L)
Tank with MOF and charging manifold	2.87
Charging manifold alone	0.58
Upper hemisphere of the tank	0.22
Discharging manifold	0.04

Finally, the volumes are calculated from the known mass flow rates of helium, the final equilibrium pressure and the temperature by considering the mass balance before and after helium is introduced into the tank. The gas density of helium gas is determined using the equation of state (EOS) of real gas available in the NIST REFPROP Standard reference database [14]. The resulting volume calibration data is shown in the table (Table 2.1). The volume of the upper hemisphere of the tank, where there is no MOF-5, is estimated from the geometry of the tank and the quantity of MOF-5.

2.3.3 Stationary storage and charging experiments

For the stationary charging tests, the all-metal valves at the exit are closed. To carry out stationary charging, the tank is initially equilibrated at 77 K and pre-

cooled hydrogen is admitted into the tank until a maximum pressure of 9 MPa is reached. The initial pressure and mass flow rate are set to 0.822 MPa and 15 SLPM. In order to compare the hydrogen uptake capacity of MOF-5 with those reported elsewhere, we measured the excess hydrogen adsorption using the test bench. This is done using step-by-step introduction of hydrogen gas into the MOF-5 tank, much similar to the protocol followed in conventional volumetric measurements. After reaching the thermal equilibrium, the pressure and temperature are recorded. The hydrogen gas densities are determined using the EOS of real gas from NIST REFPROP [14].

2.3.4 Parameters used in the simulation

The modified Benedict-Webb-Rubin real gas equation of state, as implemented in REFPROP was used to calculate the thermodynamic properties such as specific heat capacity, density, viscosity, enthalpy and thermal conductivity of hydrogen gas. Initially, the NIST database was interfaced with COMSOL Multiphysics® using Matlab (R2010b) [14, 17]. While this is a highly accurate method of importing thermodynamic data, it compromises the computational speed. Therefore, we obtained data from NIST, which is converted into a grid form in Matlab and it is implemented in COMSOL Multiphysics® platform [18]. The properties of *normal* hydrogen are used in the simulation when the *para-ortho* conversion is not taken into account. The correlations of temperature dependent thermal conductivity and the specific heat capacity of stainless steel tanks are obtained from elsewhere [19]:

$$\log k\ (\mathrm{W\ m^{-1}K^{-1}}) = -1.4087 + 1.3982\log T + 0.2543\ (\log T)^2 - 0.6260\ (\log T)^3 + 0.2334\ (\log T)^4 + 0.4256\ (\log T)^5 - 0.4658\ (\log T)^6 + 0.1650(\log T)^7 - 0.0199\ (\log T)^8 \quad (2.24)$$

$$\log C_p(\mathrm{J\ kg^{-1}K^{-1}}) = 22.0061 - 127.5528\,[\log(T\,(K)] + 303.647\,[\log(T\,(K)]^2 - 381.0098\,[\log(T\,(K)]^3 + 274.0328\,[\log(T\,(K)]^4 - 112.9212\,[\log(T\,(K)]^5 + 24.7593\,[\log(T\,(K)]^6 - 2.239153[\log(T\,(K)]^7 \quad (2.25)$$

Density of stainless steel used is 7830 (kg m^{-3}) [18]. The fitted modified D-A parameters are taken from the literature and are given in table (Table 2.2) [20]. Figure 2.3 shows fitted modified D-A parameters using experimental data [5, 20].

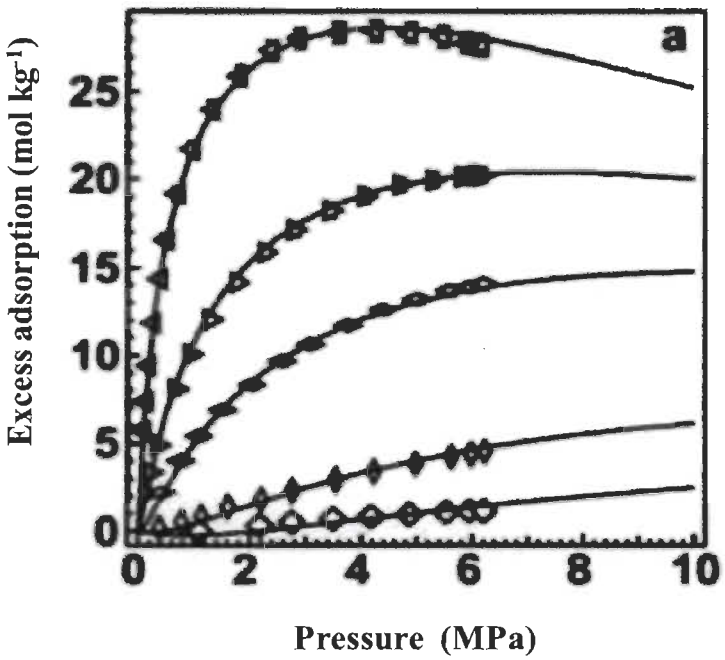

Figure 2.3: Fitted modified D-A parameters using experimental data for MOF-5 [5].

Table 2.2: Modified D-A model parameters of MOF-5 [5].

Material	n_{max} (mol kg^{-1})	P_0 (MPa)	α (J mol^{-1})	β (J mol^{-1} K^{-1})	m
MOF-5	67.5	2.75×10^{10}	3481	153.6	9.045

The experimentally measured heat capacity of MOF-5 is used for solving the energy balance equation. The measurement is conducted in the temperature range of 2–300 K by using a Calvet calorimeter and a direct adiabatic relaxation calorimeter [21]. The measured heat capacities are fitted with the 5^{th} order polynomial correlations using the Levenberg-Marquardt least-square algorithm:

$$C_{p,MOF-5} = 0.524 - 8.885 \times 10^{-3} \times \mathrm{T} + 9.624 \times 10^{-5} \times T^2 - 3.469 \times 10^{-7} \times T^3 + 4.417 \times 10^{-10} \times T^4 \quad (2.26)$$

For the thermal conductivity of MOF-5 at cryogenic temperatures, we used the reported value of 0.088 ($Wm^{-1}K^{-1}$) [22].

Table 2.3: Densities and porosities of MOF-5.

Adsorption volume, V_a ($m^3\ kg^{-1}$)		0.00123
Bulk density, ρ_b ($kg\ m^{-3}$)		155.60
Skeleton density, ρ_s ($kg\ m^{-3}$)		2000.00
Total porosity, ε_t	$1 - \frac{\rho_b}{\rho_s}$	0.92
Micro porosity, ε_{mi}	$\frac{v_a \times M_{MOF-5}}{V_{bed}}$	0.191
Bed porosity, ε_b	$\varepsilon_t - \varepsilon_{mi}$	0.73

Physical characteristics, such as the bulk density and the mass of MOF-5 are also measured. The measured bulk density and the reported skeleton density are used to calculate the total porosity of the adsorbent bed [23]. The adsorption volume, V_a obtained from the modified D-A model is used to calculate the micro porosity [2]. Adsorption volume, densities and porosities are summarised in table (Table 2.3).

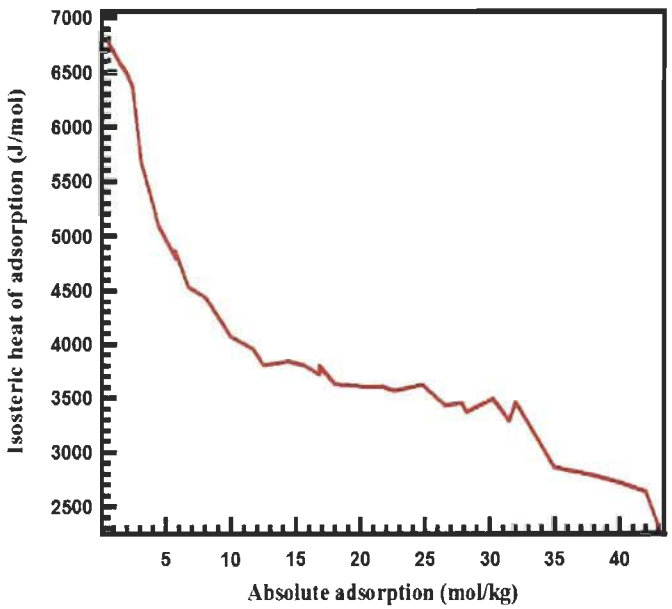

Figure 2.4: Isosteric heat as a function of absolute adsorption.

The isosteric heat of hydrogen adsorption of MOF-5 is measured experimentally using the calorimetric method [24]. The measured isosteric heat of adsorption as function of absolute adsorption obtained from modified D-A model is shown in the Figure 2.4. This data is implemented in the form look-up table into COMSOL Multiphysics® to solve the adsorption heat source in the CFD model.

2.3.5 Geometry and monitoring points

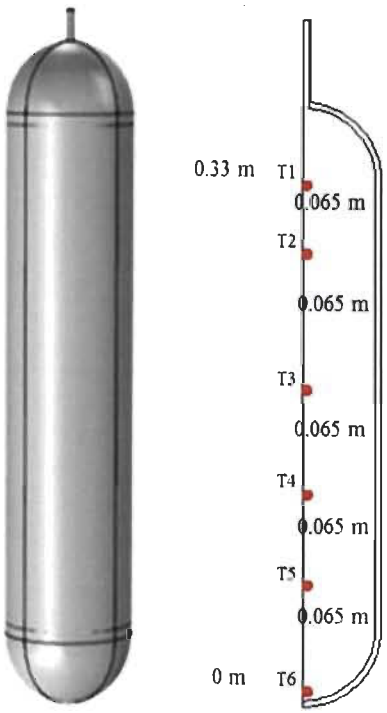

Figure 2.5: Geometry of the tank with monitoring points.

Figure 2.5 shows geometry of the tank with monitoring points. The inner and outer radii at the entrance of the 2.5 L hydrogen storage tank are 0.004 m and 0.005 m, respectively. The internal and external radii in the middle of the tank are 0.0469 m and 0.0508 m respectively. The internal and external heights of the tank are 0.45 m and 0.454 m, respectively. To compare the spatio-temporal variation of pressure and temperature obtained from the simulation with those measured experimentally, we chose four reference points in the axial direction.

2.3.6 Initial and boundary conditions

The initial and boundary conditions used for model validation are based on our experimental test bench. Due to the temperature gradient, the initial temperature of the tank in the MOF-5 test bench is not uniform, but is rather in the range of 77-79 K. To implement this temperature range in the model as an initial condition, we divided the whole bed domain into different subdomains and applied different initial temperature (corresponds to experimental initial condition) to each subdomain. The initial pressure and mass flow rate are set to 0.822 MPa and 15 SLPM. In the model, the mass flow rate is implemented in the form of mass flux of 0.0335 (kg m^{-2} s^{-1}). A heat flux boundary condition with heat transfer coefficient, 200 (W m^{-3}) is applied to the outer wall of the tank.

2.3.7 Measurement of hydrogen uptake capacity of MOF-5

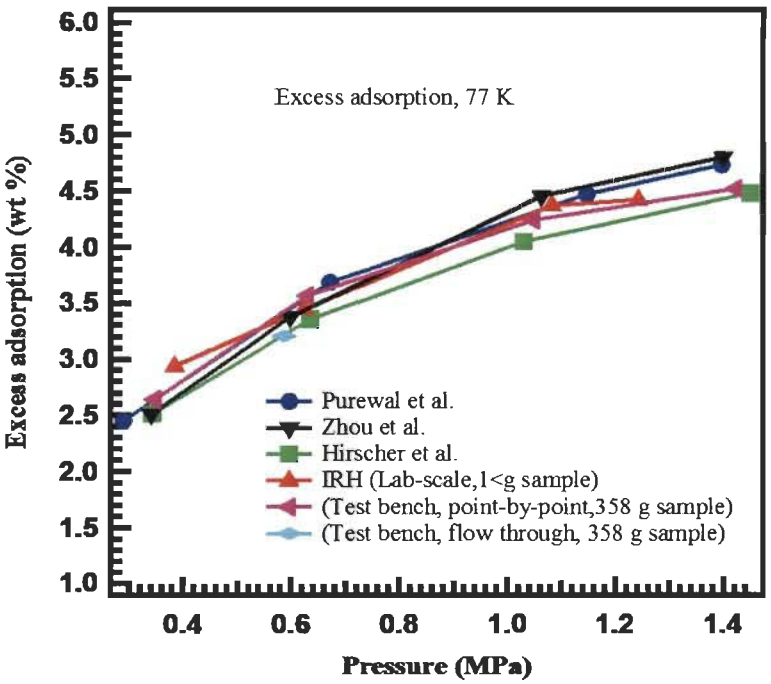

Figure 2.6: Excess adsorption of hydrogen on MOF-5 measured at 77 K using the test bench compared with the lab-scale measurements and data reported previously [6,20,25].

The excess adsorption measurement is done by using step-by-step introduction of hydrogen gas into the MOF-5 tank, much similar to the protocol followed in conventional volumetric measurements. After reaching the thermal equilibrium, the pressure and temperature are recorded and calculated the gas phase density. The calculated gas phase density and the amount of hydrogen gas introduced into the tank are used to calculate the excess adsorption data. We, then compared our excess adsorption data with other reported data and found very good agreement between our data and the data reported elsewhere (Figure 2.6).

2.3.8 Result and discussion

The validation of the CFD model, which compares the temperature and pressure of the tank during hydrogen charging obtained from simulation with those measured experimentally is presented here. Figure 2.7 shows the temperature measured along the central axial points in the tank and those obtained from the simulation. While the overall trend of the temperature evolution is clearly reproduced, the temperatures at the points T_2 and T_3 are slightly overestimated by ~2 K (Figure 2.7). We attribute the observed small difference in temperatures to differences in the positions of monitoring points in the simulation and the experiments. In the test bench storage experiment, thermocouples are implanted prior to filling MOF-5. The effects caused by filling of MOF-5 can shift the absolute positions of the thermocouples randomly by ± 0.3 cm. In addition to this, a temperature difference can be caused by the non-uniform bulk density of MOF-5 [7]. The variation of the powder bulk density within the vessel would affect the local heat generation rates, volumetric heat capacity and bed thermal conductivity [7]. The use of a temperature-invariant thermal conductivity in Eq. (2.20) and lack

LDF (Linear Driving Force) model in the mass balance equation may also contributes to the observed difference between model and experimental results.

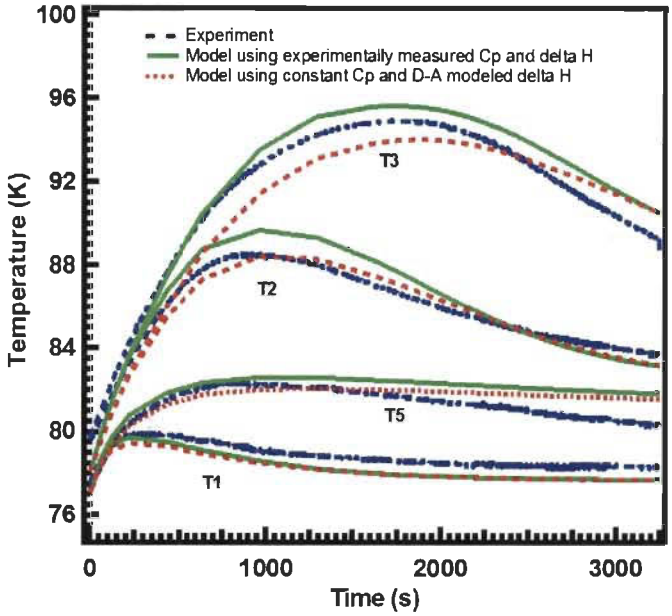

Figure 2.7: Temperature evolution during model validation with experiment in which 77 K hydrogen is charged into a 2.5 L cryo-sorptive MOF-5 tank. Model calculations are performed using experimentally measured temperature-dependent specific heats and isosteric heat.

From Figure 2.7, it is seen that the lowest temperature values are recorded at T_1 which is located at the top of the tank. This is anticipated because the top axial points are located near the inlet where the influence of incoming cold hydrogen is predominant. As a result of this temperature lowering, there will be significant adsorption which releases heat into the bed. This heat gets conductively transferred to the central part of the bed, towards points T_2 and T_3. The temperature at the point T_5 is less than that at the central regions due to the poor heat transfer stemming from the lower thermal conductivity of the MOF-5 adsorption bed. In order to understand the difference between the simulation results obtained using the experimentally measured specific heat capacity and

isosteric heat of adsorption with simulation results obtained using a constant specific heat capacity and the modified D-A modeled isosteric heat of adsorption, we then performed simulations assuming a constant specific heat capacity, 700 (J kg^{-1} K^{-1}) over all the temperature range and isosteric heat of hydrogen adsorption estimated from the modified D-A model. This results are compared with simulation results that used experimentally measured specific heat capacity and isosteric heat of adsorption. However, this presents no considerable difference in the model predictions as seen in Figure 2.7 (red profile).

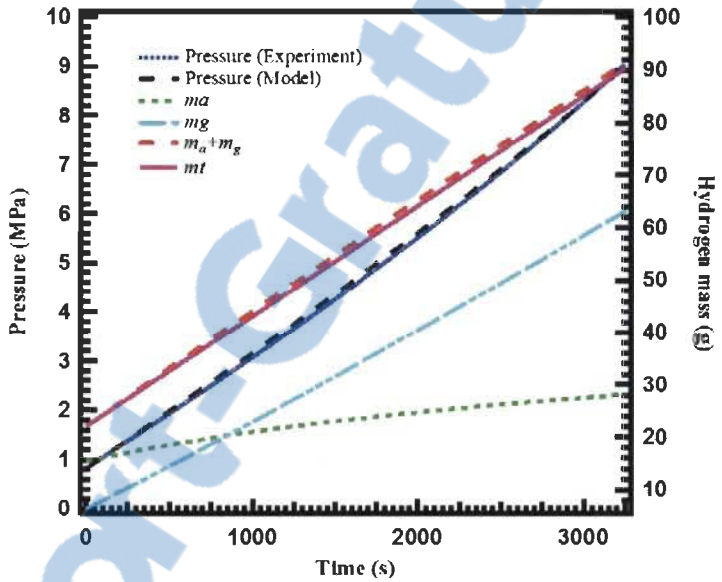

Figure 2.8: Pressure and mass evolution when 77 K hydrogen is charged into a 2.5 L cryo-sorptive MOF-5 tank.

The simulated pressure shows good agreement with experimental results which can be seen in Figure 2.8. Using the total inflow hydrogen mass (m_t) from the experiment and that from the model (m_a+m_g) adsorbed (m_a) and gas phase masses (m_g), the mass balance of the storage system is verified (Figure 2.8). To understand the contributions of various heat source terms on the observed temperature evolution in the tank, we modeled the system's temperature and heats considering adsorption heat and heat due to pressure-volume work,

separately. The heat sources and the corresponding temperature evolutions displayed in Figure 2.9 shows that, at the beginning of charging, adsorption heat (red profile) is the main contributor to the temperature evolution, while as charging progresses, the work due to compression (black profile) crosses over the heat due to adsorption.

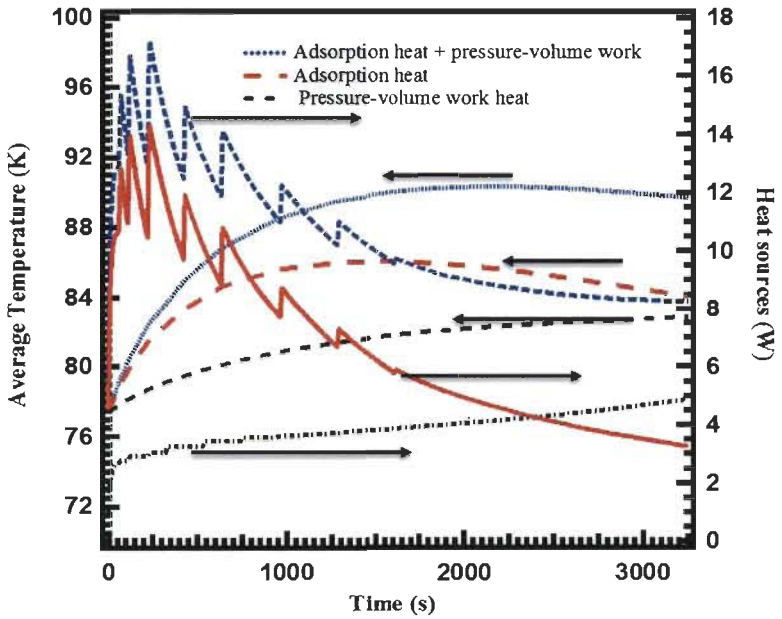

Figure 2.9: Heat source contributions and their influence on bed temperature evolutions as 77 K hydrogen is charged at a rate of 15 SLPM into 2.5 L cryo-sorptive tank filled with MOF-5. Arrows point toward the axis corresponding to the data.

As adsorption progresses, the heat released into the bed raises the average bed temperature. This eventually reduces adsorption, and the adsorptive heat is reduced consequently. The pressure work heat source increases in the beginning and stays almost uniform throughout the charging stage. The oscillating behaviour of the heat sources seen in the Figure 2.9 is an artefact probably caused by either large time steps between the model iterations or the lack LDF model in the mass balance equation.

2.4 Validation of the model with experimental data obtained from the test bench using Maxsorb™ activated carbon as an adsorbent material

The required details for performing the simulation are taken from the published literatures [7-9]. In order to avoid repetition, a brief description of the test bench, experimentation, parameters, geometry and boundary conditions are given here.

2.4.1 Test bench, experimentation geometry and monitoring points

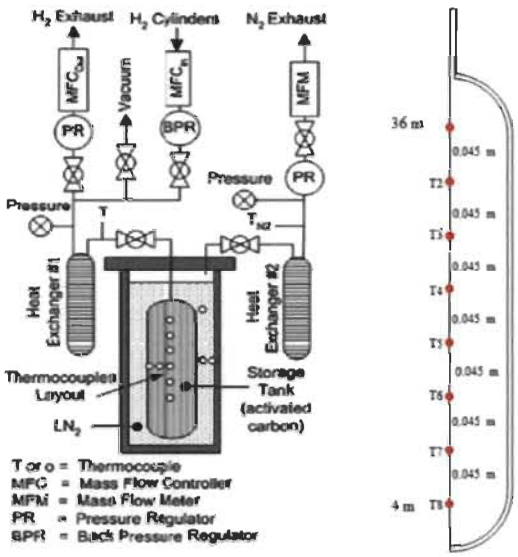

Figure 2.10: P&ID of the test bench and the monitoring points of the tank [7, 8].

The schematic of the test bench is shown in Figure 2.10 (left) [2]. The adsorption test bench consists of a 2.5 L stainless steel tank, which is filled with 670 g of Maxsorb™. To compare the spatio-temporal variation of pressure and temperature obtained from the simulation with those measured experimentally, we chose six monitoring points T_1... T_6 in the axial direction. The geometry of the tank and its monitoring points in the axial direction are shown in Figure 2.10 (right).

2.4.2 Parameters

To obtain the thermodynamic properties of hydrogen gas, the NIST standard reference database is used. The modified D-A parameters and bulk properties of Maxsorb™ required for the simulation are taken from the literature and given in the tables (Table 2.4 and 2.5) [7, 8].

Table 2.4: Modified D-A model parameters for AX-21™ [2].

D-A Parameters	n_{max} (mol kg^{-1})	P_0 (MPa)	α (J mol^{-1})	β (J mol^{-1} K^{-1})	V_a (m^3 kg^{-1})	m
	71.6	1470	3080	18.9	0.00143	2

Table 2.5: Material properties of AX-21™ [7, 8].

Bulk properties	ρ_b (kg m^{-3})	ε_b	k_s (W m^{-1} K^{-1})	C_{ps} (J kg^{-1} K^{-1})	D_p (μm)
	300	0.49	0.2	825	200

2.4.3 Initial and boundary conditions

Two simulations at different temperatures (room temperature and cryogenic temperature) were performed. The initial and boundary conditions of the simulation depend on the temperature conditions and are given in the table (Table 2.6). The initial pressure in the tank is set to 0.033 MPa for room temperature simulation. For cryogenic temperature simulation, the initial pressure in the tank is set to 0.14 MPa. The initial temperatures are set to 281 and 80 K for the simulations at room temperature and cryogenic temperatures, respectively. The mass flow rates are set to +15, -15 and 0 SLPM, respectively for charging, discharging and dormancy. Room temperature hydrogen gas is filled into the system for both simulations. A fixed temperature boundary condition, 77 K and heat flux boundary condition is applied to the outer wall of the tank [7, 8]. The

charge/discharge cycle at room temperature and charging at cryogenic temperature of Maxsorb™ carbon storage system is used for model comparison.

Table 2.6: Boundary conditions of charge/discharge cycle of AX-21™ system [7, 8].

Time (s)	Inlet	Outer wall
(*a*) *At room temperature* Charging (0-1042 s) Dormancy (1043-3189 s) Discharging (3190-4131 s) Dormancy (4132-6000s)	 297.6 K 297.8 K 282.2 K 288.9 K	 h_w = 36 (W m^{-2}K^{-1}) T_f = 282.5 K
(*b*) *At cryogenic temperature* Charging (0-1600 s)	 297 K	 77 K

2.4.4 Result and discussion

The model validation is carried out by comparing the temperatures at various points in the storage tank filled with Maxsorb™ activated carbon obtained from the simulation during hydrogen charging/discharging cycle at room temperature and charging at cryogenic temperature with those obtained from the test bench data.

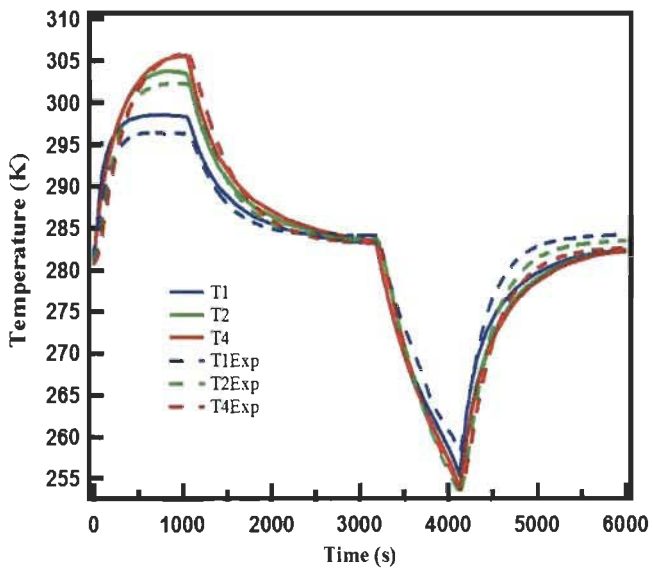

Figure 2.11: Comparison between the temperatures at points T_1, T_2 and T_4 of experimental validation and simulations at room temperature. An entire charging/discharging cycle is shown here.

The central axial points in the tank T_1, T_2, T_3, T_4 and T_6 which correspond to the positions of the thermocouples inside the test bench storage system are selected for comparing the temperatures. The temporal evolution of the temperature for both tests are shown in the Figures 2.11 and 2.12. For the room temperature data given in the Figure 2.11, we observe a very good agreement between simulation and experimental results.

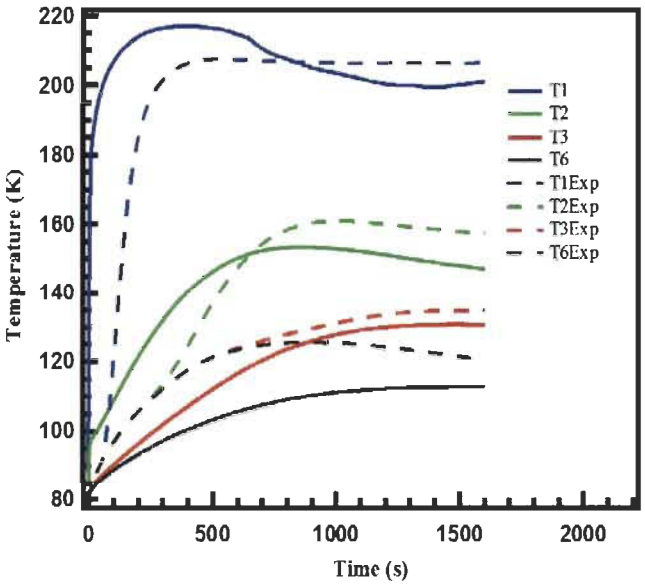

Figure 2.12: Comparison between the temperatures at points T_1, T_2, T_3 and T_6 of experimental validation and simulations at cryogenic temperature. Only the charging stage is shown here.

Although the temperatures at the monitoring points are slightly over and underestimated at cryogenic condition (Figure 2.12), the overall trend of the temperature evolution is clearly reproduced. The pressure obtained from the experimental and simulation results shows good agreement for room temperature and comparable agreement for cryogenic temperature, which are shown in Figures 2.13 and 2.14. During the charging phase, the pressure rises fast and reaches around 9 (MPa) and 5 (MPa), respectively. The pressure drops slightly

after the charging process is over owing to the decreased temperature in the tank (Figure 2.13), and it stays uniform throughout the dormancy period.

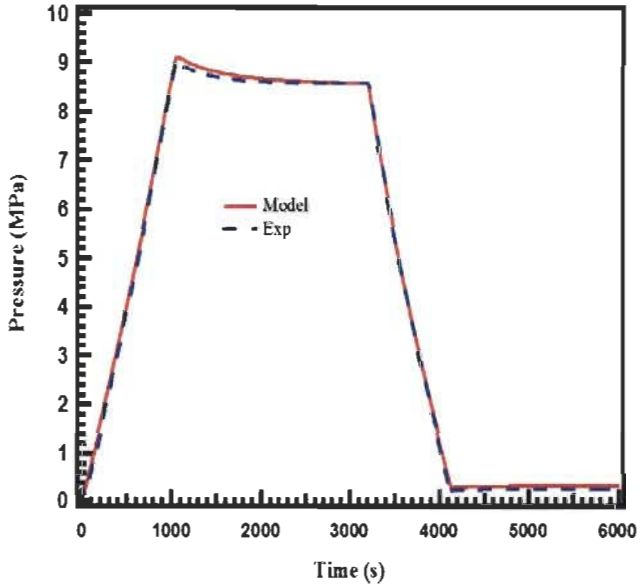

Figure 2.13: Experimental and simulation results for the pressure in the tank at room temperature

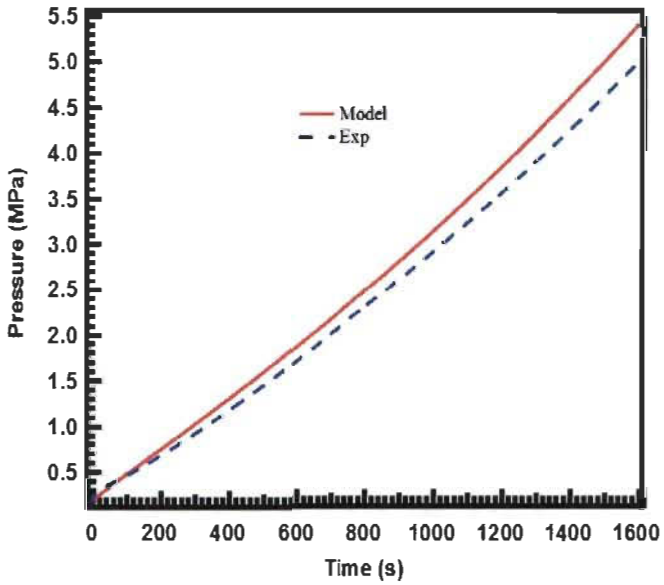

Figure 2.14: Experimental and simulation results for the pressure in the tank at cryogenic temperature.

The pressure starts dropping once the discharge is initiated due to the gas that flows out from the tank. The distribution of pressure inside the tank is uniform

owing to the small pressure gradient compared with the rate of change of pressure as function of time.

2.5 Conclusion

In conclusion, we developed a two-dimensional axisymmetric model to predict the coupled heat and mass transfer of a hydrogen adsorptive storage system. The validity of the base model is established by comparing the simulated temperatures and pressure at various points in the tank with those obtained from the experimental test bench, which is used MOF-5 as an adsorbent. The consistency checking of the adsorptive storage system model is carried out by comparing temperatures obtained from the simulation with those obtained from the bench test measurements using activated carbon (AX-21™) as an adsorbent.

References

[1] A. Dąbrowski. Adsorption-from theory to practice. Adv Colloid Interface Sci 2001; 93:135–224.

[2] Richard M.-A, Bénard P, Chahine R. Gas adsorption process in activated carbon over a wide temperature range above the critical point. Part 1: modified Dubinin-Astakhov model. Adsorption 2009; 15:43–51.

[3] Ege Dundar. Modélisation par la théorie du potentiel des processus d'adsorption dans les matériaux microporeux, Thesis, UQTR; 2014, Canada.

[4] Foo KY, Hameed BH. Insights into the modeling of adsorption isotherm systems. Chem Eng J 2010; 156:2–10.

[5] Dundar E, Zacharia R, Chahine R, Bénard P. Performance comparison of adsorption isotherm models for supercritical hydrogen sorption on MOFs. Fluid phase equilib 2014; 363:74– 85.

[6] Purewal J, Liu D, Sudik A, Veenstra M, Yang J, Maurer S, Müller U, Siegel DJ. Improved hydrogen storage and thermal conductivity in high-density MOF-5 composites. J Phys Chem C 2012; 116:20199-20212.

[7] Hardy B, Corgnale C, Chahine R, Richard M.-A, Garrison S, Tamburello D, Cossement, D, Anton D. Modeling of adsorbent based hydrogen storage systems. Int J Hydrogen Energy 2012; 37:5691-5705.

[8] Xiao J, Wang J, Cossement D, Bénard P, Chahine R. Finite element model for charge and discharge cycle of activated carbon hydrogen storage. Int J Hydrogen Energy 2012; 37:802-810.

[9] Corgnale C, Hardy B, Chahine R, Cossement D, Tamburello D, Anton D. Simulation of hydrogen adsorption systems adopting the flowthrough cooling concept. Int J Hydrogen Energy 2014; 39:17083-17091.

[10] Chen SG, Yang RT. Theoretical basis for the potential theory adsorption Isotherms. The Dubinin-Radushkevich and Dubinin-Astakhov equations. Langmuir 1994; 10:4244-4249.

[11] Ghosal R, smith DM. Micropore Characterization using the Dubinin-Astakhov Equation to Analyse High Pressure CO_2 (273 K) Adsorption Data. J Porous Mater 1996; 3:247-255.

[12] Czerny AM, Bénard P, Chahine R. Adsorption of nitrogen on granular activated carbon: experiment and modeling. Langmuir 2005; 21:2871–2875.

[13] Momen G, Hermosilla G, Michau A, Pons M, Firdaous M, Marty Ph, Hassouni K. Experimental and numerical investigation of the thermal effects during hydrogen charging in packed bed storage tank. Int J Heat Mass Transfer 2009; 52:1495–503.

[14] Lemmon EW, Huber ML, McLinden MO. NIST standard reference database 23: reference fluid thermodynamic and transport properties-REFPROP. Gaithersburg: National Institute of Standards and Technology, Standard Reference Data Program; 2007. Version 8.0.

[15] Xiao J, Tong L, Deng C, Bénard P, Chahine R. Simulation of heat and mass transfer in activated carbon tank for hydrogen storage. Int J Hydrogen Energy 2010; 35:8106-16.

[16] Xiao JS, Tong L, Cossement D, Bénard P, Chahine R. CFD simulation for charge-discharge cycle of cryo-adsorptive hydrogen storage on activated carbon. Int J Hydrogen Energy 2012; 37:12893-12904.

[17] COMSOL Multiphysics® version 4.4 4.3.1.161. Copyright 1998-2012. COMSOL AB.

[18] Ubaid S, Xiao J, Zacharia R, Chahine R, Bénard P. Effect of *para-ortho* conversion on hydrogen storage system performance. Int J Hydrogen Energy 2014; 39:11651-11660.

[19] Marquardt ED, Le JP, Radebaugh R. Cryogenic material properties database. 11th International cryo-cooler conference; June 20-22, 2000, Keystone, US.

[20] Zhou W, Wu H, Hartman RM, Yildirim T. Hydrogen and methane adsorption in metal-organic frameworks: A high-pressure volumetric study. J Phys Chem C 2007; 111:16131-16137.

[21] Kloutse FA, Zacharia R, Cossement D, Chahine R. Specific heat capacities of MOF-5, Cu-BTC, Fe-BTC, MOF-177 and MIL-53 (Al) over wide temperature ranges: Measurements and application of empirical group contribution method. Micropor Mesopor Mat 2015; 217:1-5.

[22] Ahluwalia RK, Hua TQ, Peng JK, Roh HS, Bailey J, Kumar R. System level analysis of hydrogen storage options. Presentation for DOE Hydrogen Program Review; May 14-18, 2012, Washington DC, USA.

[23] Purewal JJ, Liu D, Yang J, Sudik A, Siegel DJ, Maurer S, Müller U. Increased volumetric hydrogen uptake of MOF-5 by powder densification. Int J Hydrogen Energy 2012; 37:2723-2727.

[24] Kloutse AF, Zacharia R, Cossement D, Chahine R, Balderas-Xicohténcatl R, Oh H, Streppel B, Schlichtenmayer M, Hirscher M. Isosteric heat of hydrogen adsorption on MOFs: comparison between adsorption calorimetry, sorption isosteric method, and analytical models. Appl Phys A DOI 10.1007/s00339-015-9484-6.

[25] Schmitz B,U Müller, Trukhan N, Schubert M, Férey G, Hirscher M. Heat of adsorption for hydrogen in microporous high-surface-area materials. Chem Phys Chem 2008; 9:2181–2184.

Chapter 3

Effects of flowthrough cooling and *para-ortho* conversion on the performance of a subscale-prototype hydrogen storage tank filled with MOF-5

3.1 Background

MOF-5 has a low thermal conductivity of 0.3 $Wm^{-1} K^{-1}$ at room temperature which is nearly two orders of magnitude less than that of stainless steel. This makes the removal of heat from the MOF-5 bed is difficult [1]. Heat removal becomes even more problematic at cryogenic temperatures as MOF-5's thermal conductivity decreases further to less than 0.1 $Wm^{-1}K^{-1}$ [2].

A common approach used for enhancing the heat removal from the adsorbent bed consists in incorporating thermally conducting adsorbent additives in the bed which improves the bed's overall thermal conductivity. Liu et *al.* [2] and Purewal et *al.* [3] explored the effect of expanded natural graphite (ENG) additive on the thermal conductivity of MOF-5 at room temperature. They found that the thermal conductivity of neat MOF-5 at room temperature can be enhanced to up to 5 times by forming composite pellets with 10 % ENG, while at 77 K, the thermal conductivity increases to up to ~3 times. On the downside, ENG additive diminishes the hydrogen storage capacity of composite pellets by up to 10 % relative to neat MOF-5; this is attributed to the former's lower specific surface area. The application of this method relies on optimizing the composite's composition and pellet densities, and performing detailed parametric studies on the heat removal characteristics of the optimized composites. Inclusion of non-adsorbing metallic components in the adsorbent bed to compensate the adsorbent poor thermal conductivity is a similar approach to enhance the thermal

management inside cryo-adsorbent hydrogen storage systems. Chakraborty and Kumar modeled how an electrically heated intra-reservoir helical element accommodates the thermal requirements during endothermic hydrogen desorption from MOF-5 and AX-21™ hydrogen storage systems [4]. An important conclusion they made is that for optimum hydrogen extraction from the adsorbent bed, the thermal conductivity of the bed should be at least 0.5 W m^{-1} K^{-1}, higher than that of neat MOF-5. One could attribute this to inadequate interfacial contact between the heating element and the adsorbent. Therefore, the thermal conductivity of the adsorbent bed still is required to be high to facilitate uniform bed temperature distribution. Ahluwalia and Peng modeled adiabatic refuelling of hydrogen into an adsorptive vehicular hydrogen storage tank in which the activated carbon adsorbent is packed inside a 40-PPL 2024 aluminium alloy foam. The alloy form and an added in-tank heat exchanger are used to compensate for the adsorbent's poor thermal conductivity [5].

Due to the non-adsorbing nature of heat transfer components, both of the above approaches reduce the net volumetric hydrogen density of the storage system. In order to overcome this limitation, Schuetz et *al.* invented a hydrogen recirculation system where the adsorptive heat from the bed is removed convectively by continuous flowing cold hydrogen gas [6]. Briefly, this system consists of a loop of hydrogen gas which introduces the gas into the storage system; any non-adsorbed hot gas is recirculated back into a refrigeration unit where the hot gas is cooled and then reintroduced into the storage vessel. Numerical simulations of hydrogen charging into activated carbon tanks equipped with combined hydrogen recirculation cooling system and liquid nitrogen cooling system indicated much shorter cooling time than we would get when only

conductive heat transfer though the storage tank walls is considered [7]. In more recent works, Hardy et *al.* and Corgnale et *al.* performed numerical simulation of 'flowthrough cooling' heat removal technique for hydrogen charged into 2.5 L storage tank filled with MOF-5 using a model that was validated using experiments with the activated carbon [1, 8]. In this approach the adsorbent was maintained at cryogenic temperatures by the flow of cold hydrogen at a rate of up to 100 standard litres per minute (SLPM). The recirculation of hot hydrogen gas through the bed for transferring the heat into storage bed to enhance the hydrogen desorption is investigated [9, 10]. The result shows that heating the bed through a recirculation method is preferred over electrical heating due to the higher interfacial area between the gas and the adsorbent. Although flowthrough is increasingly considered as an efficient heat transfer mechanism for adsorptive hydrogen storage systems, all reported studies, except those in Refs. [1] and [8], are performed using solely computational simulations while experimental measurements of flowthrough are only beginning to emerge. Available experiments reported in Refs. [1] and [8], on the other hand, used flowthrough characteristics measured using activated carbon systems to model that of MOF-5 cryo-adsorptive hydrogen storage systems. While the authors observed reasonable agreements between the simulation and experiments on activated carbon, the discrepancies were attributed to experimental measurements as well as material property data used in their simulations.

In addition to the above cooling mechanism, another approach to cool the hydrogen storage medium is to convert the *para* hydrogen to the *ortho* hydrogen. Ahluwalia and his co-workers have simulated the cooling effect of *para-ortho* conversion in a MOF-5 filled hydrogen storage system [11]. The authors analysed

the MOF-5 filled system performance assuming that the system is charged with liquid *para* hydrogen, which converts to the equilibrium *para-ortho* hydrogen composition without any kinetic limitations. They reported that the storage system can reach lower temperature with equilibrium hydrogen than with *normal* hydrogen when endothermic heat of *para* to *ortho* hydrogen conversion takes place. In the absence of catalysts, however, the conversion follows slow kinetics and takes as many as several days to complete [12-15]. Recently, in a year-long project, Petitpas et *al.* conducted several experiments to study the kinetics of natural *para-ortho* conversion in a full-scale 345 bar automotive cryogenic pressure vessel filled with liquid *para*-hydrogen [16]. The authors reported that the natural conversion started in 10-15 days and was completed within 25 to 30 days. Peng and Ahluwalia developed a dynamic model which accounted for the endothermic natural *para* to *ortho* conversion kinetics to study the dormancy and hydrogen loss from an insulated pressure vessel filled with liquid *para*-hydrogen [17]. The model predicted that the hydrogen loss rate during the dormancy stage was decreased through the reduced pressure and temperature condition due to the endothermic *para-ortho* conversion. Fitzgerald et *al.* found that MOF-74 has the catalytic activity that causes conversion in the hydrogen. The authors observed that this conversion occurs on a time-scale of the order of a minute, whereas conversion is a slow process for hydrogen adsorbed on MOF-5 [18, 19]. The existing discussions reveal that the strong paramagnetic catalyst causes rapid conversion [20]. If foreign particles that can catalyze the *para-ortho* conversion are embedded in the MOF-5, the hydrogen storage system can be cooled to improve the storage capacity.

3.2 Effect of flowthrough cooling on the performance of a subscale-prototype tank filled with MOF-5

The flowthrough experiment and simulation are performed to understand the effect of flowthrough cooling on the thermal and storage performance of the 2.5 L storage tank filled with MOF-5. The details of the test bench specifications and the CFD system model are presented in Chapter 2. In order to perform the flowthrough test, 77 K pre-cooled hydrogen is charged into the tank which is initially equilibrated at 77 K and evacuated to 0.065 MPa. Hydrogen is continuously admitted into the tank at a flow rate of 20 SLPM, until a pressure 1.15 MPa is reached. When the pressure is stabilized at 1.1 MPa, the BPV#2 is adjusted so that any pressure rise due to further charging is prevented by releasing hydrogen out of the tank through the flowthrough manifold (chapter 2, Figure 2.2). This process is continued till the temperature swing that arises during the charging stage is diminished. To avoid complication in the test bench experiments, we vented the excess hydrogen and continued charging using fresh cold hydrogen instead of recirculating it after passing through external heat exchangers. Even though the test bench has the capability to perform the flowthrough experiment at high operating pressure, we limited the experiment to low pressures. This is because at high operating pressure, larger amount of hydrogen and longer time periods are required to cool the storage system during the flowthrough stage when the low mass flow rate of 20 SLPM is used in the experiment. For validating the model, we let the maximum pressure reach only 1.1 MPa. In the simulation, 77 K hydrogen at the rate of 20 SLPM is charged into the 2.5 L MOF-5 filled tank to reach 1.1 MPa pressure. Once the tank pressure has reached 1.1 MPa, a pressure boundary condition is applied to the outlet of the tank by setting the pressure to

1.1 MPa. Thus the tank pressure is 1.1 MPa throughout the flowthrough stage. The details of the adsorptive system model, parameters and geometry of the tank used in the simulation were discussed in the previous chapter. The initial and boundary conditions of the model are based on the flowthrough experiment.

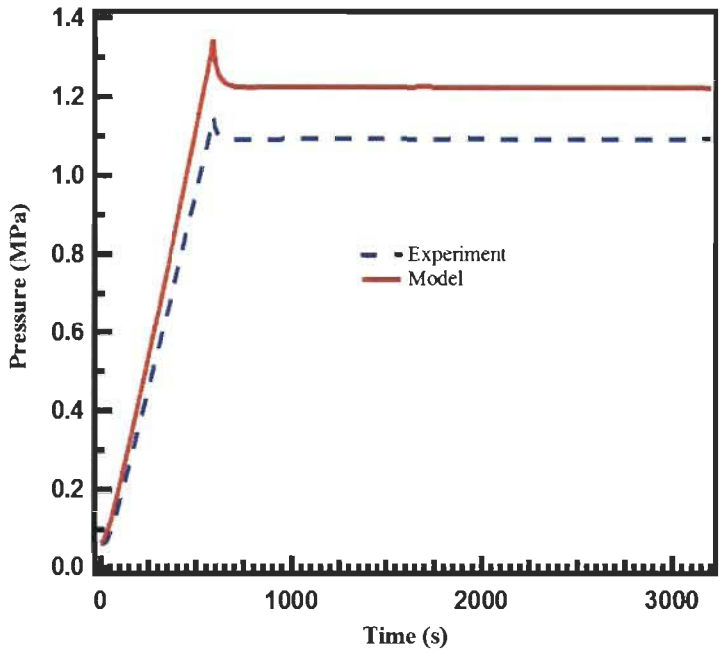

Figure 3.1: Comparison of the experimental pressure with that obtained from the simulation during a flowthrough run.

Figures 3.1 and 3.2 compares the pressure and the temperature histories in the tank obtained from experiments and simulations. The opening of BPV for releasing the excess pressure causes the sudden short rise and fall of pressure, which can be seen as a characteristic peak in Figure 3.1. Due to adsorption/pressure work heat, the bed temperature increases to a maximum of 123 K during the charging stage and then decreases to around 80 K during the flowthrough stage as the heat is transported by flowing hydrogen (Figure 3.2). While the overall behaviour of pressure and temperatures are reproduced, the model results are slightly overestimated with respect to the experiments. As discussed in the chapter 2, the

factors such as change in bulk density, using of constant contact resistance and surrounding temperature, lack LDF model in the mass balance equation, etc. may be the influencing factors for the observed difference between the simulation and experimental results.

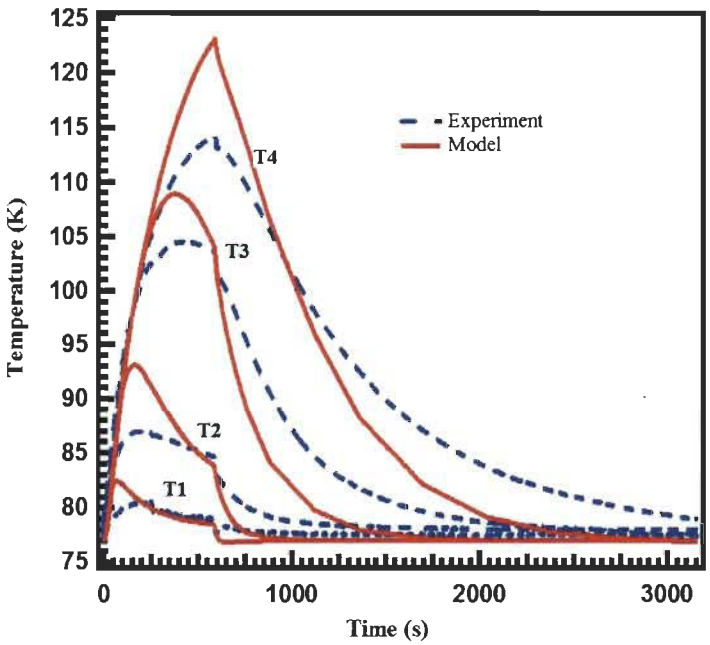

Figure 3.2: Comparison of the experimental temperature with that obtained from the simulation during a flowthrough run.

To understand how flowthrough cooling affects the storage capacity and the reduction in cooling time, we performed simulation of charging up to the same pressure as in the flowthrough runs but using only external cooling with LN_2 bath, while keeping the same inlet hydrogen temperature and charging rate as those for the flowthrough tests. After the tank pressure and the average bed temperature reached 1.4 MPa and 110 K respectively in 590 s, the charging is stopped and the storage tank is allowed to cool down to 77 K. Figure 3.3 compares the average bed temperature of the tank for the flowthrough cooling together with LN_2 cooling and the LN_2 cooling scenarios. The average bed temperature (blue profile in Figure

3.3) decreased to ~79 K while the tank pressure decreased to ~0.7 MPa (LN_2). The temperature profile indicates that for the cooling time considered (0.7 hr), there is no considerable reduction in the temperature due to flowthrough approach. This is because the flow rate used for charging hydrogen is only 20 SLPM. Faster flow rates are required for flowthrough cooling to be efficient for heat removal [1].

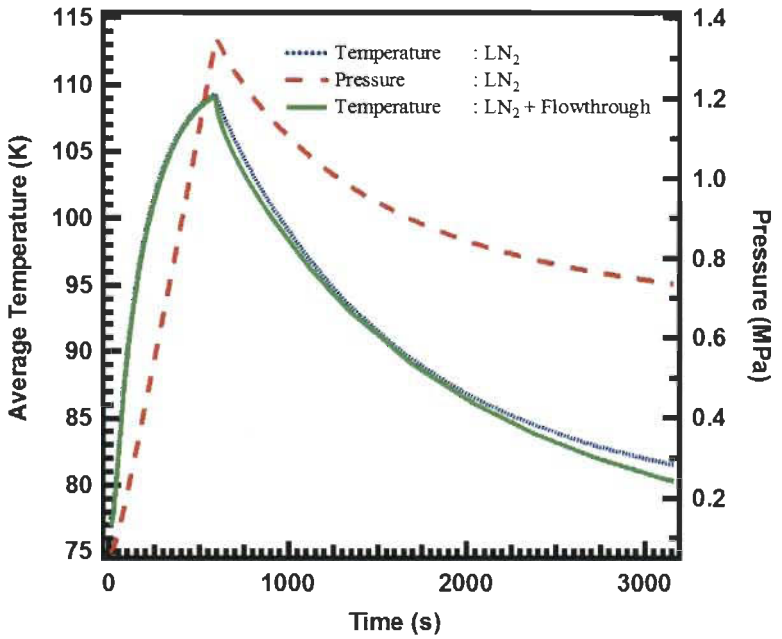

Figure 3.3: Comparison of the average bed temperatures obtained from flowthrough simulations with those obtained when only a LN_2 cooling bath was used.

In the Figure 3.4, the total amount of hydrogen stored in the system is calculated by summing the masses of hydrogen in the gas and adsorbed phases. This is in good agreement with the experimentally measured amount of hydrogen. The latter is determined from the difference between in-and out-flow mass flow meters during the experimental flowthrough runs. Masses of hydrogen, m_a and m_g in the storage system are obtained by the volume integration of adsorbed- and gas-phase hydrogen densities. Gas-phase mass increases proportionally during charging and slightly during the flowthrough stage. A significant increase in the

adsorbed-phase mass is seen during the flowthrough stage, which is attributed to a decrease of the tank temperature and the entering of additional hydrogen during the flowthrough stage. In the case of the storage system with only LN_2 as a coolant, the gas phase mass decreases and the adsorbed mass increases, but the net storage mass remains same.

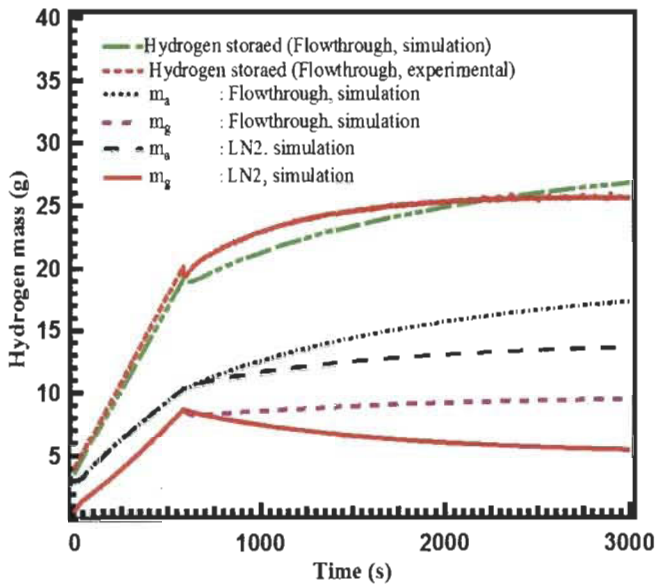

Figure 3.4: The amount of hydrogen stored in the system obtained from flowthrough simulations with those obtained when only a LN_2 cooling bath was used. The amount of hydrogen stored during flowthrough experiments are also compared with that obtained from simulation.

3.3 Effect of *para-ortho* conversion heat on the performance of a subscale-prototype storage system filled with MOF-5

The effect of *para-ortho* conversion on the thermal and storage performance of the 2.5L tank filled with MOF-5 is investigated numerically. The following assumptions are made in the simulation:

- MOF-5 has enough catalytic activities for making rapid conversion via addition of an enhancing agent.

- The material properties will not change due to the presence of the enhancing agent and we have considered only the maximum conversion effect.
- Based on the system temperature, the fraction of *para* hydrogen present in the adsorbed phase is converted to *ortho* fraction of hydrogen.

The details of the mass and energy balance equation used in the simulation are presented in the previous chapter (chapter 2, Eq. (2.11 and 2.23)). Other than the heat sources such as the adsorption heat (Q_a) and the heat due to pressure work (Q_p), an additional heat source due to *para-ortho* conversion (Q_c) is included in the energy balance equation for accommodating the *para-ortho* conversion effect in the adsorptive storage system model. We use the following approximation to calculate the conversion heat source:

$$Q_c = \frac{d}{dt}\left[(\rho_a f_{OH2} h^{po})\right] = \frac{d}{dt}\left[(n_a M_{H2} \rho_b (1 - f_{PH2}) h^{po})\right] \quad (3.1)$$

where, ρ_a in Eq. (3.1), is the adsorbed phase density. f_{ph2} and f_{oh2} are the temperature-dependent mass fraction of *para* and *ortho* fractions of hydrogen present in the equillibrium hydrogen. The fraction of *ortho* hydrogen in the equillibrium hydrogen is estimated from the temperature-induced evolution of the equilibrium mass fraction of *para* hydrogen, using the empirical relation [21]:

$$f_{PH2} = \left[0.1\left[\exp\left(\frac{-175}{T}\right) + 0.1\right]^{-1} - 7.06 \times 10^{-9} T^3 + 3.42 \times 10^{-6} T^2 - 6.2 \times 10^{-5} T - 0.00227\right] \quad (3.2)$$

In Eq. (3.1), h^{po} is the endothermic conversion enthalpy. Figure 3.5 shows the temperature-dependent *para* hydrogen content of equilibrium hydrogen and the *para* to *ortho* hydrogen energy conversion. Even though REFPROP standard reference database has the enthalpies of *ortho* and *para* hydrogen, these are

defined with the reference states of *ortho* or *para* hydrogen at the normal boiling point (20.4 K) with zero enthalpy assigned in REFPROP.

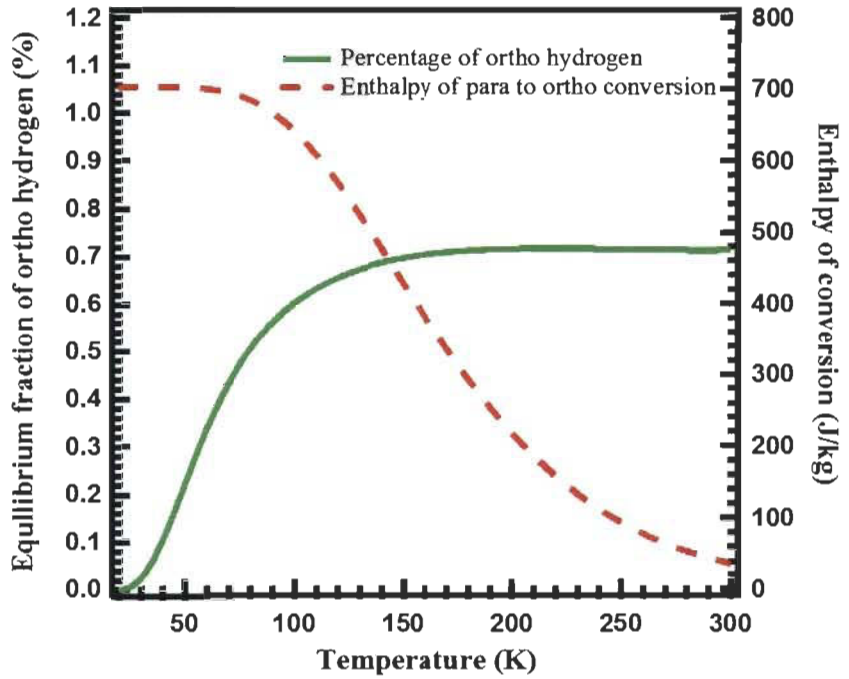

Figure 3.5: Equilibrium fraction of *para* hydrogen as function of temperature and enthalpy of *para-ortho* hydrogen conversion [17, 21].

In order to properly calculate this conversion enthalpy, a common reference state is required. Therefore, the enthalpies of *ortho* and *para* hydrogen given by the REFPROP are adjusted using a common reference state which is the *p*ara hydrogen at 0 K for which the internal energy is at its lowest quantized value. Accordingly, the enthalpy of conversion h^{po} can be written as the sum of the enthalpy from REFPROP, $h^{po}_{(refprop)}$ and the enthalpy with respect to the new reference state, $\Delta h^{po}_{(0\,K)}$:

$$h^{po} = h^{po}_{(refprop)} + \Delta h^{po}_{(0\,K)} \tag{3.3}$$

$$h^{po} = h^{o}_{(refprop)} - h^{p}_{(refprop)} \tag{3.4}$$

The enthalpy with respect to new reference state is further expressed as:

$$\Delta h^{po} = \Delta h^{o}_{(0\ K)} - \Delta h^{p}_{(0\ K)} \tag{3.5}$$

where, Δh^p, and Δh^o are the enthalpies of *para* and *ortho* at the new reference state (0 K), respectively. The values of Δh^p, and Δh^o at 0 K are -256.06 kJ kg^{-1} and 444.695 kJ kg^{-1}, respectively [16]. $h^o_{(refprop)}$ and $h^p_{(refprop)}$ are the enthalpies of *para* and *ortho* hydrogen defined in NIST REFPROP. To calculate the thermodynamic properties of hydrogen, the correlations reported in the reference [17, 22] are used.

$$\rho_g = \left(\frac{f_{oh2}}{\rho_{oh2}} + \frac{f_{ph2}}{\rho_{ph2}}\right)^{-1} \tag{3.6}$$

$$C_p = f_{oh2}C_p^{oh2} + f_{ph2}C_p^{ph2} \tag{3.7}$$

$$k = f_{oh2}k_{nh2} + f_{ph2}k_{ph2} \tag{3.8}$$

$$\mu = f_{oh2}\mu_{nh2} + f_{ph2}\mu_{ph2} \tag{3.9}$$

$$\gamma = f_{oh2}\gamma_{nh2} + f_{ph2}\gamma_{ph2} \tag{3.10}$$

$$H = f_{oh2}h_{oh2} + f_{ph2}h_{ph2} \tag{3.11}$$

where, ρ_g, C_p, k, μ, H and γ are the density, specific heat capacity, thermal conductivity, viscosity, enthalpy and ratio of specific heat capacities at constant pressure and constant volume of the hydrogen gas, respectively. In the correlation, nh_2, ph_2 and oh_2 represents *normal* hydrogen, *para* hydrogen and *ortho* hydrogen, respectively. The term f represent the mass fraction. The material properties of MOF-5 and geometry details of the2.5 L tank are discussed in the previous chapter (chapter 2). Initial temperature and pressure are set to 80 K and 0.1 MPa, respectively. Four inlet temperatures for hydrogen are considered: 35, 50, 77 and 100 K for investigating the effect of *para-ortho* conversion. An adiabatic insulated tank is assumed for the MOF-5 storage system and the estimated heat leakage rate is calculated and applied in the form of heat flux at the outer wall of the tank. For calculating the heat leakage of the storage tank, we use the data of daily

evaporation rate (%) of liquid oxygen filled tank. The mass flow rates are set to +15 and -15 and 0 SLPM, respectively for charging, discharging and dormancy of the simulation. To evaluate the maximum possible effect of an instantaneous *para* to *ortho* adsorbed hydrogen conversion on the total heat and performance of the system, the temperature and pressure data at the centre point T_4 of tank is monitored when hydrogen gas having temperatures: 35, 50, 77 and 100 K is charged into the tank maintained at 80 K. When 100 K equilibrium hydrogen, which has a composition of ~40 % *para* hydrogen, is charged into the tank, a part of the *para* fraction absorbs the heat energy from the tank and gets converted to the *ortho* fraction. This leads to a drop in the temperature at T_4 and, at the end of charging, it is 131 K, which is 10 K lower than that it would be if no conversion were considered; see Figure 3.6. When hydrogen gas having temperatures lower than 100 K is charged, temperature evolution inside the system due to adsorption and pressure work is less and the resulting fraction of *para* hydrogen converted to *ortho* hydrogen becomes less important. Furthermore, it is observed from Figure 3.6 that the effect due to the conversion is higher at 100 K inlet temperature than 35 K. Initially, the composition of *para* and *ortho* hydrogen at T_4 is ~49 and ~51 %, respectively which is the composition at 80 K. At the end of charging stage, the temperature reaches 142 K for 100 K inlet temperature and 118 K for 35 K, if no conversion heat is considered. Now, as the conversion happens, the *ortho* fraction increases from ~51 to ~67 % for 100 K inlet temperature and to 65 % for 35 K. Thus a maximum possible fraction of *para* hydrogen present at 100 K hydrogen is converted into *ortho* fraction hydrogen due to the higher temperature evolution inside the system compared to that converted at 35 K. It also is possible

that the sensible heat of *para* hydrogen influences the temperature reduction because the effect by sensible heat is more predominant at 100 K than at 35 K [21].

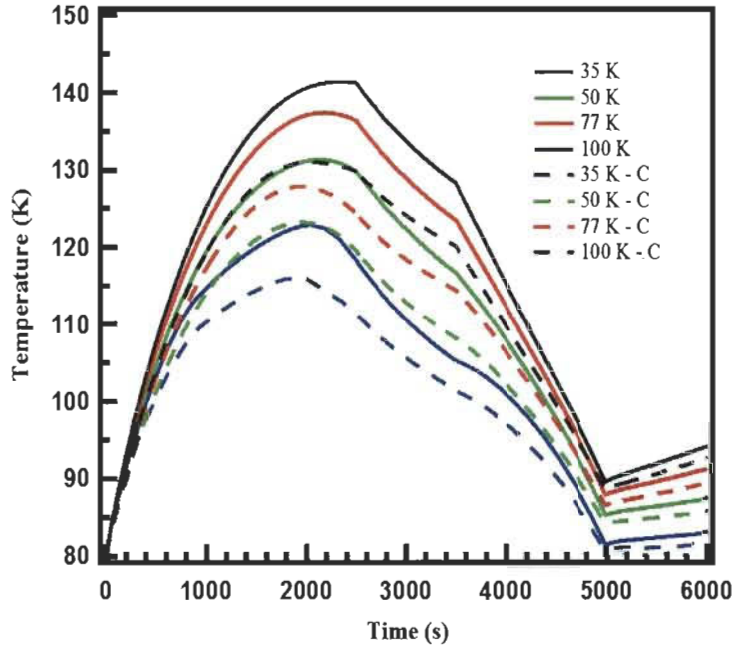

Figure 3.6: Temperature profiles at T_4 in the tank with (dashed lines) and without (solid lines) taking into account the *para-ortho* conversion at 4 inlet temperatures.

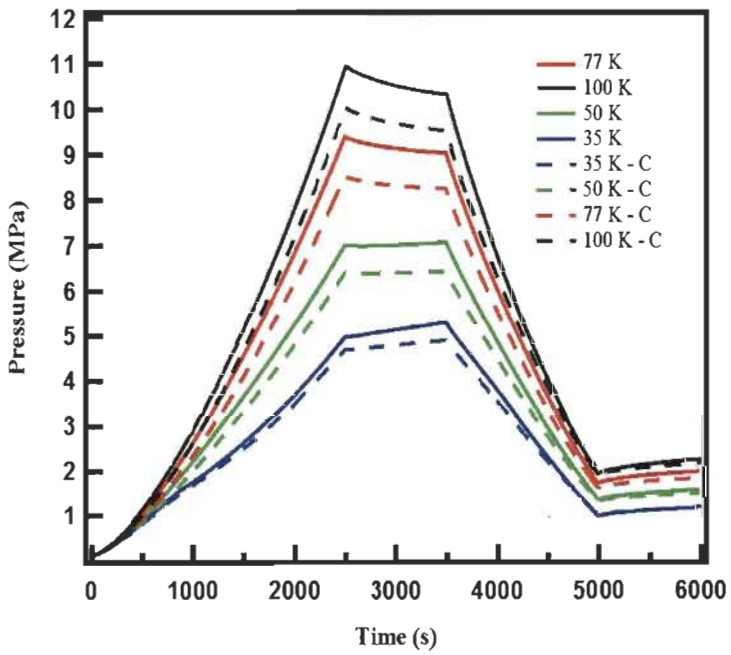

Figure 3.7: Pressure profiles at T_4 in the tank with (dashed lines) and without (solid lines) taking into account the *para-ortho* conversion at 4 inlet temperatures.

These results suggest that the temperature reduction due to *para* to *ortho* conversion helps to charge more hydrogen into the system during the charging stage. The evolution of pressure in the system at four inlet temperatures is given in the Figure 3.7. It can be seen that the pressure in the tank drops when *para-ortho* conversion is taken into account, which is due to decreased tank temperature. In general, the pressure shows similar behavior for all inlet temperatures as shown in Figure 3.7.

To account for the observed temperature evolution in the tank, we considered the contributions of adsorption heat, heat due to pressure-volume work and the conversion heat separately in the model and performed the simulation when 77 K hydrogen is charged into the tank. The point T_4 in the tank is used to monitor temperature and heat. In Figures 3.8 and 3.9, the heats and the temperature evolution at the point T_4 during the charging are shown.

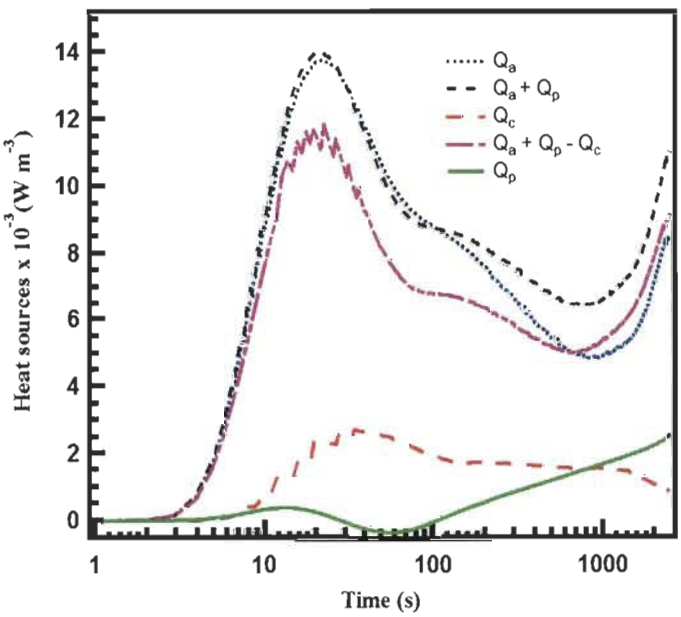

Figure 3.8: Heat sources profiles in the system at the point T_4.

First, when only the pressure work is considered, the temperature of the system initially decreased to 56 K at about 1000 s from the initial 80 K. After this, the

temperature rises to nearly 80 K as the filling progresses. The initial decrease of temperature is due to the positive Joule-Thompson (J-T) coefficient of hydrogen and hydrogen desorption from the MOF-5 bed. When charging is performed at temperatures below hydrogen's inversion temperature (T_i = 193 K), the gas undergoes expansion into the tank and the positive J-T effect leads to decreased temperature. While the charging is in progress, the temperature of the tank increases owing to the heat produced by pressure work. When the heat due to adsorption alone is considered, temperature at T_4 increases to 127 K, due to endothermic adsorption process. If both the adsorption heat and pressure work heat are considered, the resulting temperature at T_4 increases to 135 K from 80 K. If conversion heat is considered along with the other forms of heat, the final temperature decreases by 10 K.

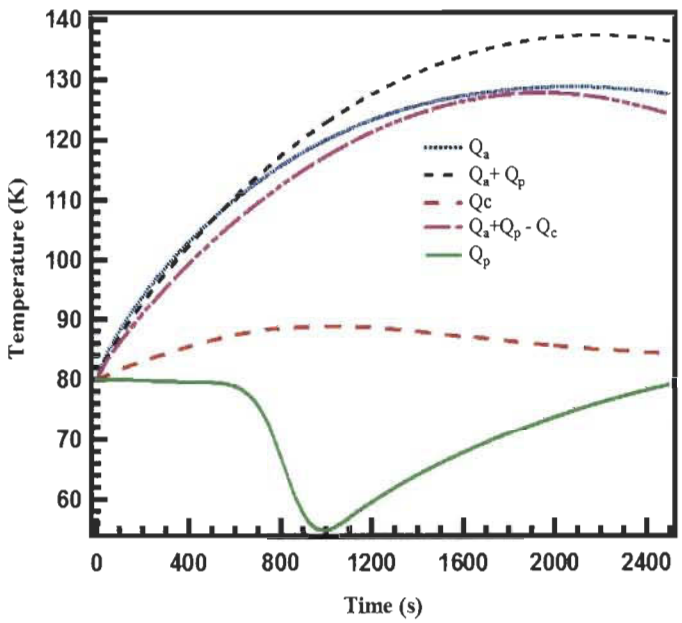

Figure 3.9: Temperature profiles at the point T_4 when different heat source terms are considered separately.

Figure 3.10 shows the effect of *para-ortho* conversion on the storage system capacity; we find that the gas phase mass (m_g) is larger in the storage system

without conversion than the gas phase mass (m_g-C) of the system with conversion. In other words, the adsorbed phase (m_a) has lower mass of hydrogen without conversion than has with conversion (m_a-C). The total mass of hydrogen (m_t) is the same in the both cases because of the same mass flow rate and filling time. In summary, due to the lowering of the system temperature by *para-ortho* conversion, the adsorbed phase mass increases and the gas phase mass decreases in the storage system which help to fill more hydrogen gas into the system at the storage conditions than that can be filled when no conversion takes place.

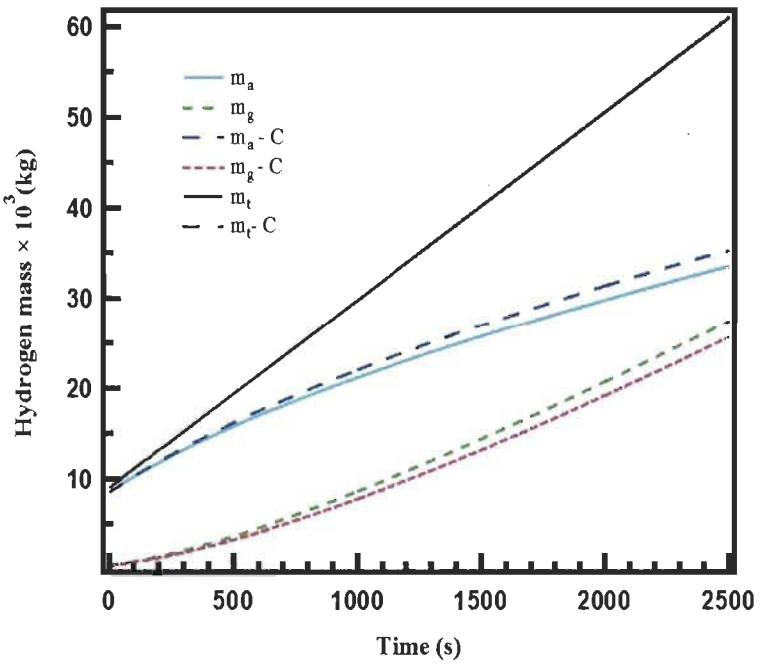

Figure 3.10: Hydrogen mass balance in the system with and without conversion.

3.4 Conclusion

In this chapter, the effects of flowthrough cooling and *para-ortho* conversion on the performance of a MOF-5 filled 2.5 L cryo-adsorptive hydrogen storage system is investigated. The result from the "effect of flowthrough cooling on the performance of the storage system" shows that the advantage of the flowthrough cooling technique is not only cooling the storage system but comes also from the

fact that the process enhances the storage capacity. The comparison of average bed temperature profiles between the flowthrough cooling and LN_2 cooling scenarios indicates that faster flow rate is required for flowthrough cooling to be efficient for heat removal. In the case of the *para-ortho* conversion effect on the storage system performance, the results revealed that the endothermic conversion reduces the system temperature; this is supported by the analysis of the various heat sources and the corresponding temperatures.

References

[1] Hardy B, Corgnale C, Chahine R, Richard M.-A, Garrison S, Tamburello D, Cossement D, Anton D. Modeling of adsorbent based hydrogen storage systems. Int J Hydrogen Energy 2012; 37:5691-5705.

[2] Liu D, Purewal JJ, Yang J, Sudik A, Maurer S, Mueller U, Ni J, Siegel DJ. MOF-5 Composites exhibiting improved thermal conductivity. Int J Hydrogen energy 2012; 37:6109-6117.

[3] Purewal J, Liu D, Sudik A, Veenstra M, Yang J, Maurer S, Müller U, Siegel DJ. Improved hydrogen storage and thermal conductivity in high-density MOF-5 composites. J Phys Chem C 2012; 116:20199-20212.

[4] Chakraborty A, Kumar S. Thermal management and desorption modeling of a cryo-adsorbent hydrogen storage system. Int J Hydrogen Energy 2013; 38:3973-3986.

[5] Ahluwalia RK, Peng JK. Automotive hydrogen storage system using cryo-adsorption on activated carbon. Int J Hydrogen Energy 2009; 34:5476-5487.

[6] Schuetz W, Michl F, Polifke W, Paggiaro R. Storage system for storing a medium and method for loading a storage system with a storage medium

and emptying the same therefrom. US patent. US 2008/0020250 A1, Jan. 24, 2008.

[7] Paggiaro R, Michl F, Bénard P, Polifke W. Cryo-adsorptive hydrogen storage on activated carbon. II: Investigation of the thermal effects during filling at cryogenic temperatures. Int J Hydrogen Energy 2010; 35:648-659.

[8] Corgnale C, Hardy B, Chahine R, Cossement D, Tamburello D, Anton D. Simulation of hydrogen adsorption systems adopting the flowthrough cooling concept. Int J Hydrogen Energy 2014; 39:17083-17091.

[9] Air Liquide; 2006. private communication

[10] Kumar VS, Raghunathan K, Kumar SA. Lumped-parameter model for cryo-adsorber hydrogen storage tank. Int J Hydrogen Energy 2009; 34:5466-545.

[11] Ahluwalia RK, Hua TQ, Peng JK, Papadias D, Kumar R. System level analysis of hydrogen storage options. Presentation, DOE Hydrogen Program Review; May 9-13, 2011, Washington DC, USA.

[12] Weitzel DH, Loebenstein WV, Draper JW, Park OE. *Ortho-Para* Catalysis in liquid-hydrogen Production. J Res Nat Bur Stand 1958; 60:221-227.

[13] Buntkowsky G, Walaszek B, Adamczyk A, Xu Y, Limbach HH, Chaudret B. Mechanism of nuclear spin initiated *para*-H_2 to *ortho*-H_2 Conversion. Phys Chem Chem Phys 2006; 8:1929-1935.

[14] Minaev BF, Agren H. Spin Catalysis of *ortho-para* hydrogen conversion. J Phys Chem 1995; 99: 8936-8940.

[15] Milenko YY, Sibileva RM. Natural *ortho-para* conversion rate in liquid and gaseous hydrogen. J Low Temp Phys 1997; 107:77-92.

[16] Petitpas G, Aceves SM, Matthews MJ, Smith JR. *Para*-H_2 to *ortho*-H_2 conversion in a full-scale automotive cryogenic pressurized hydrogen storage up to 345 bar. Int J Hydrogen Energy 2014; 39:6533-6547.

[17] Peng JK, Ahluwalia RK, Enhanced dormancy due to *para*-to-*ortho* hydrogen conversion in insulated cryogenic pressure vessels for automotive applications, Int J Hydrogen Energy 2013; 38:13664-13672.

[18] FitzGerald SA, Hopkins J, Burkholder B, Friedman M. Quantum dynamics of adsorbed normal- and *para*-H_2, HD, and D_2 in the microporous framework MOF-74 analyzed using infrared spectroscopy. Phys Rev B 2010; 81: 104305-104309.

[19] FitzGerald SA, Allen K, Landerman P, Hopkins J, Matters J, Myers R, Rowsell JLC. Quantum dynamics of adsorbed H_2 in the microporous framework MOF-5 analyzed using diffuse reflectance infrared spectroscopy. Phys Rev B 2008; 77:224301-224309.

[20] Rossington DR, Capozzl VF. *Para*-to-*Ortho* H_2 Conversion on Gd, Y, Gd_2O_3, and Y_2O_3. J Am Ceram Soc 1974; 57:474-477.

[21] James Patrick Meagher. Modeling of hydrogen liquefiers with kinetic conversion of *ortho* to *para* hydrogen in plate-fin heat exchangers. Thesis, University at Buffalo; 2009, USA.

[22] Ubaid S, Xiao J, Zacharia R, Chahine R, Bénard P. Effect of *para-ortho* conversion on hydrogen storage system performance. Int J Hydrogen Energy 2014; 39:11651-11660.

Chapter 4

Multiphysics performance of a bulk cryo-adsorptive hydrogen storage reservoir filled with MOF-5

In this chapter, the multiphysics performance such as the thermal and storage performances of a bulk (20 m^3) cryo-adsorptive hydrogen reservoir filled with MOF-5 is presented. A 2D-axisymmetric CFD model is used to conduct this study. The details of the general CFD model and its validation, and the implementation of flowthrough cooling and *para-ortho* conversion in the model are discussed in the previous chapters (Chapter 2 and 3).

Figure 4.1: Storage reservoir and its 2d-axisysmmetrical representation.

We used the geometric parameters of Celine 3 type bulk storage tank available from the reference [1] for developing the geometric model. The inner and outer radii at the entrance and middle of the 20 m^3 tank are 0.04 m, 0.046 m, 0.907 m and 0.918 m, respectively. The internal and external heights of the tank are 8.58

m and 8.98 m, respectively. The maximum allowed pressure of the bulk tank is assumed to be 4 MPa. The Celine 3 type storage reservoir and the 2d-axisysmmetrical representation used in the simulations are shown in Figure 4.1. In the simulation, an adiabatic insulated tank is assumed and the estimated heat leakage rate is calculated and applied in the form of a heat flux (0.8287 Wm^{-2}) at the outer wall of the tank. For calculating the heat leakage of the storage tank, we use the data of daily evaporation rate (%) of liquid oxygen filled tank. The initial pressure, initial temperature and the mass flowrate are set to 0.1 MPa, 300 K and 10000 SLPM, respectively. In the beginning, we simulated the effects of charge-discharge cycles to reduce the tank temperature from 300 K to 77 K. Once the tank's temperature is brought down to 77 K, the filling of hydrogen is performed until the maximum pressure capacity is reached. Then, the simulation is focused to achieve maximum hydrogen storage capacity in the tank using flowthrough cooling technique. In the next step, we investigated the effect of flowthrough cooling together with instantaneous *para-ortho* hydrogen conversion on the thermal and storage capacity of the tank. A parametric study of the effects of mass flowrate on cooling time reduction during the flowthrough stage is also investigated. In the final part, the hydrogen loss rate during the 10 days dormancy stage is estimated.

4.1 Thermal and storage performance of the bulk tank

At first, the simulation is performed for reducing the tank temperature to 80 K from 300 K. To this end, hydrogen gas pre-cooled at 77 K is charged into the tank until 4 MPa pressure is reached, and then 3 MPa of hydrogen is released from the reservoir to the ambient. In order to implement the discharging of the gas from the reservoir, the outflow velocity boundary condition (1.5 m s^{-1}) is applied at the

outlet of the tank. Even though the model can accommodate high outflow gas velocity value as a boundary condition at the outlet of the tank, we used low outflow gas velocity value (1.5 m s^{-1}). This is because the convergence during the simulation is complex when high value is taken into account; therefore we used low value to get smooth convergence during the simulation. The adjustment of the relative tolerance in the time dependent solver may be helpful to solve this convergence issue. The charging-discharging cycle is repeated until the tank's temperature is reduced to 77 K.

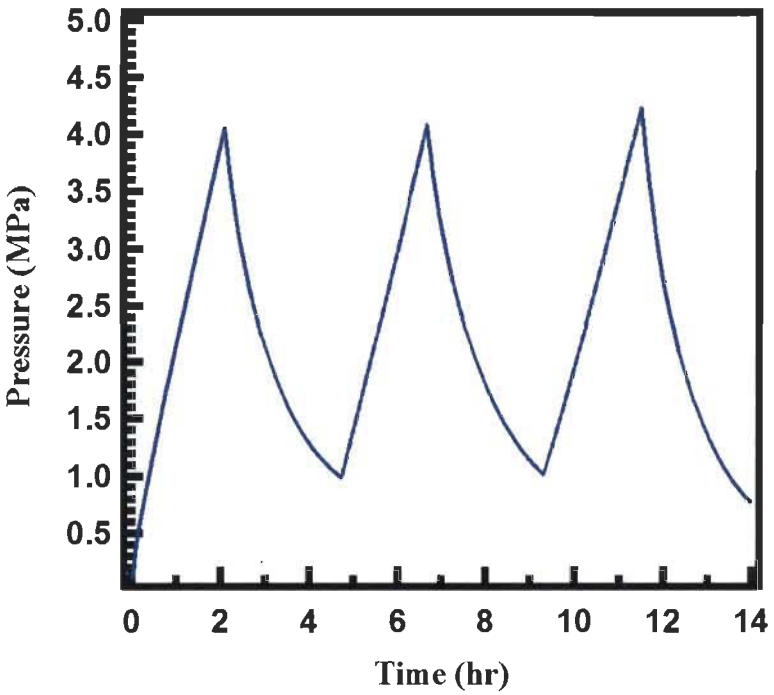

Figure 4.2: Pressure of the tank during the charging/discharging cycles.

The result (Figure 4.2) shows that, at the end of the first filling stage, the temperature of the tank's lower half section is increased due to the adsorption and pressure work heat energy (Figure 4.3). The maximum temperature is observed at the bottom of the tank followed by middle and top parts of the system (Figure 4.3). The temperatures at the bottom, middle and top shows 341 K, 321 K and 77 K, respectively.

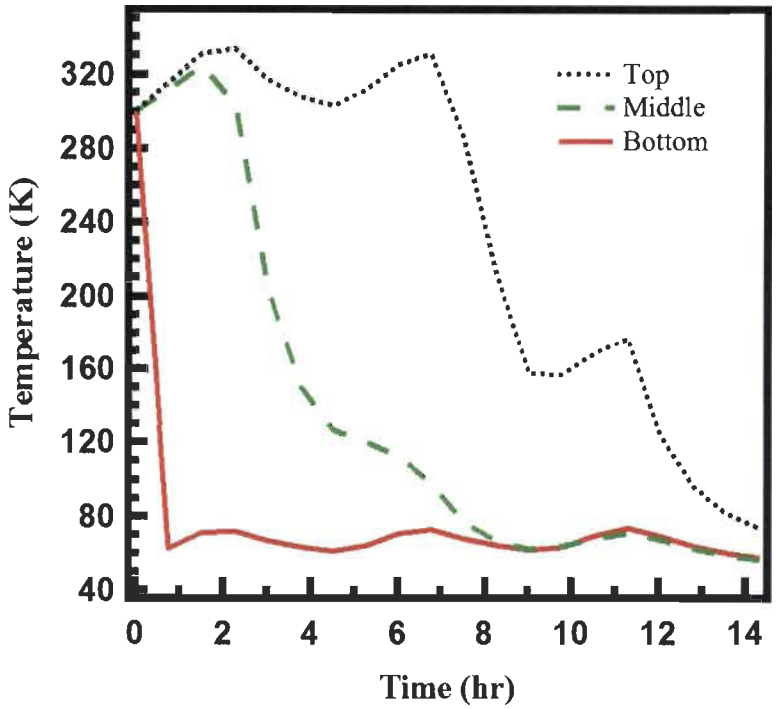

Figure 4.3: Temperature of the tank during the charging/discharging cycles.

During the discharging stage, convective heat transfer (heat energy inside the system is transported out of the reservoir with the outflow of hydrogen) and desorption of hydrogen are takes place, subsequently the temperature at the bottom, middle and top parts of the tank is reduced to 300 K, 122 K and 60 K, respectively. Once the tank pressure is reduced to 1 MPa from 4 MPa during the discharging (Figure 4.2), a second charging-discharging cycle is carried out. The resulting temperature history shows that the temperature is increased to 73 K from 60 K at the top of the tank (Figure 4.3), which is due to the liberated heat energy during the charging time. This increased heat energy is transferred to the middle of the tank, which leads to desorption of hydrogen from the middle point and results in further temperature reduction to 103 K from 122 K at the middle point. Due to the decreased temperature in the middle section, adsorption heat is released which is then transferred to the bottom part of the tank. This results in a temperature rise to 321 K from 300 K in the bottom section. During the third

charging-discharging cycle, the temperature at the top, middle and bottom points are reduced to 60 K, 65 K and 145 K.

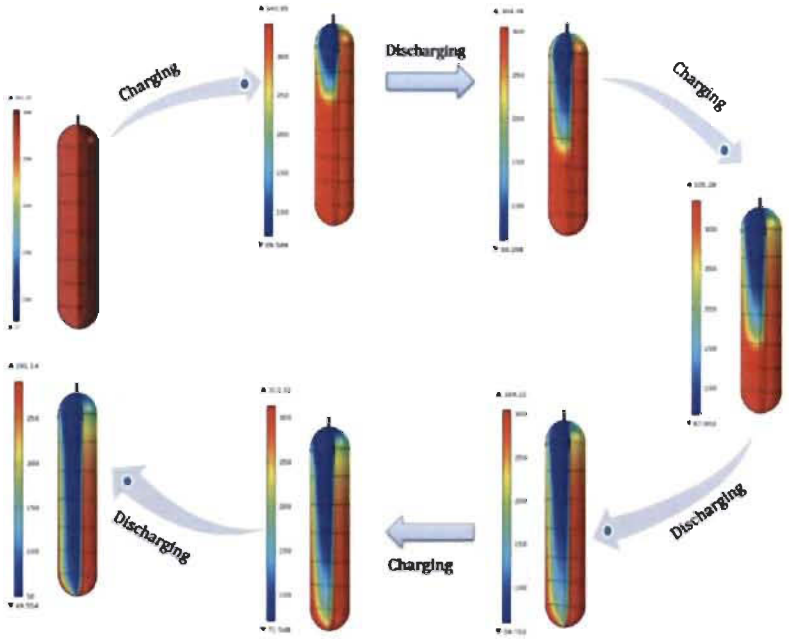

Figure 4.4: Pictorial representation of tank's temperature profile during the charging/discharging cycles.

Figure 4.4 shows the pictorial representation of the tank's temperature variations during the three charging-discharging cycles. At 0 second, the temperature of the whole system is 300 K, which is represented by red color. The red color at the top of the tank has disappeared when the first filling stage is finished. At the top part, the red color is replaced by blue color, which means the heating effect at that section is diminished due to the influence of incoming cold hydrogen. After releasing 3 MPa hydrogen from the reservoir, the blue color extends from the top to the middle of the tank, which indicates that the tank's temperature is further reduced due to the convective heat transfer during the hydrogen discharging. At the end of the third charging-discharging cycle, the red color has completely disappeared and is replaced by blue color, which indicates that the average temperature of the whole bed in the tank is reduced to 80 K from 300 K.

Once the average temperature of the system has reached to 80 K, this temperature becomes the initial condition of the tank and the filling is carried out using 77 K hydrogen till a pressure of 4 MPa is reached (the initial pressure was set to 0.1 MPa). After reaching the maximum capacity of the tank, the simulation is then focussed to achieve the overall maximum storage capacity of the tank by decreasing the tank temperature. In order to achieve this, the heat energy due to the adsorption and pressure work must be again removed.

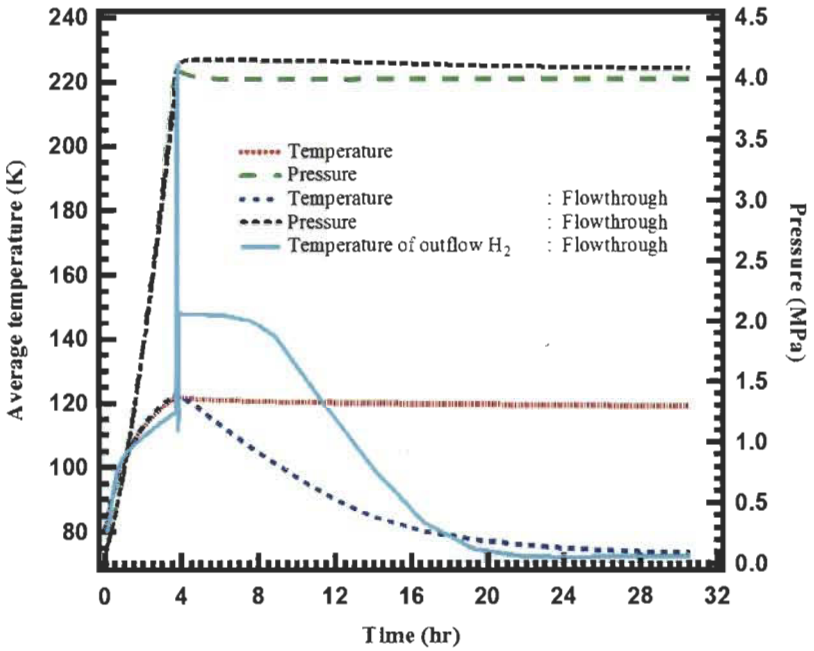

Figure 4.5: Average bed temperature, pressure and outlet temperature during the whole charging/flowthrough stage.

Even though a charge-discharge cycle can remove the heat energy and enhance the storage capacity after several cycles, the model implemented flowthrough cooling, there cooling and charging takes place simultaneously. In order to accommodate the flowthrough cooling in the simulation, at the end of the charging stage, a pressure boundary condition is applied to outlet of the tank and the value of pressure is set to 4 MPa. The results from the simulation shows that the

pressure and average bed temperature of the tank reach 4 MPa and ~125 K, respectively (Figure 4.5) at the end of the charging stage. During the flowthrough, the tank pressure remains stable due to the continuous filling of hydrogen whereas the temperature decreases to 77 K.

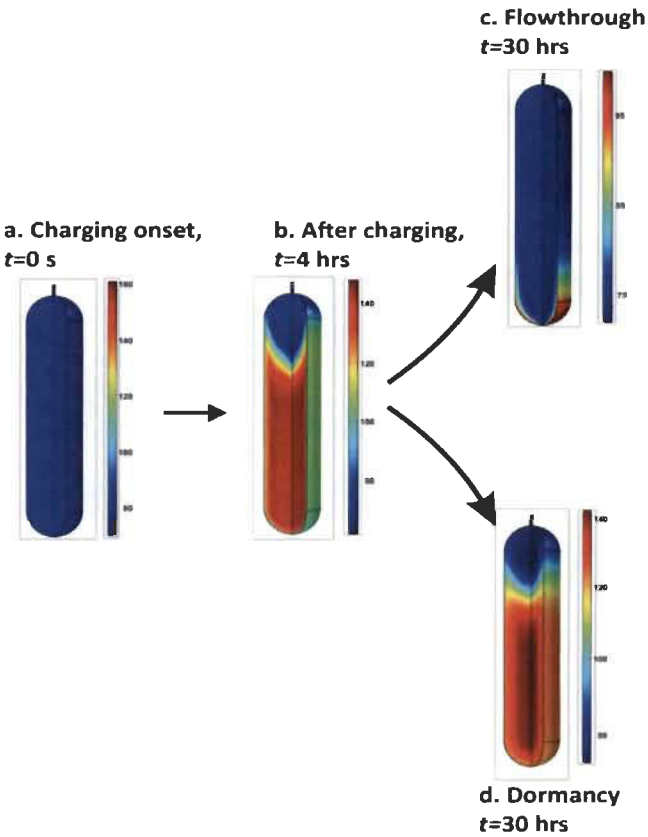

Figure 4.6: Evolution of the temperature inside the 20 m^3 bulk storage tank containing MOF-5. (a) at the onset of charging, (b) after charging hydrogen at a rate of 10000 SLPM, (c) during flowthrough for 30 hours and (d) during idling for 30 hours (without flowthrough).

In Figure 4.6, snapshots of temperature gradients inside the tank during the flowthrough heat removal is compared with what would happen in the absence of flowthrough. At the onset of charging (Figure 4.6, a), the system is equilibrated at 80 K with 0.1 MPa hydrogen present. As hydrogen is charged into the system, the average temperature rises to ~125 K. Until the end of charging (Figure 4.6, b, 4

hr), adsorption enthalpy/pressure work enthalpy enhances the temperature in the bed and the heat front (red hue) is conductively transported to the centre of the tank. During the flowthrough (Figure 4.6, c), the heat is transported out of the vessel by the hydrogen leaving the vessel, indicated by the cold front (blue hue) advancing down. It is noted that the temperature at the top of the tank reduces to less than liquid nitrogen temperature. This is because of the cooling effects contributed by the positive Joule-Thomson effect as hydrogen gas expands while it enters the tank and the cooling effect produced by partial desorption of hydrogen that was initially adsorbed. A tentative scenario without the flowthrough cooling is active is shown in Figure 4.6, d. Here, after 4 hours of hydrogen charging, the system is allowed to be in dormancy for 30 hours. The poor thermal conduction of the MOF-5 bed will cause the system to remain hot at ~125 K as indicated by the red hue in Figure 4.6, d.

In Figure 4.7, the effect of flowthrough cooling on the system storage capacity obtained using mass analysis is shown. The gas-phase mass increases linearly during the charging stage, however the rate decreases during the flowthrough as addition of hydrogen is compensated by simultaneous outflow. Adsorbed phase mass increases throughout the charging and flowthrough regimes. The calculated total mass (m_t) of hydrogen when flowthrough is operational is 460 kg (in 30 hr, Figure 4.7, blue). The total hydrogen storage at the end of the charging stage is ~255 kg, which is increased to 460 kg when the ~30 hr flowthrough cooling regime is finished. When there is no flowthrough cooling in MOF-5 reservoir, the heat of adsorption and the heat due to pressure work raise the temperature inside the tank to ~125 K (Figure 4.6). The maximum amount of hydrogen stored is ~255

kg as the storage pressure reaches a maximum of 4 MPa when no further storage is possible (Figure 4.7, red).

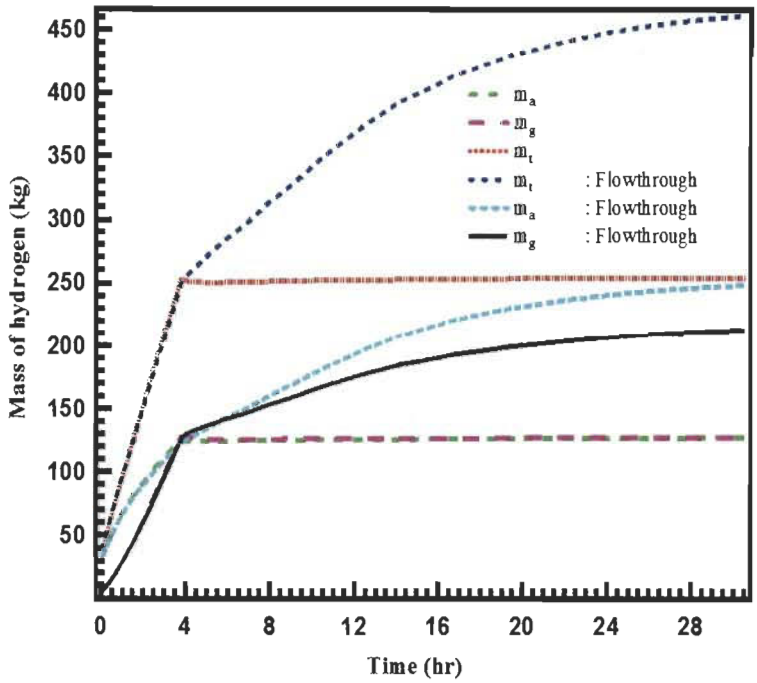

Figure 4.7: Stored mass of hydrogen during the whole charging/flowthrough stage.

In the flowthrough cooling system, within ~5.5 hours, the storage system stored ~275 kg of hydrogen, which is equal to net storage amount in a cryo-compressed tank with hydrogen maintained at 77 K and 4 MPa. Above 5.5 hours of flowthrough cooling, a cryo-sorptive MOF-5 tank stores significantly more hydrogen than a cryo-compressed storage tank maintained at 77 K and 4 MPa. The time taken for cooling the tank from ~125 K to 80 K is 13.1 hr, in the meantime 707 kg of hydrogen is used to diminish the effect of 45 K temperature swing. Out of this 707 kg of hydrogen, 157 kg is stored in the tank and the remaining 550 kg of hydrogen is eventually recovered. We assumed here that the excess hydrogen is vented and that the charging is continued using fresh cold hydrogen instead of recirculating it after passing through any external heat exchangers. Even though we assumed here

that the excess hydrogen is not re-circulated; the model is further used to study the temperature of the exhaust hydrogen gas during the flowthrough cooling stage. The estimation of exhaust hydrogen temperature profile is useful for calculating the required energy for cooling the exhaust hydrogen when the re-circulation is taken into account. The point, which is located at the outlet of the tank is selected for monitoring the temperature of the outgoing gas. The result (Figure 4.5, cyan colour) shows that the temperature rises during the charging time and decreases during the flowthrough stage, thus, the required energy for cooling the exhaust hydrogen can be reduced when the flowthrough cooling is on progresses.

4.2 Effect of flowthrough cooling together with *para-ortho* conversion on the storage tank performance

In chapter 2, we studied the maximum possible effect of an instantaneous *para* to *ortho* conversion on the total heat in the 2.5 L storage system. There, we reported that the endothermic *para* to *ortho* conversion in the equilibrium hydrogen reduces the system storage temperature. Here, the model is applied to a 20 m^3 storage reservoir and simulation is performed for understanding the combined heat removal effect of *para* to *ortho* conversion and flowthrough cooling technique. To perform the simulation, hydrogen gas at 77 K is charged in the tank until 4 MPa is reached. At the end of the charging stage, the system is set to flowthrough. In order to implement the *para-ortho* conversion effect in the storage system, the heat source term due to *para-ortho* conversion is included in the energy balance equation of the adsorptive system model. Also, we assumed here that equilibrium hydrogen at 77 K consists of ~49 of *ortho* hydrogen and ~51 %

of *para* hydrogen is used for filling the storage tank. Figure 4.8 compares the average bed temperature and pressure of the tank for flowthrough cooling together with the *para-ortho* conversion and flowthrough cooling alone scenarios. It shows that if no conversion heat is considered, the allowable pressure of the tank 4 MPa reaches in ~4 hr. If the *para-ortho* conversion is taken into account, the maximum pressure reaches in 4.17 hr.

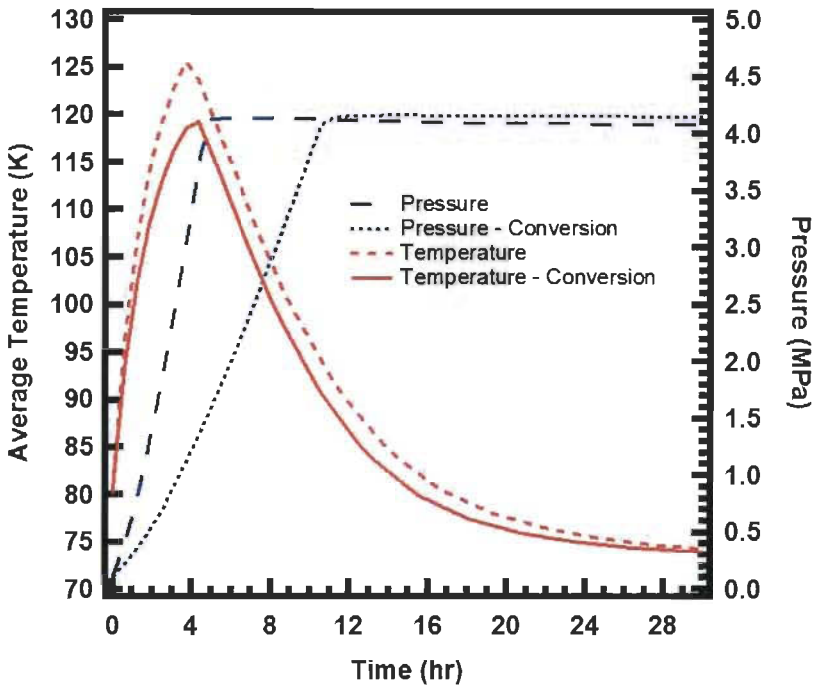

Figure 4.8: Average temperature and pressure in the system when *para-ortho* conversion together with flowthrough cooling and flowthrough cooling alone scenario.

The average temperature of the tank at the end of the charging stage is ~119 K when *para-ortho* conversion takes place, which is lower compared to the system that has no *para-ortho* conversion, there the final average temperature at the end of the charging stage is 125 K. During the flowthrough stage, the generated heat is convectively transferred out of the reservoir with outflow hydrogen. If *para-ortho* conversion and flowthrough cooling are considered together, temperature

reduction due to conversion helps to charge more hydrogen into the system during the charging stage and the storage capacity can be accelerated during the flowthrough cooling stage.

4.3 Effect of the mass flow rate on the cooling time reduction during the flowthrough cooling stage

To understand the effect of the mass flow rate on the cooling time reduction during the flowthrough cooling stage, 77 K pre-cooled hydrogen is charged at the rate of 10000 SLPM into the storage system initially equilibrated at 80 K and 0.1 MPa until the pressure reaches 4 MPa. At the end of the charging stage, the model is used to test the effects of different flowthrough-mass flow rates: 10000 SLPM, 15000 SLPM and 20000 SLPM on heat removal.

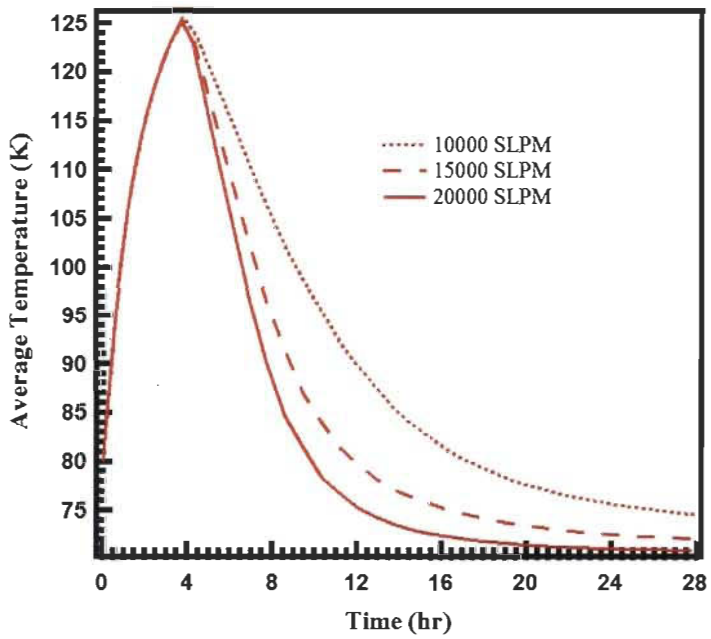

Figure 4.9: Effect of the mass flow rate on the temperature reduction during the flowthrough stage.

Figure 4.9 compares the average bed temperatures of the system when different mass flow rates are considered. The result shows that the time taken for cooling

the storage system from ~125 K to 80 K is 6 hr when 20000 SLPM flowrate is considered, which is less compared to 8 hr for 15000 SLPM and 13 hr for 10000 SLPM. Higher flow rate enhances the velocity of the hydrogen gas inside the tank during the flowthrough cooling stage; therefore it results in faster heat removal from the system compared to the lower flow rates, such as 15000 SLPM and 10000 SLPM.

4.4 Performance of the bulk tank during the dormancy stage

It is important to understand the hydrogen loss rate of large storage reservoir during the long term dormancy stage. The hydrogen loss during the dormancy stage depends highly on the tank insulation. If the tank is not well insulated, the possible heat leak of the tank causes the heat increment in the storage system. This leads to a buildup of excess pressure inside the tank, which need to be removed for complying with safety regulations. Here, the model tries to simulate the thermal and storage performance of the MOF-5 filled 20 m^3 bulk tank during the 10 days dormancy stage. An adiabatic insulated tank is assumed and the estimated heat leakage rate is applied in the form of heat flux (0. 8287 W m^{-2}) at the outer wall of the tank. In order to understand the storage and thermal performance of the tank during the dormancy stage, the 80 K maintained reservoir is charged with 77 K hydrogen to reach maximum storage pressure, 4 MPa. At the end of the charging stage, the tank is cooled down using the flowthrough cooling method. Once the system reaches to 80 K, the inlet is closed, we set pressure boundary condition (4 MPa) at the inlet of the tank, and keep the tank for 10 days. The result (Figure 4.10) shows that ~24 kilogram of hydrogen is lost during the dormancy stage of 10 days. For the storage duration between 0.8 and 1 day, around ~4

kilogram of hydrogen should be exhausted to maintain the tank pressure within the allowed maximum pressure of 4 MPa.

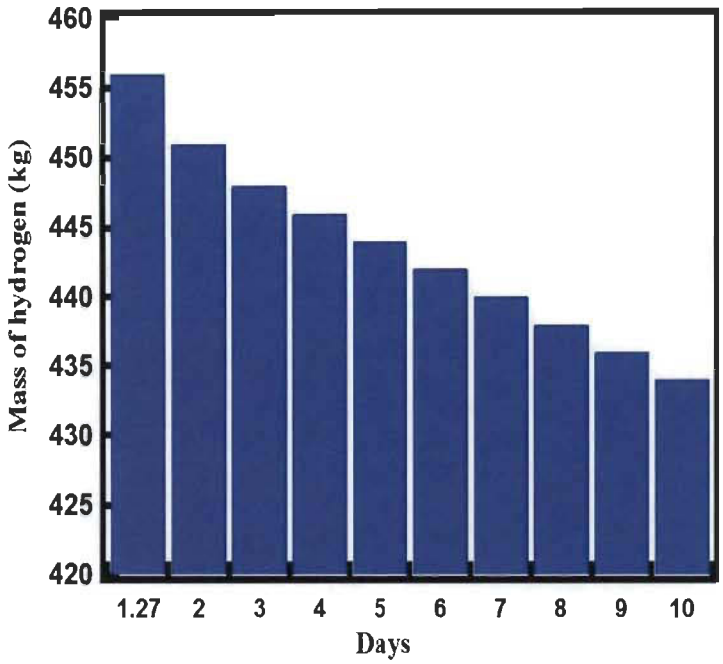

Figure 4.10: Hydrogen loss during the dormancy stage.

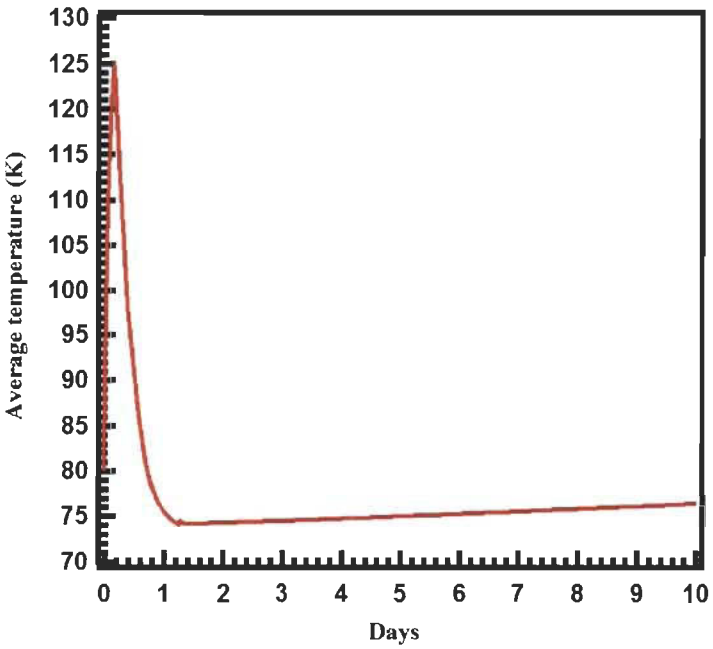

Figure 4.11: Temperature history during the 10 days dormancy stage.

For the storage from day 1 to 10, ~2.4 kilogram of hydrogen should be vented per day for avoiding the excess pressure inside the tank. Between 0.8 and 1 day, ~2 kg

of extra hydrogen is required to be vented than that required to be vented on following days. This may be due to the sudden temperature rise in the tank immediately after the flowthrough cooling is stopped. The temperature profile in the Figure 4.11 shows that temperature rises during the charging stage and it starts to decrease when the flow through cooling is in progress. During the dormancy stage, temperature slightly increases due to the heat transfer from the ambient to the tank.

4.5 Conclusion

To conclude this chapter, the CFD model is used to study the multiphysics performance of a 20 m^3 storage reservoir filled with MOF-5. In this study, at first, we used charge-discharge cycles to reduce the tank temperature from 300 K to 80 K. The result shows that the temperature of the system is reduced to 80 K after three charging-discharging cycles. Once the temperature of the whole tank reaches to 80 K, the tank filled to 4 MPa pressure and then the outlet of the tank is opened for flowthrough cooling, which is for to diminishing the temperature swing and increase the storage capacity. By performing flowthrough cooling for ~30 hrs, the average temperature of the adsorbent bed can be brought down to 77 K; this results in a hydrogen storage capacity of 460 kg at the tank maximum pressure of 4 MPa, which is even higher than the storage capacity of a cryo-compressed hydrogen tank equilibrated at 77 K and 4 MPa (275 kg).The temperature of the exhaust hydrogen gas during the flowthrough cooling time is simulated; the result shows that the required energy for cooling the exhaust hydrogen which is for further use can be reduced when the flowthrough cooling is on progresses. The simulation is then used to study the effect of *para-ortho* conversion together with flowthrough cooling on temperature reduction in the

tank. We found that instantaneous *para-ortho* conversion reduced the system temperature during the charging stage and the temperature reduction is accelerated during flowthrough stage. Further, the effect of mass flow rate on heat removal from the system during the flowthrough stage has been evaluated. The observed result reveals that a high mass flow rate of 20000 SLPM accelerates the heat removal from the storage tank and cooling of the tank compared to low mass flow rates such as 10000 SLPM and 15000 SLPM. Finally, the hydrogen mass loss during the 10 days dormancy period is calculated. It is necessary to vent out 24 kg of hydrogen over 10 days to comply with the maximum pressure rating of the tank.

Reference

[1]. http://www.cryolor.com/en/notre-offre/cryogenic-storage-vessels/tanks-for-lin-lox-and-lar.html(accessed Feb.10, 2014).

Chapter 5

Summary of the thesis and future work

We studied the problem of thermal management due to the poor thermal conductivity of MOF-5 and investigated the multiphysics performance of a cryo-adsorptive hydrogen storage reservoir filled with MOF-5. In order to solve the problem of thermal management due to the poor thermal conductivity of MOF-5, we used flowthrough cooling and charge-discharge cycles methods. The results shows that these methods accelerated the heat removal rate from the system without affecting the system's storage capacity. We also studied the effect of *para-ortho* hydrogen conversion on the temperature reduction in the storage system. The result shows that instantaneous *para-ortho* conversion in the storage system reduced the temperature during the charging time. For a better understanding of the overview of the thesis, chapter wise summary is included in this section. In addition to this, the recommendations and suggestions for future research are included at the end of this section.

5.1 Adsorptive storage system model development and its validation

The aim of the work presented in the first chapter is to develop and validate a computation fluid dynamics adsorptive hydrogen storage system model. Darcy's equation combined with the continuity equation is used for solving the mass and the momentum balance governing equations of the adsorptive storage system. Standard energy balance equation for gas flowing through the adsorbent bed is used to describe energy conservation in the adsorptive storage system. Accurate thermophysical and physicochemical properties are used in the mathematical

model. The modified Benedict-Webb-Rubin real gas equation of state, as implemented in NIST REFPROP is used to obtain the thermodynamics parameters such as specific heat capacity, density, viscosity, enthalpy and thermal conductivity of *ortho*, *para* and *normal* hydrogen. The parameters such as the thermal conductivity of MOF-5 at cryogenic temperature and the skeleton density of MOF-5 are obtained from the literature. Experimentally measured specific heat capacity of MOF-5, isosteric heat of adsorption and bulk density of MOF-5 are used in the model. The properties of the tank material are adapted from the literature.

The test bench consisting of a 2.5 L tank filled with MOF-5 is used to perform the experiment for comparing the experimental results with simulation results. While comparing the simulation results and experimental results, we found that the simulation results shows good agreement with the experimental results. The consistency checking of the adsorptive storage system model is carried out by comparing temperatures obtained from the simulation with those obtained from the bench test measurements using activated carbon (AX-21™) as an adsorbent.

5.2 Effects of flowthrough cooling and *para-ortho* conversion on the performance of a subscale-prototype hydrogen storage tank filled with MOF-5

The aim of the work presented in the second chapter is to use the model validated in chapter one to investigate the effects of flowthrough cooling and endothermic *para-ortho* conversion on the thermal and storage performance of the subscale-prototype (2.5 L) storage system filled with MOF-5. In order to study the effect of flowthrough cooling, flowthrough experiments are performed. The results show that the heat energy, which arises during the charging is removed

convectively during the flowthrough cooling stage. In the flowthrough test bench, LN_2 is used as coolant at the exterior of the tank. In order to understand the effect of flowthrough cooling on storage capacity and reduction in cooling time, simulation of charging to the same pressure is performed using only LN_2 as an exterior tank coolant, while keeping the same inlet hydrogen temperature and charging rate than for the flowthrough tests. The results indicate that the advantage of flowthrough cooling technique is not only in the cooling the storage system but the process enhances the storage capacity also whereas the storage system considering only LN_2 as a coolant, there is no additional hydrogen is entering the tank. The result of the average bed temperature profiles for flowthrough cooling and LN_2 cooling scenarios indicates that faster flow rates are required for flowthrough cooling to be efficient for heat removal. The flowthrough experimental results compares well with the simulation results. We obtained good agreement in temperature, pressure and mass balance.

To investigate the effect of endothermic *para-ortho* hydrogen conversion on the storage system, the following assumptions are made in the simulation:

- MOF-5 has enough catalytic activities for making rapid conversion via addition of an enhancing agent.
- The material properties will not change due to the presence of the enhancing agent and we have considered only the maximum conversion effect.
- Based on the system temperature, the fraction of *para* hydrogen present in the adsorbed phase is converted to *ortho* fraction of hydrogen.

The simulation results show that the endothermic conversion reduces the system temperature; this is supported by the analysis of the various heat sources such as

adsorption heat, heat due to pressure work and *para-ortho* conversion effect and the corresponding temperatures.

5.3 Multiphysics performance of a cryo-adsorptive bulk hydrogen storage reservoir filled with MOF-5

In chapter 4, we numerically investigated the multiphysics performance of a bulk hydrogen storage reservoir filled with MOF-5 when 77 K hydrogen is charged into the tank, which is maintained at room temperature. At first, a charge-discharge cycle method is used for achieving the cryogenic condition (80 K) in the tank. The result shows that the temperature of the system is reduced to 80 K after three charging-discharging cycles. Once the temperature of the tank has gone down to 80 K, the filling is carried out using 77 K hydrogen to reach the tank's maximum pressure, 4 MPa. After this, flowthrough cooling is implemented in the simulation. The simulation result shows that, when flowthrough cooling is operational for ~30 h, the total hydrogen mass that can be stored before the tank reaches its maximum pressure capacity of 4 MPa is 460 kg. This is significantly more than the storage capacity (~275 kg) of cryo-compressed tank in which hydrogen is maintained at 77 K and 4 MPa. The model then studied the effect of *para-ortho* conversion together with flowthrough cooling on temperature reduction in the tank. We found that instantaneous *para-ortho* conversion reduced the system temperature during the charging stage and the temperature reduction is accelerated during flowthrough stage. Further, the model tested the effect of the mass flow rate on heat removal from the system during the flowthrough stage. The results reveal that high mass flow rate 20000 SLPM accelerates the heat removal from the storage tank and cools the tank in 6 hr, which is less compared to 8 hr for

15000 SLPM and 12.8 hr for 10000 SLPM. Finally, the hydrogen mass loss during the 10 days dormancy stage is calculated. We find that each day ~2.4 kilograms of hydrogen should be removed from the reservoir to maintain the pressure below the maximum allowable pressure of the tank.

5.4 Future work

In the model, we assumed that MOF-5 has enough catalytic activity for making temperature dependent instantaneous *para-ortho* conversion, this assumption need to be proved by experiment. Moreover, the experimental data is important for developing the adsorptive storage system model that accommodates *para-ortho* conversion. The existing discussions reveal that the strong paramagnetic moment of catalyst causes rapid conversion [1, 2]. Fitzgerald et *al.* found that MOF-74 has a magnetic moment that causes conversion in the hydrogen. The authors observed that this conversion occurs in a time-scale of the order of a minute, whereas conversion is a slow process for hydrogen adsorbed on MOF-5 [3, 4]. Some literatures suggest certain strategies for increasing the magnetic strength of MOFs, such as embedding catalytic particles inside the MOF-5 [5].

Another recommendation for future work is related to the model improvement. In the adsorptive storage system model, we used heat flux boundary condition at the outer wall of the tank, there we set at constant ambient temperature condition, 77 K. For convenience, the possibility of LN_2 evaporation is ignored. For improvement of the model, an estimation of LN_2 evaporation rate is necessary. Also, we used constant heat transfer coefficient in the energy balance model that can be changed when the ambient temperature is changed. It would be better if we could implement heat transfer coefficient that are functional on the ambient temperature changes. In addition to this, a complete understanding of

software platform for solving the governing equation is important. Design with exact geometry, proper meshing, perfect adjustment of the time dependent solver etc., are important for improving the accuracy of the final results.

References

[1] Weitzel DH, Loebenstein WV, Draper JW, Park OE. *Ortho-Para* Catalysis in liquid-hydrogen Production. J Res Nat Bur Stand 1958; 60:221-227.

[2] Buntkowsky G, Walaszek B, Adamczyk A, Xu Y, Limbach HH, Chaudret B. Mechanism of nuclear spin initiated *para*-H_2 to *ortho*-H_2Conversion. Phys Chem Chem Phys 2006; 8:1929–1935.

[3] FitzGerald SA, Hopkins J, Burkholder B, Friedman M. Quantum dynamics of adsorbed normal- and *para*-H_2, HD, and D_2 in the microporous framework MOF-74 analyzed using infrared spectroscopy. Phys Rev B 2010; 81: 104305.

[4] FitzGerald SA, Allen K, Landerman P, Hopkins J, Matters J, Myers R, Rowsell JLC. Quantum dynamics of adsorbed H_2 in the microporous framework MOF-5 analyzed using diffuse reflectance infrared spectroscopy. Phys Rev B 2008; 77:224301-224309.

[5] Falcaro P, Normandin F, Takahashi M, Scopece P, Amenitsch H, Costacurta S, Doherty CM, Laird JS, Lay MDH, Lisi F, Hill AJ, Buso D. Dynamic Control of MOF-5 Crystal Positioning Using a Magnetic Field. Adv Mater 2011; 23: 3901–3906.

Section B

Articles

Article – 1

Effect of *para-ortho* conversion on hydrogen storage system performance

S. Ubaid*, J. Xiao, R. Zacharia, R. Chahine, P. Bénard.

Institut de recherche sur l'hydrogène, Université du Québec à Trois-Rivières, P.O. Box 500, Trois-Rivières, Québec G9A 5H7, Canada

Abstract

We present a study of the effects of *para-ortho* conversion on the performance of an adsorption-based hydrogen storage system using finite element method implemented in COMSOL Multiphysics® 4.3a platform. The base model which does not take into account the *para-ortho* conversion is validated using the experimental data of Maxsorb™ activated carbon measured with a test bench at room and cryogenic temperatures. The validated model is subsequently applied to simulate the storage system filled with MOF-5 and then extended to investigate the effects of endothermic *para-ortho* conversion of hydrogen isomers on storage and thermal performances during hydrogen charging/discharging cycle for four inlet temperatures, 35, 50, 77 and 100 K. Our results show that the endothermic conversion reduces the system temperature and increases the net storage capacity. The temperature changes due to the different heat sources are used to investigate the effect of conversion on the temperature reduction. The adsorbed and gas phase masses in the storage system with and without conversion at the end of the charging time are used to determine the effect of conversion on the storage system capacity. Even though the conversion is more significant at low temperature (35 K), the gains are larger at high temperature (100 K).

INTERNATIONAL JOURNAL OF HYDROGEN ENERGY 39 (2014) 11651–11660

Available online at www.sciencedirect.com

ScienceDirect

journal homepage: www.elsevier.com/locate/he

Effect of *para–ortho* conversion on hydrogen storage system performance

S. Ubaid*, J. Xiao, R. Zacharia, R. Chahine, P. Bénard

Institut de recherche sur l'hydrogène, Université du Québec à Trois-Rivières, P.O. Box 500, Trois-Rivières, Québec G9A 5H7, Canada

ARTICLE INFO

Article history:
Received 12 March 2014
Received in revised form
9 May 2014
Accepted 16 May 2014
Available online 16 June 2014

Keywords:
Hydrogen storage
Adsorption
Metal-organic frameworks
System modelling
Para–ortho conversion

ABSTRACT

We present a study of the effects of *para–ortho* conversion on performance of an adsorption-based hydrogen storage system using finite element methods implemented in COMSOL Multiphysics 4.3a platform. The base model which does not take into account the *para–ortho* conversion is validated using the experimental data of Maxsorb activated carbon measured with a test bench at room and cryogenic temperatures. The validated model is subsequently applied to simulate the storage system filled with MOF-5 and then extended to investigate the effects of endothermic *para–ortho* conversion of hydrogen isomers on storage and thermal performances during hydrogen charging/discharging cycle for four inlet temperatures, 35, 50, 77 and 100 K. Our results show that the endothermic conversion reduces the system temperature and increases the net storage capacity. The temperature changes due to the different heat sources are used to investigate the effect of conversion on the temperature reduction. The adsorbed and gas phase masses in the storage system with and without conversion at the end of the charging time are used to determine the effect of conversion on the storage system capacity. Even though the conversion is more significant at low temperature (35 K), the gains are larger at high temperature (100 K).

Introduction

Sorptive hydrogen storage in which hydrogen is physisorbed on high surface area porous materials, such as metal organic frameworks (MOFs) is widely recognized as a promising option for automobile energy storage applications [1]. In order for these technologies to be feasible for on-board applications, the adsorption-based hydrogen storage systems must meet certain specific system-level performance criteria [2]. Even though several MOFs can achieve the storage densities necessary for on-board applications purely on the basis of their adsorption capacity, it is evident that any realistic hydrogen storage system built using these MOFs cannot readily meet all required system performance targets [3]. This is because the overall performance of a storage system not only depends on material's hydrogen storage densities, but also on the storage and thermal behaviour of the entire storage system, which includes the storage material as well as other structural components, such as tank, heat transfer materials, heating elements, valves, sensors etc. [4].

* *Corresponding author.* Tel.: +1 819 376 5011x4463; fax: +1 819 376 5164.
E-mail addresses: siyad.ubaid@uqtr.ca, siyanet04@gmail.com (S. Ubaid).
http://dx.doi.org/10.1016/j.ijhydene.2014.05.101

Computational fluid dynamics (CFD) simulation is a powerful tool that can help us quickly forecast a storage system's performance without actually relying on routine bench-level experiments, which are complex, time-consuming and requires high-level safety infrastructures and large quantities of sorbent materials. In recent years, CFD has allowed the prediction of system performance of hydrogen storage tanks filled with MOF-5 and Cu-BTC [5]. The authors adapted a previously developed 2D axisymmetric model that was originally validated using experimental data of activated carbon Maxsorb. Irrespective of the temperature conditions imposed in these simulations and others [2,5], the hydrogen gas is typically treated as "normal hydrogen" whose hydrogen's nuclear spin isomers composition of 75% *ortho* and 25% *para*–hydrogen [6], which is the composition at room temperature. Below the room temperature, the composition of *para–ortho* fraction present in the hydrogen is defined as equilibrium hydrogen. The composition of these isomers is known to evolve to 100% *para* form as the temperature decreases to 20 K. In the absence of catalysts, however, the conversion follows slow kinetics and takes as many as several days to complete. Recently, in a year-long project, Petitpas et al. conducted several experiments to study the kinetics of natural *para–ortho* conversion in a full scale 345 bar automotive cryogenic pressure vessel filled with liquid *para*–hydrogen [7]. The authors reported that the natural conversion started in 10–15 days and it was completed with 25–30 days. Peng and Ahluwalia developed a dynamic model which accounted endothermic natural *para* to *ortho* conversion kinetics to study the dormancy performance and hydrogen loss from an insulated pressure vessel filled with liquid *para* hydrogen [8]. The model predicted that the hydrogen loss rate during the dormancy stage was decreased through the reduced pressure and temperature condition due to the endothermic *para–ortho* conversion.

The existing discussions reveal that the strong paramagnetic moment of catalyst cause rapid conversion [9–11]. Fitzgerald et al. found that MOF-74 has a magnetic moment that causes conversion in the hydrogen. The authors observed that this conversion occurs on the order of a minute, whereas conversion is a slow process for hydrogen adsorbed on MOF-5 [12,13]. In the present model, we assumed that MOF-5 has enough catalytic activity to make instantaneous conversion of adsorbed hydrogen. Our assumption is valid under the condition that the paramagnetic moment of pristine MOF-5 could be increased by embedding the paramagnetic particles in the MOF-5, for example, using the method discussed by Paolo et al. [14]. If foreign particles that can catalyse the conversion are embedded in the MOF-5, the overall thermal performance of the hydrogen storage system may have non-trivial contributions from endothermic heat of conversion. For example, the *para–ortho* conversion in the equilibrium hydrogen in a storage system filled with MOF-5 at different storage temperatures resulted in temperature swing while recovering the fractions of sorbed hydrogen from the system, as shown by Ahluwalia and co-workers [15]. The authors concluded that an additional external cooling is not necessary for the system to reach theoretical gravimetric and volumetric capacities if the *para–ortho* conversion occurs with no kinetic limitations, inside the system containing MOF-5.

The objective of the work presented in this paper is to develop a computational fluid dynamics model that accommodates the endothermic heat of *para–ortho* hydrogen conversion in a realistic axisymmetric 2D hydrogen storage tank filled with powder MOF-5 and to understand its effects on overall thermal and storage behaviour of the storage system. In this model, we assume that charged liquid *para* hydrogen converts to equilibrium *para–ortho* composition solely as a function of the prevailing pressure and temperature without kinetic limitations [15]. Since no system-level experimental data of MOF-5 adsorption is yet available for validating the model, we validated the base model using the data from bench tests of Maxsorb performed at room temperature and 77 K. Similar methods have been previously adopted by Hardy et al. and Xiao et al. [16,17]. The system of differential equations governing the mass and energy balance in the system subjected to initial and boundary conditions is solved using finite element platform COMSOL Multiphysics 4.3a to obtain the spatio-temporal evolution of heat and mass characteristics. To implement the heat of conversion Q_C, we include the enthalpy of conversion of adsorbed hydrogen in the energy source term. The present model is an attempt to understand the consequences of conversion on charging and discharging by examining an extreme limit, namely maximum conversion effect during the charging time.

Description of the model

We begin with the standard equations of energy and mass conservation to study the multiphysics performance of the storage system. The modified Benedict-Webb-Rubin real gas equation of state, as implemented in NIST REFPROP was used to calculate the thermodynamics properties such as specific heat capacity, density, viscosity and thermal conductivity of *ortho*, *para*, normal and equilibrium hydrogen [18]. The base model which is validated using Maxsorb and the model extension to MOF-5 system does not take into account the *para–ortho* conversion heat.

Mass conservation equation and Darcy law

The rate of change of mass of hydrogen entering or leaving the storage tank is described using the Darcy's law of fluid flow in the porous media. This is given by:

$$\frac{\partial}{\partial t}(\rho\varepsilon_b) + \nabla\cdot(\rho\vec{u}) = S_m. \tag{1}$$

In Eq. (1), ρ is the density of the hydrogen gas, ε_b and u are the adsorbent bed porosity and the Darcy velocity of gas flow through the adsorbent, respectively. The mass of hydrogen added to the adsorbed phase per unit volume per unit time is given by the mass source term S_m:

$$S_m = -\rho_b M_{H_2}\frac{\partial n_a}{\partial t}, \tag{2}$$

where ρ_b,M_{H2} and n_a are the adsorbent bed density, molar mass of hydrogen gas and absolute adsorption, respectively. The negative sign of S_m implies that desorption increases the amount of gaseous hydrogen. The Darcy velocity of the

hydrogen gas flowing through the porous adsorbent is related to the Darcy permeability κ, gas viscosity μ and pressure gradient ∇p by Darcy law:

$$\vec{u} = -\frac{\kappa}{\mu}\nabla p. \tag{3}$$

The Darcy permeability is valid over the range of Reynolds numbers and superficial velocities considered in this work [19]. The operator ∇ is defined in the spherical polar coordinates. Darcy permeability can be written as:

$$\kappa = \frac{1}{150}\frac{D_p^2 \varepsilon_b^3}{(1-\varepsilon_b)^2}, \tag{4}$$

where D_p is the diameter of adsorbent particles, for which we use the reported values of $D_p = 0.25$ μm for MOF-5 [20] and 200 μm for Maxsorb [17]. n_a in Eq. (2) is the absolute adsorption obtained using modified Dubinin–Astakhov (D–A) adsorption model. In this model, absolute adsorption is related to the state variables, temperature T and pressure P using Eq. (5).

$$n_a = n_{max}\exp\left[-\left(\frac{RT}{\alpha+\beta T}\right)^m \ln^m\left(\frac{p_0}{p}\right)\right], \tag{5}$$

where R is the universal gas constant. m is the heterogeneity parameter of the sorbent material. It is typically assumed 2 for activated carbon, which is also used here for MOF-5. Unrestricted fit using m in modified D–A model has recently shown that the value of m can be as high as ~7 for MOF-5 [21]. Nevertheless, we use the original 5-parameter model with $m = 2$ which still can accurately predict the adsorption isotherms in the pressure and temperature range we consider [22]. n_{max} represents the maximum value of absolute adsorption corresponding to limiting saturating pressure p_0. α and β are the enthalpic and entropic contributions to the free energy of adsorption. To implement the modified D–A model in the simulation, we use to parameterize the model using the reported excess adsorption of MOF-5 [23]. The resulting D–A parameters of MOF-5 and Maxsorb carbon are given in Table 1. ε_b in Eq. (4) is the effective porosity which is determined from the system void volume, V_v and adsorption volume, V_a using Eq. (6) [16].

$$\varepsilon_b = \rho_b(V_v - V_a), \tag{6}$$

where, V_a is determined using the modified D–A model: $n_{ex} = n_a - V_a\,\rho_g$. For V_v we use 0.0029 and 0.0062 $m^3\ kg^{-1}$, respectively for Maxsorb and MOF-5 [16].

Energy conservation equation

To describe the energy conservation of the storage system, we use the standard energy balance equation for hydrogen gas flowing through the adsorbent bed:

$$(\rho C_p)_{eq}\frac{\partial T}{\partial t} + \rho C_p\,\vec{u}\cdot\nabla T = \nabla\cdot(k_{eq}\nabla T) + Q. \tag{7}$$

In Eq. (7), the equivalent volumetric heat capacity of the adsorbent-gas system is given by:

$$(\rho C_p)_{eq} = \varepsilon_b\rho_g C_{pg} + (1-\varepsilon_b)\rho_s C_{ps}, \tag{8}$$

where ρ_g, ρ_s, C_{pg} and C_{ps} are densities and specific heat capacity of the adsorbent and gas phase, respectively. For C_p of MOF-5 and Maxsorb, we use a constant value equivalent to the C_p at the room temperature. There is no reported low temperature C_p data of MOF-5. The equivalent conductivity of the adsorbent-gas system in Eq. (7) is the net conductivity of the medium including that of the adsorbent k_s and of the gas k_g, weighed using the effective porosity. It can be written as:

$$k_{eq} = \varepsilon_b k_g + (1-\varepsilon_b)k_s. \tag{9}$$

The heat source term, Q in Eq. (7) is the sum of the contributions from the adsorption heat Q_a, the heat produced by pressure-volume work Q_p and the heat due to *para–ortho* conversion Q_c. The heat generated due to pressure-volume work is defined in the spherical polar coordinates as:

$$Q_p = \varepsilon_b\frac{\partial p}{\partial t} + u_r\frac{\partial p}{\partial r} + u_z\frac{\partial p}{\partial z}, \tag{10}$$

where u_r and u_z are the components of velocity field along the radial and axial directions. The heat of adsorption Q_a is given by:

$$Q_a = \rho_b\frac{\partial n_a}{\partial t}q_{st}, \tag{11}$$

where q_{st} is the isosteric heat of adsorption, which is given by the modified D-A model as:

$$q_{st} = \alpha\sqrt{-\ln\frac{n_a}{n_{max}}}. \tag{12}$$

To calculate the conversion heat, we considered that the equilibrium hydrogen gas entering into the MOF-5 storage system is divided into two phases: gaseous and adsorbed. Based on the system temperature, the fraction of *para* hydrogen present in the adsorbed phase is converted to *ortho* fraction of hydrogen, while no conversion is considered in the gas phase because the gas phase hydrogen has no direct contact with MOF-5. Here we assume that the conversion is instantaneous. We use the following expression to calculate the conversion heat source

$$Q_c = \frac{d}{dt}\left[(\rho_a f_{OH2}\Delta H_{p-o})\right] = \frac{d}{dt}\left[(n_a M_{H2}\rho_b(1-f_{PH2})\Delta H_{p-o})\right], \tag{13}$$

where ΔH_{p-o} is the endothermic conversion energy 527 kJ kg^{-1} [24], ρ_a in Eq. (13) is the adsorbed phase density and foh_2 is the temperature dependent mass fraction of *ortho* hydrogen present in the equilibrium hydrogen. The fraction of *ortho* hydrogen in the equilibrium hydrogen is estimated from the temperature-induced evolution of equilibrium mass fraction of *para* hydrogen, using the empirical relation [6]:

Table 1 – Modified D-A model parameters of Maxsorb and MOF-5.

	n_{max} (mol kg^{-1})	P_0 (MPa)	α (J mol^{-1})	β (J $mol^{-1}\ K^{-1}$)	V_a ($m^3\ kg^{-1}$)	V_v ($m^3\ kg^{-1}$)
Maxsorb	71.6	1470	3080	18.9	0.001473	0.0029
MOF-5	91.1	837.1	3031.6	11.3	0.00179	0.0062

$$f_{PH2} = 0.1\left[\exp\left(\frac{-175}{T}\right) + 0.1\right]^{-1} - 7.06 \times 10^{-9}T^3 + 3.42 \times 10^{-6}T^2 - 6.2 \times 10^{-5}T - 0.00227 \quad (14)$$

The temperature-dependent *para* hydrogen content of equilibrium hydrogen calculated using Eq. (14) is shown in Fig. 1.

Geometry of the tank and material properties of adsorbents

The geometry of the storage tank and boundary conditions used for model validation are based on our experimental test bench. The schematic of our test bench is shown in Fig. 2, the detailed description of the test bench is presented elsewhere [2]. The adsorption test bench consists of a 2.5 L stainless steel tank, which is typically filled with 670 g of Maxsorb. To compare the spatio-temporal variation of pressure and temperature obtained from the simulation with those measured experimentally we chose eight monitoring points T1, ..., T8 in the axial direction and three monitoring points, T4, Tr and Tw in the central radial direction. The geometry of the tank which is the same as that of the experimental test system used in the simulations and its monitoring points of axial and radial directions are depicted in Fig. 2, right panel. The geometry is implemented with extra fine mesh having 2077 triangular elements.

To calculate the thermodynamic properties of gaseous hydrogen, the real gas equation of state (EOS) implemented in the NIST REFPROP standard Reference Database is used.

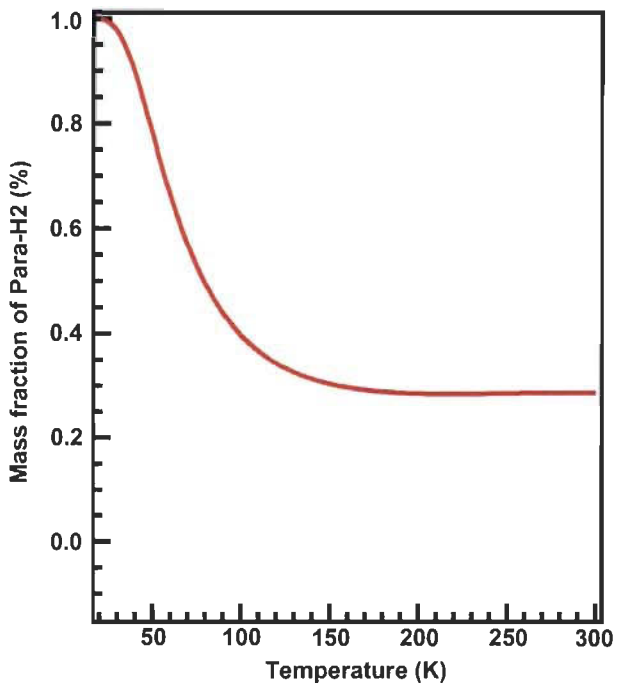

Fig. 1 – Equilibrium fraction of *para* hydrogen as function of temperature.

Initially, the NIST database was interfaced with COMSOL using Matlab (R2010b). While this is a highly accurate method of importing thermodynamic data, it compromises the computational speed. Therefore, we obtained data from NIST which is converted into a grid form in MATLAB and is implemented in COMSOL Multiphysics platform. The bulk properties of Maxsorb and MOF-5 required for the simulation are taken from the literature and given in Table 2 [2,16].

Initial and boundary conditions

We have three sets (a, b and c) of initial and boundary conditions depending on the simulations performed and are given in Table 3: (a) For the validation of model we used the initial and boundary conditions similar to those used in the experiments. For this the initial pressure in the tank is set to 0.033 MPa for room temperature validation. For cryogenic temperature validation, the initial pressure in the tank is set to 0.14 MPa. The initial temperatures are set to 281and 80 K for the simulations at room temperature and cryogenic temperatures, respectively. The mass flow rates are set to +15, −15 and 0 SLPM, respectively for charging, discharging and dormancy. The room temperature hydrogen gas is filled into the system for both experimental validations. A fixed temperature boundary condition, 77 K and heat flux boundary condition is applied to the outer wall of the tank [16,17]. The charge/discharge cycle at room temperature and charging at cryogenic temperature of Maxsorb carbon storage system is used for model validation. (b) For MOF-5 storage system, the initial temperature and pressure are set to 80 K and 0.1 MPa, respectively. The mass flow rate and the inlet temperature are set to 15 SLPM and 77 K, respectively. (c) For model extension to the effect of *para–ortho* conversion, four inlet temperatures for hydrogen are considered: 35, 50, 77 and 100 K. An adiabatic insulated tank is assumed for the MOF-5 storage system and the estimated heat leakage rate is calculated and applied in the form of heat flux at the outer wall of the tank. For calculating the heat leakage of the storage tank, we use the data of daily evaporation rate (%) of liquid oxygen filled tank. The duration of each step is given in the parenthesis of column 1.

Results and discussion

Validation of the model at room and cryogenic temperature using the experimentally measured temperatures of bench tests with Maxsorb

We begin with discussing the validation of the base model which does not take into account the *para–ortho* conversion heat. Even though the activated carbon is a known catalyst for the *ortho–para* conversion, we do not consider the conversion in our model validation. This is because validation is performed with hydrogen at room temperature where the effects are not significant over the timescales considered [25]. The validation is carried out by comparing temperatures at various points in the storage tank filled with Maxsorb obtained from the simulation during hydrogen charging/discharging cycle at room temperature and charging at cryogenic temperature

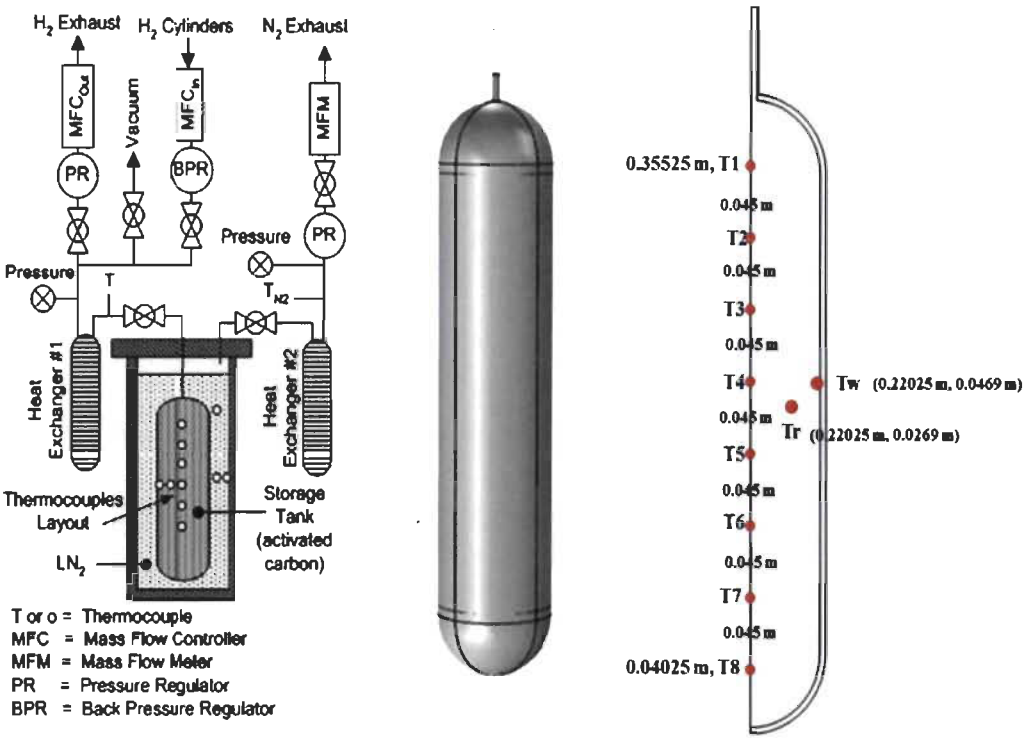

Fig. 2 – On the left, P&ID of the test bench used for the validation experiments. On the right, geometry of the tank used in the simulation with reference points.

with those obtained using from our test bench experiments. The central axial points in the tank T1, T2, T3, T4 and T6 which correspond to the positions of thermocouples inside the test bench storage system are selected for comparing the temperatures. Ice water and liquid nitrogen are used as tank coolants for room temperature and for cryogenic temperature tests, respectively. The temporal evolution of temperature for both tests is shown in Fig. 3. For room temperature data given in the left panel of Fig. 3, we observe a very good agreement between simulation and experimental results. Although the temperatures at points T3 and T6 are slightly over and underestimated at cryogenic condition (right panel, Fig. 3), overall trend of temperature evolution is clearly reproduced. The difference between experiment and simulation primarily stems from the constant heat capacity assumed overall temperatures. Other factors, such as bulk density of the material and sensitive boundary conditions may also contribute to the difference between experimental data and simulation results at cryogenic temperature, as discussed by Hardy et al. [16]. The results of pressure and mass balance are very similar to those available in the published data and hence not presented here for brevity. Through the validation of model at two different temperature conditions, we found that the model shows adaptability and consistency with experimental data even though slight differences shown between the experimental data and the model.

Table 2 – Material properties of Maxsorb and MOF-5.

	ρ_b (kg m^{-3})	ε_b	k_s (W m^{-1} K^{-1})	C_{ps} (J kg^{-1} K^{-1})
Maxsorb	300	0.49	0.2	825
MOF-5	190	0.57	0.088	700

Extension of the validated model to simulate the performance of the storage system filled with MOF-5 at 77 K

For the simulation of storage performances of tank filled with MOF-5, the initial and boundary conditions used are those given in Section 4. In Fig. 4 (left), the verification of mass balance is shown. Here, total mass of hydrogen in the tank while charging obtained by integrating the experimental charging

Table 3 – Boundary conditions of charge/discharge cycle of Maxsorb and MOF-5 system.

Time (s)	Inlet	Outer wall
(a) Validation of Model *(Maxsorb)*		
Charging (0–1042 s)	297.6 K	$h_w(T_f - T)$ W m^{-2}
Dormancy (1043–3189 s)	297.8 K	h_w = 36 W m^{-2} K^{-1}
Discharging (3190–4131 s)	282.2 K	T_f = 282.5 K
Dormancy (4132–6000 s)	288.9 K	
(b) Simulation of System filled with MOF-5		
Charging (0–2500 s)	77 K	3 W m^{-2}
Dormancy (2501–3500 s)	Insulation	
Discharging (3001–5000 s)	3 W m^{-2}	
Dormancy (5001–6000 s)	Insulation	
(c) Simulation of System filled with MOF-5 with para–ortho conversion		
Charging (0–2500 s)	100 K, 77 K, 50 K, 35 K	3 W m^{-2}
Dormancy (2501–3500 s)	Insulation	
Discharging (3001–5000 s)	3 W m^{-2}	
Dormancy (5001–6000 s)	Insulation	

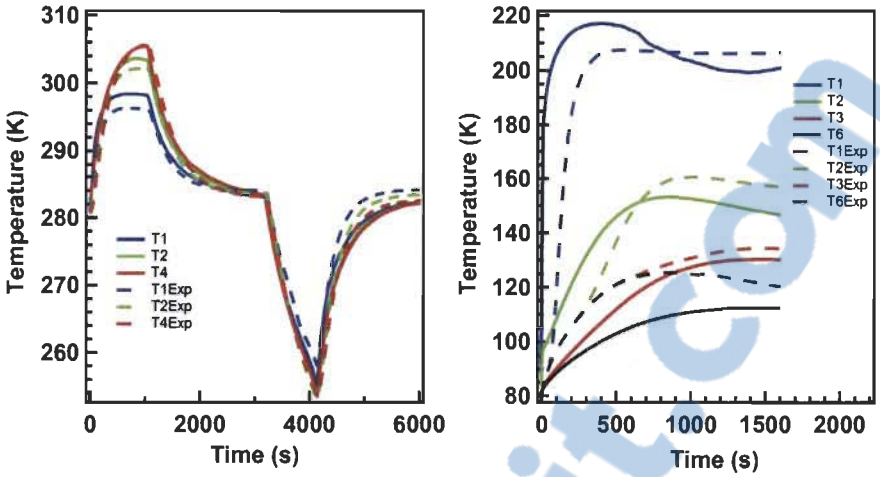

Fig. 3 – Comparison between the temperatures at points T1, T2 and T4 of experimental validation and simulations at room temperature (left panel) and at points T1, T2, T3 and T6 at cryogenic temperature (right panel). For room temperature entire charging/discharging cycle is shown. For cryogenic temperature, only the charging stage is shown.

rate over the charging time is compared with the sum of the amounts hydrogen present in gas and adsorbed phases. The latter ones are obtained from the simulation using the modified DA model and real gas EOS, respectively. Fig. 4 (left panel) clearly shows that a consistent mass balance is manifested throughout the charging time. Fig. 4 (right panel) shows the uniform behaviour of pressure in the tank which increases almost linearly with time while charging and falls slightly while idling. During discharging, pressure drops sharply as the hydrogen gas is flowing out of the tank.

Temperature profiles along several axial points during charging–discharging cycles are shown in Fig. 5. At T1, temperature rises sharply the onset of charging until 100 s; as cold hydrogen flow into the tank, the adsorption takes place and heat is released into to bed. The resulting adsorption heat is conductively transferred from the entry to the point T1. The temperature at T1 then drops sharply to 56 K until before 360 s. This drop in temperature arises because of the positive Joule-Thompson (J-T) coefficient of hydrogen and also due to hydrogen desorption from the MOF-5 bed. When charging is performed at temperatures below hydrogen's inversion temperature (T_i = 193 K), the gas undergoes expansion into the tank and positive $J-T$ effect leads to decreased temperature. In addition, the mass source term at T1 increases until 100 s as shown in Fig. 6, which indicates the desorption of hydrogen. Desorption being an endothermic process; the heat required is absorbed from the system, which leads to decreased temperature. Since the axial point T1 is the one closest to the gas inlet, it is reasonable to think that the effect will be more pronounced at this point as compared with other axial points as seen in Fig. 5. Desorption takes the heat from the bed and causes the temperature reduction in the tank.

Once T1 is cooled down, adsorption increases again as hydrogen is flowing past T1while continuous charging, which is consistent with decreasing mass source term at T1. This releases heat into the bed and subsequently increases the temperature to nearly 80 K at T1 in Fig. 5. Note that desorption while charging takes places only at top most points in the tank which can be concluded for the mass source terms at points T4 and T8 (Fig. 6). Additionally, there is no sharp temperature

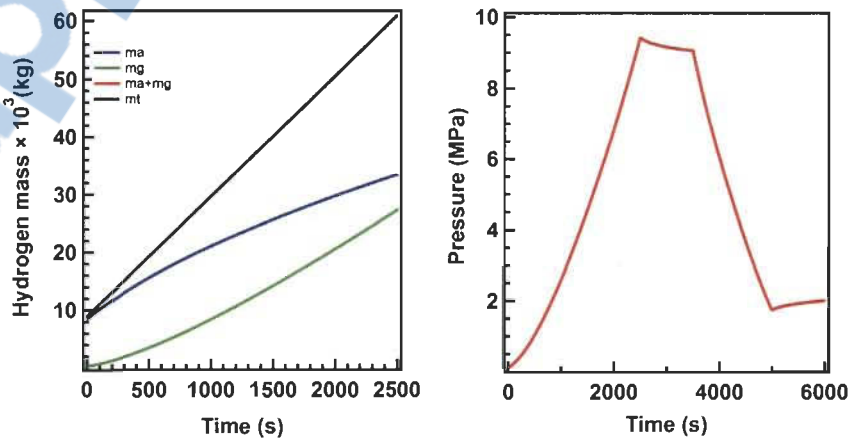

Fig. 4 – (Left panel): Mass balance during charging and (right panel) pressure during the charge/discharge cycle.

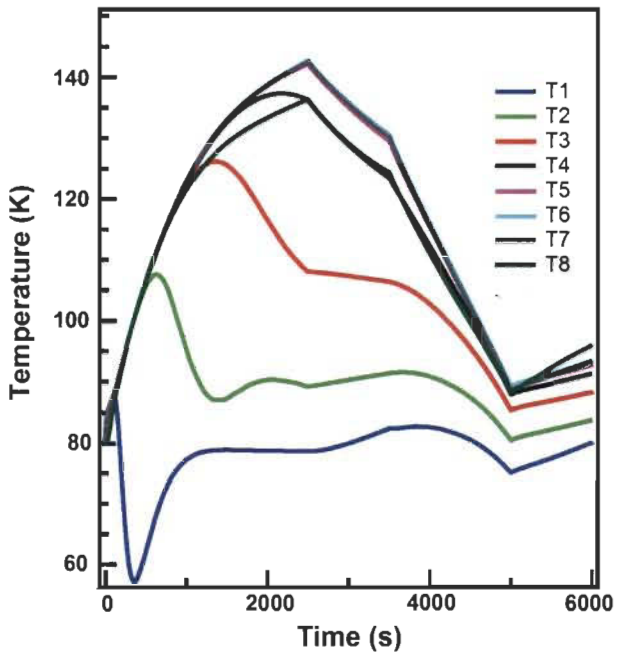

Fig. 5 – Temperature variations along the axial points.

reduction at the point T1 contrary to that observed when tank filled with Maxsorb activated carbon. This is because, when adsorption is performed at temperatures higher than hydrogen's inversion temperature, hydrogen heats up as it throttles through the adsorption bed. Also higher thermal conductivity of Maxsorb and adsorption heats of Maxsorb as compared to that of MOF-5 rises the temperature at T1 during charging [16].

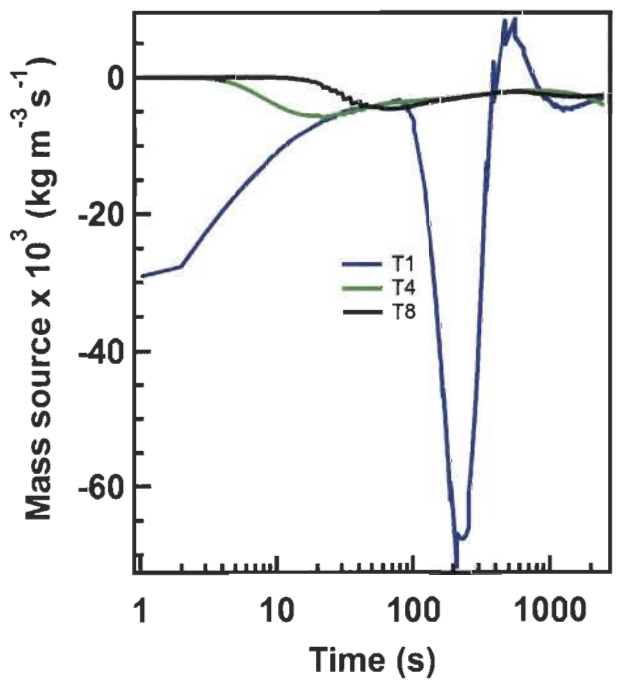

Fig. 6 – Mass source term variations at points T1, T4 and T8 while charging.

At T2 and T3, temperature rises at the onset of charging stage due to the heat of adsorption and heat produced by pressure work. Since these points are located near the inlet region of the tank, effect of cooling due to the inflow of 77 K hydrogen causes temperature drop at T2 and T3. The cooling effect by inflow of 77 K hydrogen disappears completely at points T4 to T7 as filling continues because the adsorption heat and heat by pressure work from the top points are transferred towards the bottom of the tank. Temperature at the point T8 is less than that at the central regions due to the poor heat transfer stemming from the lower thermal conductivity of MOF-5 adsorption bed. During the idling stage, after the charging, all points show temperature drop due to the heat transfer from cold region to bottom region. While discharging, the temperature drops drastically because of hydrogen desorption and outflow of heat with hydrogen. Comparison of temperature profiles along the radial direction is shown in Fig. 7. While the overall radial temperature evolution follow the temperature profiles elsewhere, as we move outwards to the wall, the temperature decreases due to the poor thermal conductivity of MOF-5.

Effect of para–ortho *conversion heat on the performance of the storage system filled with MOF-5*

Currently, the method for vehicular storage system fuelling is using either pre-cooled hydrogen at liquid nitrogen temperature or at cryo compressed supercritical hydrogen [9,26]. In such cases, if the cryogenic hydrogen is not already at equilibrium *ortho–para* composition, a significant volume of hydrogen would be lost during the storage time due to heat release during the conversion. A method to avoid this storage loss is to convert hydrogen to the *para* form after the cooling. If *para* hydrogen enters the storage tank, the temperature of the tank will be reduced due to the instantaneous conversion because of the catalytic activity of MOF-5. If the conversion is not instantaneous, temperature reduction by conversion may be negligible during the short time period of charging which for vehicular applications lasts typically 3–4 min. Here, we made an attempt to understand the maximum possible effect of an instantaneous *para* to *ortho* adsorbed hydrogen conversion on the total heat and performance of the system by monitoring the temperature and pressure data at the centre point T4 of tank when hydrogen gas at temperatures: 35, 50, 77 and 100 K is charged into the tank which is maintained at 80 K.

When 100 K equilibrium hydrogen which has a composition of ~40% *para* hydrogen is charged into the tank, a part of *para* fraction absorbs 527 kJ kg^{-1} of energy from tank and gets converted to *ortho* fraction. This leads to drop in the temperature at T4 at the end of charging is 131 K which is 10 K lower than it would if no conversion is considered; see Fig. 8 (left panel). As the hydrogen gas with temperatures lower than 100 K is charged, temperature evolution inside the system by adsorption and pressure work is less, the resulting fraction of *para* hydrogen converted to *ortho* hydrogen becomes lesser. Furthermore, it is observed from Fig. 8(a) (left panel) that the effect due to the conversion is higher at 100 K inlet temperature than 35 K.

Initially, the composition of *para* and *ortho* hydrogen at the T4 is ~49 and ~51%, respectively which is the composition at

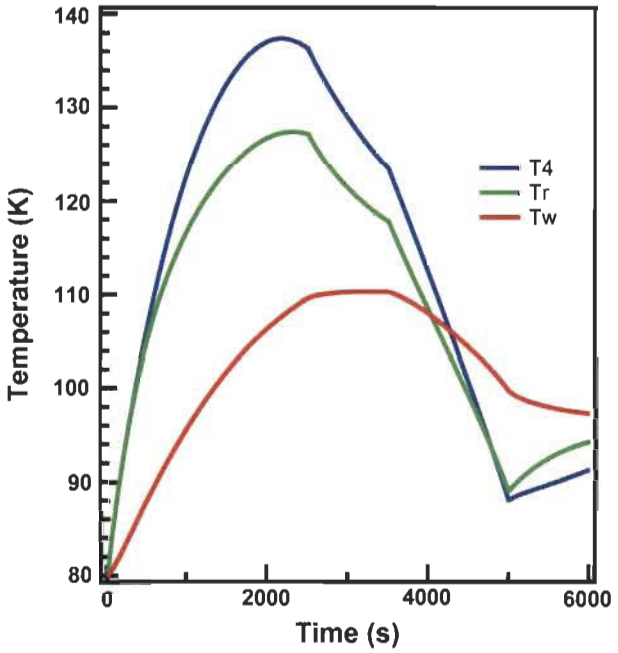

Fig. 7 – Temperature profiles at radial points while charging, discharging and dormancy.

80 K. At the end of charging stage the temperature reaches 142 K for 100 K inlet temperature and 118 K for 35 K, if no conversion heat is considered. Now, as the conversion happens, *ortho* fraction increases from ~51 to ~67% for 100 K inlet temperature and to 65% for 35 K. Thus the maximum possible fraction of *para* hydrogen present at 100 K hydrogen is converted into *ortho* fraction hydrogen due to the higher temperature evolution inside the system compared to that converted at 35 K. It also is possible that the sensible heat of *para* hydrogen influences for temperature reduction because the effect by sensible heat is predominant at 100 K than at 35 K. These results suggest that the temperature reduction due to *para* to *ortho* conversion helps to charge more hydrogen into the system. The evolution of pressure in the system at four inlet temperatures is given in Fig. 8 (right panel). It can be seen that the pressure in tank is dropped when *para–ortho* conversion is taken into account, which is due to decreased tank temperature. In general, the pressure shows similar behaviour for all inlet temperatures as shown in Fig. 8 (right panel).

To account for the observed temperature evolution in the tank, we modelled the system's temperature and heats at the point T4 when 77 K hydrogen is charged into the tank by considering the contributions of adsorption heat, heat due to pressure-volume work and the conversion heat, separately. In Fig. 9 left and right panels the heats and the temperature evolution at the point T4 during the charging are shown. First, when only the pressure work is considered, the temperature of the system initially decreased to 56 K at about 1000 s from the initial 80 K. After this, the temperature rises to nearly 80 K as the filling progresses. As discussed previously, the initial decrease is explained as hydrogen undergoes expansion below its inversion temperature. While the charging is in progress, the temperature of the tank increases owing to the heat produced by pressure work. When the heat due to adsorption alone is considered, temperature at T4 increases to 127 K, due to endothermic adsorption process. If both the adsorption heat and pressure work heat are considered, the resulting temperature at T4 increases to 135 K from 80 K. If conversion heat is considered along with the other forms of heat, the final temperature decreases by 10 K. In summary, the heat of adsorption (Q_a) and heat generation due to the pressure work (Q_p) causes the temperature at T4 to rise while the endothermic conversion reduces the temperature.

To understand the effect of conversion on the storage capacity, we compared the final gas phase mass and adsorbed mass of the storage system without conversion and with conversion during the charging stage. Fig. 10 shows the effect of *para–ortho* conversion on the storage system capacity; we find that the gas phase mass (mg) is larger in the storage system without conversion than the gas phase mass (mg-C) of the system with conversion. In other words, the adsorbed phase (ma) has lower mass of hydrogen without conversion than has with conversion (ma-C). The total mass of hydrogen (mt) is the same in the both cases because of the same mass

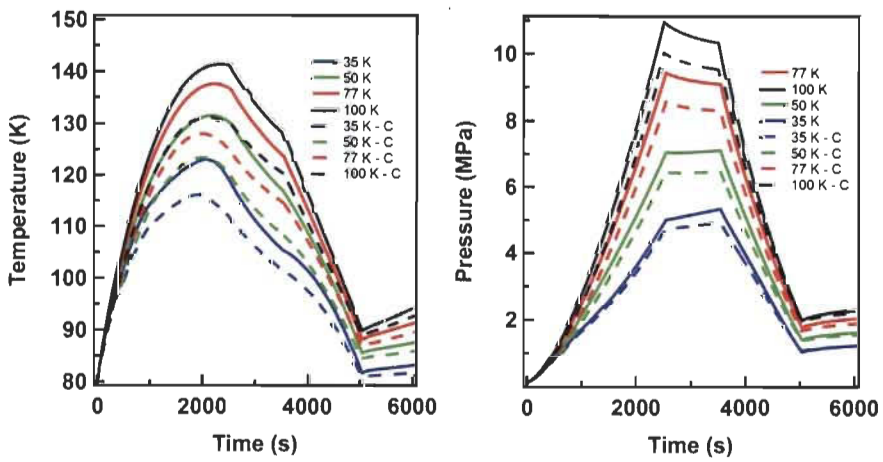

Fig. 8 – (Left panel): Temperature and (right panel) pressure profiles at T4 in the tank with (solid lines) and without (dashed lines) taking into account the *ortho–para* conversion at 4 inlet temperatures.

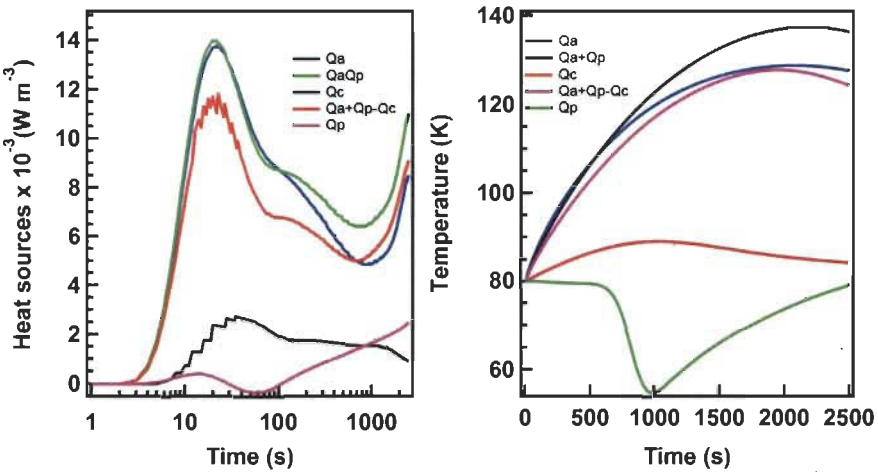

Fig. 9 – (Left panel): Heat source and (right panel) temperature profiles at the point T4 when different heat source terms are considered separately.

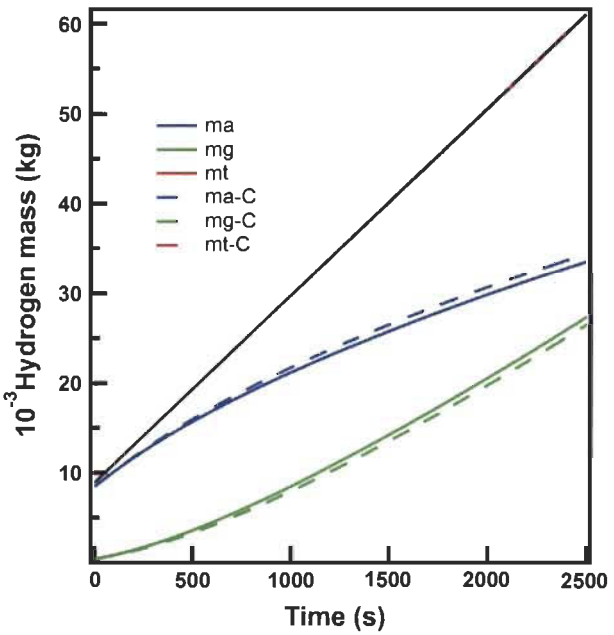

Fig. 10 – Hydrogen mass balance in the system with and without conversion.

flow rate and filling time. To conclude, due to the lowering of the system temperature by *para–ortho* conversion, the adsorbed phase mass increases and the gas phase mass decreases in the storage system which help to fill more hydrogen gas into the system at the storage conditions studied than that can be filled when no conversion takes place.

Conclusions

In conclusion, we developed a two-dimensional axisymmetric geometric hydrogen storage system model which takes into account the *para–ortho* conversion to predict of coupled heat and mass transfer of the storage system and implemented it in the computational software COMSOL multiphysics 4.3a platform [27]. The validity of the base model was established by comparing the simulated temperatures at various points in the tank with those obtained from an experimental bench test performed using Maxsorb. The validated base model is extended to check the adaptability to a storage system filled with MOF-5 at cryogenic temperature and the mass balance is verified. This showed that the hydrogen gas expansion at below inversion temperature, i.e., 193 K and hydrogen desorption from MOF-5 bed induce a cooling effect at the central point of tank filled with MOF-5 tank at cryogenic condition. The base model is further extended to study the effects of endothermic *para* to *ortho* hydrogen conversion in a storage system filled with MOF-5 at cryogenic temperatures, assuming that the conversion occurs with no kinetic limitation. The obtained results revealed that the endothermic conversion reduces the system temperature; this is supported by the analysis of the various heat sources and the corresponding temperatures. Finally, the effect of conversion on the storage mass shows that the conversion helps to fill more hydrogen in the storage tank. The conversion gain is larger at higher temperature (100 K) than that at the lower temperature (35 K) even if the percentage of *para* hydrogen is larger at lower temperature.

Acknowledgement

The authors acknowledge the Natural Science and Engineering Research Council (NSERC) of Canada, Air Liquide, and the H2Can Network for providing the financial support for this work.

REFERENCES

[1] Panella B. Hydrogen storage by physisorption on porous materials [Thesis]. Stuttgart, Germany: Max-Planck-Institut für Metallforschung; September 2006.

[2] Richard M-A, Cossement D, Chandonia P-A, Chahine R. Preliminary evaluation of the performance of an adsorption-based hydrogen storage system. AIChE J 2009;55:2985–96.
[3] Ahluwalia RK, Hua TQ, Peng JK. On-board and off-board performance of hydrogen storage options for light-duty vehicles. Int J Hydrogen energy 2012;37:2891–910.
[4] Jorgensen Scott W. Hydrogen storage tanks for vehicles: recent progress and current status. Curr Opin Solid State Mater Sci 2011;15:39–43.
[5] Xiao J, Zhou T, Bénard P, Chahine R. Thermal effect simulation of hydrogen cryo-adsorption storage system. J Renew Sustain Energy 2013;021415:1–10.
[6] Meagher James Patrick. Modeling of hydrogen liquefiers with kinetic conversion of *ortho* to *para* hydrogen in plate-fin heat exchangers [Thesis, Department of Chemical and Biological Engineering, University at Buffalo]. USA: State University of New York; April 22–2008.
[7] Petitpas G, Aceves SM, Matthews MJ, Smith JR. Para-H2 to ortho-H2 conversion in a full-scale automotive cryogenic pressurized hydrogen storage up to 345 bar. Int J Hydrogen Energy 2014;39:6533–47.
[8] Peng JK, Ahluwalia RK. Enhanced dormancy due to para-to-ortho hydrogen conversion in insulated cryogenic pressure vessels for automotive applications. Int J Hydrogen Energy 2013;38:13664–72.
[9] Weitzel DH, Loebenstein WV, Draper JW, Park OE. Ortho–para catalysis in liquid–hydrogen production. J Res Nat Bur Stand 1958;60:221–7.
[10] Buntkowsky G, Walaszek B, Adamczyk A, Xu Y, Limbach HH, Chaudret B. Mechanism of nuclear spin initiated *para*-H2 to *ortho*-H2 Conversion. Phys Chem Chem Phys 2006;8:1929–35.
[11] Minaevt Boris F, Agren Hans. Spin catalysis of ortho–para hydrogen conversion. J Phys Chem 1995;99:8936–40.
[12] FitzGerald SA, Hopkins J, Burkholder B, Friedman M. Quantum dynamics of adsorbed normal- and para-H2, HD, and D2 in the microporous framework MOF-74 analyzed using infrared spectroscopy. Phys Rev B 2010;81:104305.
[13] FitzGerald SA, Allen K, Landerman P, Hopkins J, Matters J, Myers R. Quantum dynamics of adsorbed H_2 in the microporous framework MOF-5 analyzed using diffuse reflectance infrared spectroscopy. Phys Rev B 2008;77:224301.
[14] Falcaro Paolo, Normandin Francois, Takahashi Masahide, Scopece Paolo, Amenitsch Heinz, Costacurta Stefano, et al. Dynamic control of MOF-5 Crystal positioning using a magnetic field. Adv Mater 2011;23:3901–6.
[15] Ahluwalia RK, Hua TQ, Peng JK, Roh HS, Bailey J, Kumar R. System Level Analysis of Hydrogen Storage Options. Presentation for DOE Hydrogen Program Review; May 14–18, 2012. pp. 12–6. Washington, DC, USA.
[16] Hardy B, Corgnale C, Chahine R, Richard M-A, Garrison S, Tamburello D, et al. Modeling of adsorbent based hydrogen storage systems. Int J Hydrogen Energy 2012;37:5691–705.
[17] Xiao J, Wang J, Cossement D, Bénard P, Chahine R. Finite element model for charge and discharge cycle of activated carbon hydrogen storage. Int J Hydrogen Energy 2012;37:802–10.
[18] EW Lemmon MLH, McLinden MO. NIST standard reference database 23: reference fluid thermodynamic and transport properties-REFPROP. Gaithersburg: National Institute of Standards and Technology, Standard Reference Data Program; 2007. Version 8.0.
[19] Xiao J, Tong L, Deng C, Bénard P, Chahine R. Simulation of heat and mass transfer in activated carbon tank for hydrogen storage. Int J Hydrogen Energy 2010;35:8106–16.
[20] Purewal JJ, Liu D, Yang J, Sudik A, Siegel DJ, Maurer S, et al. Increased volumetric hydrogen uptake of MOF-5 by powder densification. Int J Hydrogen Energy 2012;37:2723–7.
[21] Purewal J, Liu D, Sudik A, Veenstra M, Yang J, Maurer S, et al. Improved hydrogen storage and Thermal conductivity in high-density MOF-5 composites. J Phys Chem C 2012;116:20199–212.
[22] Richard M-A, Bénard P, Chahine R. Gas adsorption process in activated carbon over a wide temperature range above the critical point. Part 1: modified Dubinin–Astakhov model. Adsorption 2009;15:43–51.
[23] Zhou W, Wu H, Hartman RM, Yildirim T. Hydrogen and methane adsorption in metal-organic frameworks: a high-pressure volumetric study. J Phys Chem C 2007;111:16131–7.
[24] Amos Wade A. Costs of storing and transporting hydrogen. Golden, CO, USA: National Renewable Energy Laboratory; 1998.
[25] Larsen AH, Simon FE, Swenson CA. The rate of evaporation of liquid hydrogen due to the ortho–para hydrogen conversion. Rev Sci Instrum 1948;19:266–9.
[26] Aceves SM, Espinosa-Loza F, Ledesma-Orozco E, Ross TO, Weisberg AH, Brunner TC, et al. High-density automotive hydrogen storage with cryogenic capable pressure vessels. Int J Hydrogen Energy 2010;35:1219–26.
[27] Comsol Multiphysics 4.3a version 4.3.1.161 Copyright 1998–2012. Comsol AB.

Nomenclature

C: conversion
C_{pg}: specific heat capacity of hydrogen gas, J kg^{-1} K^{-1}
C_{ps}: specific heat capacity of adsorbent, J kg^{-1} K^{-1}
D_p: particle diameter, mm
κ: permeability, m^2
k_{eq}: equivalent thermal conductivity, W m^{-1} K^{-1}
k_s: thermal conductivity of adsorbent, W m^{-1} K^{-1}
k_g: thermal conductivity of hydrogen gas, W m^{-1} K^{-1}
M_{H2}: molecular mass of hydrogen, kg mol^{-1}
ma: mass of adsorbed phase, kg
mg: mass of a gas phase, kg
mt: total mass, kg
n_a: absolute adsorption amount/unit adsorbent, mol kg^{-1}
n_{max}: limit adsorption amount per unit adsorbent, mol kg^{-1}
p: pressure, Pa
p_0: limiting pressure at which n_{max} is observed, Pa
Q: heat source term, W m^{-3}
Q_a: adsorption heat, W m^{-3}
Q_p: heat produced due to pressure work, W m^{-3}
Q_c: conversion heat, W m^{-3}
q_{st}: isosteric heat of adsorption, J mol^{-1}
R: universal gas constant, J mol^{-1} K^{-1}
S_m: mass source term, kg s^{-1} m^{-3}
T: temperature, K
$\vec{u}$: Darcy velocity vector, m s^{-1}
α: enthalpic factor, J mol^{-1}
β: entropic factor, J mol^{-1} K^{-1}
μ: dynamic viscosity, Pa s
ρ_g: density of hydrogen gas, kg m^{-3}
ρ_s: particle density of adsorbent, kg m^{-3}
ε_b: bed porosity

Article – 2

Effect of flowthrough cooling heat removal on the performances of MOF-5 cryo-adsorptive hydrogen reservoir for bulk storage applications

Siyad Ubaid [*,‡], Renju Zacharia[*,‡], Jinsheng Xiao[‡], Richard Chahine[‡], Pierre Bénard[‡], Pascal Tessier[§]

[‡]Institut de recherche sur l'hydrogène, Université du Québec à Trois-Rivières, P.O. Box 500, Trois-Rivières, Québec G9A 5H7, Canada

[§]Air Liquide Research and Development, Delaware Research and Technology Center, 200 GBC Drive, Newark, DE 19702, USA

Abstract

We numerically investigated the effect of flowthrough cooling heat removal on the storage and thermal performances of a 20 m^3 MOF-5 cryo-adsorptive bulk hydrogen reservoir. To validate the models, detailed experimental measurements of flowthrough cooling using a 2.5 L storage tank filled with MOF-5 are used for the first time. As the hydrogen gas is charged into the large reservoir, the temperature of the system raise from 77 to 121 K. When the flowthrough cooling is active for ~30 hrs, the average temperature of the adsorbent bed is cooled down to 77 K; this results in a hydrogen storage capacity of 460 kg at tank's maximum pressure of 4 MPa, which is even higher than the storage capacity of a cryo-compressed hydrogen tank equilibrated at 77 K and 4 MPa. Our work establishes that flowthrough cooling is an efficient heat removal approach for bulk hydrogen reservoirs filled with MOF-5.

Available online at www.sciencedirect.com

ScienceDirect

journal homepage: www.elsevier.com/locate/he

Effect of flowthrough cooling heat removal on the performances of MOF-5 cryo-adsorptive hydrogen reservoir for bulk storage applications

Siyad Ubaid [a,*], Renju Zacharia [a,**], Jinsheng Xiao [a], Richard Chahine [a], Pierre Bénard [a], Pascal Tessier [b]

[a] Institut de recherche sur l'hydrogène, Université du Québec à Trois-Rivières, P.O. Box 500, Trois-Rivières, Québec G9A 5H7, Canada

[b] Air Liquide Research and Development, Delaware Research and Technology Center, 200 GBC Drive, Newark, DE, 19702, USA

ARTICLE INFO

Article history:
Received 27 February 2015
Received in revised form
8 May 2015
Accepted 16 May 2015
Available online 12 June 2015

Keywords:
Hydrogen storage
Adsorption
Metal-organic frameworks
Flowthrough heat removal
System modelling
Bulk reservoir

ABSTRACT

We numerically investigated the effect of flowthrough cooling heat removal on the storage and thermal performances of a 20 m^3 MOF-5 cryo-adsorptive bulk hydrogen reservoir. To validate the models, detailed experimental measurements of flowthrough cooling using a 2.5 L storage tank filled with MOF-5 are used for the first time. As the hydrogen gas is charged into the large reservoir, the temperature of the system raise from 77 to 121 K. When the flowthrough cooling is active for ~30 h, the average temperature of the adsorbent bed is cooled down to 77 K; this results in a hydrogen storage capacity of 460 kg at tank's maximum pressure of 4 MPa, which is even higher than the storage capacity of a cryo-compressed hydrogen tank equilibrated at 77 K and 4 MPa. Our work establishes that flowthrough cooling is an efficient heat removal approach for bulk hydrogen reservoirs filled with MOF-5.

Introduction

Bulk reservoirs in which hydrogen is stored conventionally as compressed gas (CGH_2) or cryogenic liquid (LH_2) are important supply-chain elements used in state-of-the-art hydrogen refuelling and dispensing stations, tube-trailer loading terminals and centralized hydrogen production facilities. Hydrogen stored in these reservoirs, nevertheless, suffers from technical limitations such as low net volumetric energy density in the case of CGH_2 and fuel-loss due to liquid hydrogen boil-off in the case of LH_2 [1–3]. Adsorptive hydrogen storage on microporous metal-organic frameworks (MOFs) is a potential alternative hydrogen storage approach which could overcome the above limitations of conventional hydrogen storage technologies [4,5]. However, unlike CGH_2 approach, adsorptive hydrogen storage approach requires the hydrogen stored in the adsorbent medium to be maintained at

* *Corresponding author.* Tel.: +1 819 376 5011x4463.
** *Corresponding author.* Tel.: +1 819 376 5011x3433; fax: +1 819 376 5164.
E-mail addresses: siyad.ubaid@uqtr.ca (S. Ubaid), renju.zacharia@uqtr.ca (R. Zacharia), Jinsheng.Xiao@uqtr.ca (J. Xiao), Richard.Chahine@uqtr.ca (R. Chahine), Pierre.Benard@uqtr.ca (P. Bénard), pascal.tessier@airliquide.com (P. Tessier).
http://dx.doi.org/10.1016/j.ijhydene.2015.05.097

cryogenic temperatures for attaining high volumetric storage density [6]. Furthermore, unlike in the case of LH_2 storage, as the filling of hydrogen gas into adsorptive tanks generates significant amounts of heat due to both exothermic adsorption and gas compression, appropriate heat management strategies should be implemented to minimize the heat swings during hydrogen filling and discharging [7].

Removal of heat from adsorptive bed is expected to be difficult due to adsorbents' poor thermal conductivity. For example, the room temperature thermal conductivity of MOF-5 which is the primary candidate adsorbent down selected by the Hydrogen Storage Engineering Center of Excellence for cryo-adsorptive vehicular hydrogen storage, is 0.3 $Wm^{-1}\ K^{-1}$ which is nearly two orders of magnitude less than that of stainless steel. Heat removal becomes even more problematic at cryogenic temperatures as MOF-5's thermal conductivity decreases further to less than 0.1 $Wm^{-1}\ K^{-1}$ at cryogenic temperatures [8]. A common approach used for enhancing the heat removal from the adsorbent bed is incorporating thermally conducting adsorbent additives in the bed which improves the bed's overall thermal conductivity. Liu et al. [8] and Purewal et al. [9] explored the effect of expanded natural graphite (ENG) additive on room temperature thermal conductivity of MOF-5. They found that the room temperature thermal conductivity of neat MOF-5 can be enhanced to up to 5 times by forming composite pellets with 10% ENG, while at 77 K, the thermal conductivity enhances to only up to ~3 times [8,9]. On the downside, ENG additive diminishes the hydrogen storage capacity of composite pellets by up to 10% relative to neat MOF-5 which is attributed to the former's lower specific surface area. The application of this method relies on optimizing the composites' composition and pellet densities and also performing detailed parametric studies on the heat removal characteristics of optimized composites. Inclusion of non-adsorbing metallic components in the adsorbent bed to compensate the adsorbent's poor thermal conductivity is a similar approach to enhance the thermal management inside cryo-adsorbent hydrogen storage systems. Chakraborty and Kumar modelled how an electrically heated intra-reservoir helical element accommodates the thermal requirements during endothermic hydrogen desorption from MOF-5 and AX-21 hydrogen storage systems [10]. An important conclusion they made is that for optimum hydrogen extraction from the adsorbent bed, the thermal conductivity of the bed should be at least 0.5 $W\ m^{-1}\ K^{-1}$, higher than that of neat MOF-5. One could attribute this to inadequate interfacial contact between the heating element and the adsorbent; so the thermal conductivity of the adsorbent bed still is required to be high to facilitate uniform bed temperature distribution and faster heat removal. Ahluwalia and Peng modelled adiabatic refuelling of hydrogen into an adsorptive vehicular hydrogen storage tank in which the activated carbon adsorbent is packed inside a 40-PPL 2024 aluminium alloy foam. The alloy form and an added in-tank heat exchanger are used to compensate for the adsorbent's poor thermal conductivity [11]. Due to non-adsorbing nature of heat transfer components, these approaches reduce the net volumetric hydrogen density of the storage system [11,12]. An alternative method for heat removal is passing cold hydrogen through the storage reservoir contains storage material to transfer heat by convection [13]. Schuetz et al. invented a hydrogen recirculation system where the adsorptive heat from the bed is removed convectively by continuous flowing of cold hydrogen gas [14]. Briefly, this system consists of a loop of hydrogen gas using which the gas is introduced into the storage system and any non-adsorbed hot gas is recirculated back into a refrigeration unit, the hot gas is cooled and then reintroduced into the storage vessel. Numerical simulations of hydrogen charging into activated carbon tanks enabled with combined hydrogen recirculation cooling system and liquid nitrogen cooling system indicated much shorter cooling time than that would result when only conductive heat transfer though the storage tank walls was considered [15]. In much recent works, Hardy et al. and Corgnale et al. performed numerical simulation of 'flowthrough cooling' heat removal technique for hydrogen charged into 2.5 L storage tank filled with MOF-5 using a model that was validated using experiments with the activated carbon [7,16]. In this approach the adsorbent was maintained at cryogenic temperatures by the flow of cold hydrogen at a rate of up to 100 standard litres per minute (SLPM). They concluded that no additional cooling system is required when flowthrough cooling approach is implemented. Senthil Kumar et al. likewise used a complementary approach of recirculating the storage bed with hot hydrogen gas to transfer heat into storage bed which enhanced the hydrogen desorption [17]. They suggested that heating the bed through recirculation method is more preferred than by electrical heating due to the higher interfacial area between the gas and the adsorbent. Although the flowthrough method is increasingly considered as an efficient heat transfer mechanism for adsorptive hydrogen storage systems, all reported studies, except those in Refs. [7] and [16], are performed using solely computational simulations while experimental measurements of flowthrough are only beginning to emerge. Available experiments reported in Refs. [7] and [16], on the other hand, used flowthrough characteristics measured using activated carbon systems to model that of MOF-5 cryo-adsorptive hydrogen storage systems. While the authors observed reasonable agreements between the simulation and experiments on activated carbon, the discrepancies were attributed to experimental measurements as well as material property data used in their simulations. For instance, the cryogenic heat capacity of Maxsorb used in their simulation is estimated from the room temperature data using the general Tarasov correlation for pyrolytic graphite [18] while the cryogenic specific heat capacity of MOF-5 was approximated by scaling [7] the room temperature C_p of Maxsorb. Likewise, the isosteric heat of hydrogen adsorption used in the model is derived using modified Dubinin-Astakhov (D-A) thermodynamic model [7]. Though the model fits the experimental isotherm data of activated carbon very well, model predictions deviate from the isotherms of MOF-5 especially at initial loading [8]. An alternate option is the use of isosteric heats measured with direct calorimetric or isosteric methods [19,20]. Therefore, not only it is necessary to develop experimental benchmarks of flowthrough cooling heat removal from a MOF-5 cryo-adsorptive storage system but also to develop computational simulations by taking into account appropriate experimental conditions and material properties, so that comparison between experiments and simulations can be made on equal

footing. To this end, we implemented an experimental flow-through test-bench equipped with a 2.5 L cryo-adsorptive tank filled with MOF-5 and measured the thermal as well as the storage performances of this system during hydrogen charging (at a rate of 15 SLPM) and flowthrough (at a rate of 20 SLPM). Further to this, a computational fluid dynamics model of hydrogen charging and flowthrough into this MOF-5 cryo-adsorptive storage tank is developed by accommodating initial and boundary conditions from the experiment as well as using experimentally measured thermophysical and physicochemical properties of MOF-5. The model is validated by comparing the simulated temperature, pressure and storage mass during hydrogen charging and flowthrough in the cryo-adsorptive tank with those obtained from an experimental test bench.

For large bulk reservoirs of capacities around 20 m^3, such as those used in hydrogen distribution infrastructures, hydrogen charging is done at rates of around 10000 SLPM, – much faster than the charging rates typically considered for vehicular subscale prototype reservoirs simulations and experiments [21,22]; this faster charging rate is expected to render flowthrough cooling more effective [7,16]. For large adsorptive storage reservoirs heat removal might rely on solely flowthrough as liquid nitrogen cooling is less feasible due to the scale of the system. While direct experimental measurements using bulk reservoirs are impractical, we scale up our validated flowthrough model to study the effect of flowthrough cooling on the thermal and storage performances of a 20 m^3 MOF-5 cryo-adsorptive bulk reservoir filled at a rate of 10000 SLPM with 77 K hydrogen until a maximum pressure of 4 MPa.

Experimental section

Flowthrough experimental setup

The schematic of the bench-scale test system used to probe hydrogen charging and flowthrough is shown in Fig. 1. A detailed description of the adsorptive storage tank geometry is presented elsewhere [7,16]. The test bench consists of a charging manifold, discharging manifold and flowthrough manifold all tethered to a 2.5 L stainless steel tank filled with MOF-5 adsorbent. For charging experiments, hydrogen gas (99.999%, Praxair) is admitted into the tank by means of a thermal mass flow controller (TMFC, Brooks 0–100 SLPM) and a back pressure regulator (BPR, TESCOM) installed on the charging manifold. A bypass manifold and a manual valve connected across TMFC help to maintain the required 50 psia pressure difference between the inlet and outlet of TMFC at the start of flow control. Once admitted into the tank, the pressure of the hydrogen gas is monitored using a pressure transducer, PT (Dresser DXD, 0–3000 psia). For cryogenic charging tests, hydrogen gas is pre-cooled to ~80 K before it enters the storage tank by means of a helical cooling loop immersed inside a liquid nitrogen (LN_2)-filled 40 L cryogenic vessel, while the storage tank is vertically immersed in a 125 L cryogenic vessel (CryoFAB) filled with LN_2. Nine k-type thermocouples are attached along the axial (T_1–T_6 along axial from top to bottom) and radial (T_7–T_9 along radial from axis to tank wall) directions within the tank to monitor spatial distribution of tank temperature, while a single k-type thermocouple inserted at the entrance of storage tank monitors the inlet hydrogen's temperature. To isolate hydrogen manifolds from the storage tank, two all-metal valves (Swagelok) are attached on entrance and exit of the tank. To measure the flow of the gas during discharging and flowthrough, two thermal mass flowmeters are used (TMFR, Brooks 0-30 SLPM, Bronkhorst TMFC (0-150 SLPM). A rotary vane pump is attached to the charging manifold to evacuate the whole system prior to all experiments. The data acquisition and control of valves, mass flow controllers and temperature sensors are made possible using National Instruments Compact FieldPoint communication system which is interfaced to PC using NI LabVIEW professional development software suite. Pressure data are acquired by interfacing the transducer to PC using RS-232 Serial communication protocol.

Sample loading and void volume measurement

MOF-5 required in our tests is obtained from BASF. Since this adsorbent is sensitive to moisture and air, it was stored and handled within a dry argon-filled glove box workstation. After embedding thermocouples in the storage tank, the tank is transferred into the glove box and 358 g of MOF-5 is added into the tank. After filling, all-metal valves on both sides of the tank are closed until the tank is re-engaged back into the test bench setup. Once attached, the argon gas is out-gassed by means of the mechanical pump. Empty tank volume, manifold volume (volume between MFC and all-metal valve of tank inlet) and the void volume of MOF-5 tank are estimated by admitting known amounts of ultrapure helium (99.999%, Praxair) into the system. Void volume measurements with MOF-5 are carried out at room temperature and final

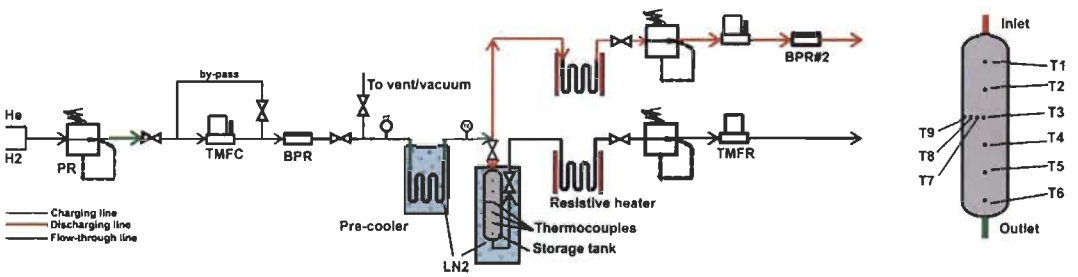

Fig. 1 – Schematic representation of flowthrough experimental test bench.

equilibrium pressures of less than 2 MPa so as to minimize any potential He adsorption. Finally, the volumes are calculated from known mass flow rates of helium, final equilibrium pressure and temperature by considering the mass balance before and after helium is introduced into the tank. The gas densities of He gas are determined using the equation of state (EOS) of real gas available at NIST REFPROP Standard reference database. The resulting data are shown in the volume calibration table (Table 1). The volume of the upper hemisphere of the tank where there is no MOF-5 is estimated from geometry of the tank and the quantity of MOF-5.

Stationary storage, charging and flowthrough experiments

In order to compare the hydrogen uptake capacity of MOF-5 with those reported elsewhere, we measured excess adsorption using the test bench. This is done using step-by-step introduction of hydrogen gas into the MOF-5 tank, much similar to the protocol followed in conventional volumetric measurements. After reaching the thermal equilibrium, the pressure and temperature are recorded. The hydrogen gas densities are determined using the EOS of real gas from NIST REFPROP. For stationary charging tests all-metal valve at the exit is maintained closed while it is kept open for the flow-through tests. To carry out stationary charging, tank is initially equilibrated at 77 K and pre-cooled hydrogen is admitted into the tank until a maximum pressure of 9 MPa. For this base model validation, the initial pressure and mass flow rate are set to 0.822 MPa and 15 SLPM. To perform the flowthrough cooling experiments, the storage tank is charged with 77 K hydrogen at a flow rate of 20 SLPM to a maximum pressure of ~1.15 MPa while the back pressure regulator, BPR#2 of the tank is adjusted to control and maintain the set pressure of 1.1 MPa. Once the pressure stabilized at1.1 MPa, the BPR is opened and the excess pressure due to further charging hydrogen is released outside of the tank. In order to avoid complication in the test bench experiments, we vented the excess hydrogen and continued charging using fresh cold hydrogen instead of recirculating it after passing through external heat exchangers. This process is continued till the average temperature of the bed reached to maximum possible lowest temperature of 80 K.

Material properties of MOF-5, hydrogen and stainless steel

Accurate thermophysical and physicochemical properties of all materials used in the simulation are necessary to obtain comparable results with experiments. These properties include specific heat capacity, thermal conductivity, isosteric heat of adsorption, bulk densities, etc. The properties of hydrogen and stainless steel are adapted from in the literature, while most of the properties of MOF-5 are measured. To calculate the thermodynamic properties of gaseous hydrogen we use the real gas EOS implemented in the NIST Standard Reference Database [23]. Temperature dependent thermal conductivity and specific heat capacity of stainless steel tanks are obtained from the polynomial correlation [24]:

$$\begin{aligned}\log[k\ (Wm^{-1}K^{-1})] = &-1.4087 + 1.3982\ [\log\ (T\ (K))\ ] \\ &+ 0.2543\ [\log\ (T\ (K))]^2 \\ &- 0.6260\ [\log\ (T\ (K))]^3 \\ &+ 0.2334\ [\log\ (T\ (K))]^4 \\ &+ 0.4256\ [\log\ (T\ (K))]^5 \\ &- 0.4658\ [\log\ (T\ (K))]^6 \\ &+ 0.1650\ [\log\ (T\ (K))]^7 \\ &-\ 0.0199\ [\log\ (T\ (K))]^8 \end{aligned} \quad (1)$$

$$\begin{aligned}\log\ [C_p(J\ kg^{-1}K^{-1})] = &\ 22.0061 - 127.5528\ [\log\ (T\ (K))\ ] \\ &+ 303.647\ [\log\ (T\ (K))]^2 \\ &- 381.0098\ [\log\ (T\ (K))]^3 \\ &+ 274.0328\ [\log\ (T\ (K))]^4 \\ &- 112.9212\ \ [\log\ (T\ (K))]^5 \\ &+ 24.7593\ [\log\ (T\ (K))]^6 \\ &- 2.239153\ [\log\ (T\ (K))]^7 \end{aligned} \quad (2)$$

Density of stainless steel used is 7830 kg m^{-3} [25] Heat capacity of MOF-5 used is the one measured in temperature range of 2–300 K by combining the measurements using a Calvet calorimeter and a direct adiabatic relaxation calorimeter [20]. The measured heat capacities, which in the range of 100–800 (J kg^{-1} K^{-1}) are fitted with the 5th order polynomial correlations using the Levenberg–Marquardt least-square algorithm:

$$\begin{aligned}C_{p,MOF-5}\ (J\ kg^{-1}K^{-1}) = &\ 0.524 - 8.885\ \times 10^{-3} \times T\ (K) + 9.624 \\ &\times 10^{-5} \times T^2(K) - 3.469 \times 10^{-7} \times T^3(K) \\ &+ 4.417\ \times 10^{-10} \times T^4(K). \end{aligned} \quad (3)$$

Due to the lack of temperature dependent thermal conductivity of MOF-5, we used the data (0.088 W m^{-1} K^{-1}) measured at cryogenic temperature [26]. The isosteric heat of hydrogen adsorption of MOF-5 required for calculating the heat adsorption is measured experimentally using calorimetric method [21]. To determine the isosteric heats using sorption method, independent measurements of isotherms were carried out at different temperatures (77–296 K) and pressure (0–20 MPa) using coupled adsorption calorimetric measurement system. The measured isosteric heat of adsorption, which is in the range of (7000–3200 J kg^{-1}) is implemented in the model using interpolation method. Bulk density of MOF-5 is determined following the procedure given in ASTM standard D 2854-96. The skeleton density of the MOF-5 is estimated by comparing the volumes of empty tank and tank containing MOF-5 obtained from the helium gas flow experiments. The bulk and skeleton density are used to

Table 1 – Volume calibration of different parts of flowthrough test bench system.

Part	Volume (L)
Tank with MOF and charging manifold	2.87
Charging manifold alone	0.58
Upper hemisphere of the tank	0.22
Discharging manifold	0.04

calculate total porosity of the adsorbent bed. The adsorption volume V_a obtained from modified D-A model is used to calculate the microporosity [27]. The bed porosity of the storage system is determined using the microporosity and total porosity. The properties of MOF-5 are summarized in Table 2.

Simulations

Mass and energy conservation equations of hydrogen flowing through MOF-5

We start with a generalized two dimensional axy-symmetrical model of coupled mass–momentum and energy conservation equations which governs the incompressible hydrogen gas flow in free volume. This model is adapted to describe the hydrogen flow through isotropic porous MOF-5 bed. We used the Darcy's law without Ergun's or Brinkman extensions to describe the flow through the porous bed because the estimated Reynolds numbers for hydrogen charging and flow-through tests in the 2.5 L tank are found to be 0.09 and 0.01, respectively. In these laminar flow regimes characterized by Reynolds number <10, Darcy's law is valid. Furthermore, we assumed that Darcian momentum conservation is valid also when hydrogen is charged through the adsorbent bed in large 20 m^{-3} bulk hydrogen reservoir. Although the mass flow rate of 10000 SLPM is applied in this case, small particle diameter of MOF-5 (0.25 μm) renders a borderline Reynolds number of 9.8 for which the flow is still considered to be laminar [28]. This specialized model is adapted for charging or flowthrough scenarios by applying the necessary boundary and initial conditions. The conservation equation of mass–momentum balance is given by:

$$\frac{\partial}{\partial t}(\rho\varepsilon_b) + \nabla\cdot(\rho\vec{u}) = S_m, \tag{4}$$

where ρ, ε_b, and u are the density of the hydrogen gas, the adsorbent porosity and the Darcy velocity of gas flow through the adsorbent, respectively. The mass of hydrogen adsorbed in the sorbent is given by the mass source term, S_m:

$$S_m = -\rho_b M_{H2}\frac{\partial n_a}{\partial t}, \tag{5}$$

where ρ_b, M_{H_2} and n_a are the bed density, molar mass of hydrogen gas and absolute adsorption, respectively. The Darcy velocity of the hydrogen gas flowing through the porous adsorbent is related to the Darcy permeability κ, gas viscosity μ and pressure gradient ∇p:

$$\vec{u} = -\frac{\kappa}{\mu}\nabla p. \tag{6}$$

Darcy permeability is determined from the diameter of the adsorbent particles (D_p = 0.25 μm for MOF-5) [29], and porosity using the relation:

$$\kappa = \frac{1}{150}\frac{D_p^2\varepsilon_b^3}{(1-\varepsilon_b)^2}, \tag{7}$$

Absolute adsorption of hydrogen on MOF-5, n_a is calculated using the modified D-A adsorption model [27,30]. In the modified D-A model, absolute adsorption is related to the state variables, temperature T and pressure P using Eq. (8).

$$n_a = n_{max}exp\left[-\left(\frac{RT}{\alpha+\beta T}\right)^m ln^m\left(\frac{P_0}{P}\right)\right], \tag{8}$$

where R is the universal gas constant, m is the heterogeneity parameter of the sorbent material, n_{max} represents the limiting absolute adsorption corresponding to the limit $p \to p_0$, where p_0 is the saturation pressure. α and β are enthalpy and entropic contributions to the free energy of adsorption. m is typically 2 for microporous activated carbons. For MOF-5 the best fitted value of m can be higher than 2 as shown by recent non-linear regression using 6-parameter modified D-A model [27]. We used the reported best fit value of m = 9.045 [27]. The model parameters are obtained by fitting the modified D-A model with the reported experimental excess hydrogen adsorption on MOF-5 [31]. The model parameters used in our simulations are n_{max} = 67.5 mol kg^{-1}, $P_0 = 2.75 \times 10^{10}$ MPa, α = 3481 J mol^{-1} and β = 153.6 J mol^{-1} K^{-1} [27].

The standard energy balance equation for hydrogen gas flowing through the adsorbent bed is used to describe the thermal response of the storage system. This is given by:

$$(\rho C_p)_{eq}\frac{\partial T}{\partial t} + \rho C_p\vec{u}\cdot\nabla T = \nabla\cdot(k_{eq}\nabla T) + Q. \tag{9}$$

In Eq. (9) $(\rho C_p)_{eq}$ is the equivalent volumetric heat capacity of the adsorbent-gas system. It is given as a combination of the volumetric heat capacities of adsorbed hydrogen and adsorbent, weighed using respective porosity factors:

$$(\rho C_p)_{eq} = \varepsilon_b\rho_g C_{pg} + (1-\varepsilon_b)\rho_s C_{ps}, \tag{10}$$

where ρ_g, ρ_s, C_{pg} and C_{ps} are densities and specific heat capacity of the gas phase and adsorbed phase, respectively. The equivalent conductivity of the adsorbent-gas system is the net conductivity of the medium which includes the conductivity of the adsorbent k_s and that of the gas k_g, weighed using the corresponding porosity factors. It is given by:

$$k_{eq} = \varepsilon_b k_g + (1-\varepsilon_b)k_s. \tag{11}$$

The heat source term Q is the sum of the contributions due to the heat produced by pressure-volume work Q_p and the adsorption heat Q_a. The general three-dimensional (3D) form of the pressure work in energy equation is given by [32]:

$$Qp = \left[\varepsilon_b\frac{\partial p}{\partial t} + (\vec{u}\,.\,\nabla)p\right] \tag{12}$$

Table 2 – Properties of MOF-5.

Adsorption volume, V_a (m^3 kg^{-1})		0.00123
Bulk density, ρ_b (kg m^{-3})		155.60
Skeleton density, ρ_s (kg m^{-3})		2000.00
Total porosity, ε_t	$1-\frac{\rho_b}{\rho_s}$	0.92
Microporosity, ε_{mi}	$\frac{V_a\times M_{H_2}\times\rho_b}{V_{bed}}$	0.191
Bed porosity, ε_b	$\varepsilon_t - \varepsilon_{mi}$	0.73
Specific heat capacity, C_p (J kg^{-1} K^{-1})		T-dependent, exptal [19].
Isosteric heat, q_{st} (J mol^{-1})		Coverage-dependent, exptal [20].
Thermal conductivity, k (W m^{-1} K^{-1})		0.088

where $\vec{u}$ is the superficial velocity or Darcy's velocity through porous media. An expanded form of the above formula for the axisymmetric (2D) geometry is used in current model. Heat of adsorption Q_a is given by:

$$Q_a = \rho_b \frac{\partial n_a}{\partial t} \Delta H, \quad (13)$$

where, ΔH is the isosteric heat of adsorption.

The constituting equations governing the mass and energy conservation are solved using finite element platform COMSOL Multiphysics version 4.4 to obtain the storage and thermal characteristics of the tank [33]. Based on the experimental test bench, a 2D axisymmetric geometry of the 2.5 L storage tank is used for model validation. The storage tank of the experimental test bench consist of adsorbent bed and the thermocouples. However, we neglected the thermocouples in the model and considered only the adsorbent bed. To monitor the variations of temperature and pressure in the simulation, we chose four monitoring points in the axial direction. The monitoring points are T1 (0, 0.33 m), T2 (0, 0.26 m), T3 (0, 0.19 m) and T5 (0, 0.064 m), which are based on the thermocouple positions. The numbers in the parenthesis give the distance of thermocouples from the inlet of the tank. We used default mesh setting of COMSOL. Accordingly, the 2.5 L tank has extra-fine triangular mesh with 4004 domain elements and 1349 boundary elements while the 20 m^3 storage reservoir consists 12,603 domain elements and 1187 boundary elements.

The initial temperature of the tank in the test bench is not uniform but is found to be in the range of 77–79 K. To implement this temperature range in the model as one of the initial conditions in the model, we divided the whole bed domain into different subdomains whose initial temperatures are assigned based on measured temperature data. Although we replenished the lost LN_2 intermittently throughout our experiments, the transient boil-off quantity could not be characterized. Therefore, we assumed a constant heat transfer coefficient of 200 W m^{-2} K^{-1} to describe convection heat transfer from the storage vessel to the liquid and gas phase nitrogen occupying the Dewar. This heat transfer coefficient is based on available experimental data of boiling heat transfer coefficient of a stainless steel block immersed in LN_2 bath [34]. It is known that heat transfer coefficients in boiling nitrogen are extremely difficult to characterize due to complex thermal boundary conditions. In comparison, Paggiaro et al. and Ahluwalia and Peng have used 2000 and 100 W m^{-2} K^{-1}, respectively, as a heat transfer coefficient in their models [11,15].

Results and discussion

Excess adsorption from static storage test

Fig. 2 shows the excess adsorption isotherm of hydrogen on MOF-5 at measured at 77 K using storage test bench. As noted early on these measurements are made using point-by-point introduction of hydrogen gas from the charging manifold into the tank containing MOF-5. The excess adsorption is calculated from the amount of hydrogen gas introduced into the tank and gaseous hydrogen present after adsorption equilibrium is reached. For comparison, we also provide excess adsorption measurement of the same sample (<1 g) performed using our lab-scale volumetric Sievert's apparatus. As seen in the Fig. 2, our measurements agree well with data reported elsewhere [8,31,35].

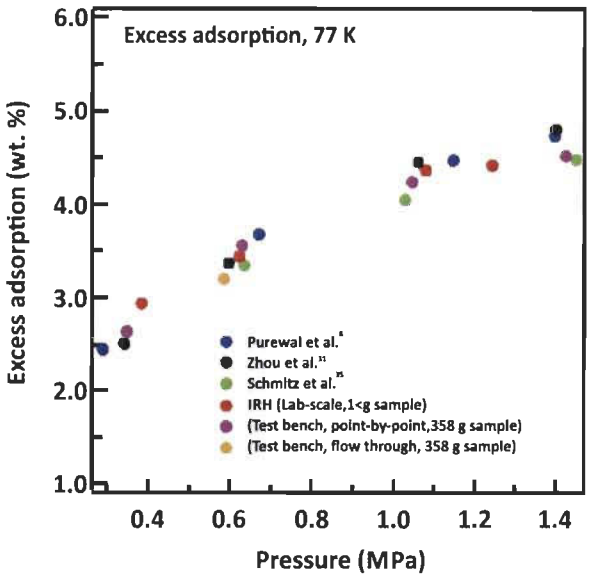

Fig. 2 – Excess adsorption of hydrogen on MOF-5 measured at 77 K using the test bench compared with the lab-scale measurements and data reported previously [8,31,35]. Excess adsorption in flowthrough measurements are carried out after thermal equilibrium is reached.

Hydrogen charging without flowthrough and comparison with the base model

A series of hydrogen charging tests is performed without flowthrough cooling to validate the base simulation model. The MOF-5 tank is initially evacuated to a pressure of 0.822 MPa and is cooled to 77 K by immersing the tank in LN_2 cryogenic vessel. Hydrogen gas pre-cooled to 77 K is admitted into the 2.5 L MOF-5 tank at rate of 15 SLPM until a final pressure of ~9 MPa is reached. In the model, the equivalent mass flow rate is set by a mass flux of 0.0335 kg m^{-2} s^{-1} flowing through the tank inlet orifice of 6.2 × 10^{-4} m^2. To compare the evolution of the distribution of pressure and temperature obtained from the simulation with those measured experimentally four reference thermocouple positions T_1, T_2, T_3 and T_5 in the axial direction are selected. Fig. 3 (left, red) shows the temperature measured along the central axial points in the tank and those obtained from the simulation. While the overall trend of the temperature evolution is clearly reproduced, the temperatures at points T_2 and T_3 are slightly overestimated by <2 K (Fig. 3 (left, green)). We attribute the observed small difference in temperatures to several reasons. First of all, the effects caused by filling MOF-5 into the storage tank containing thermocouples randomly shift the absolute positions of thermocouples by as much as by ±0.3 cm. In addition to this, temperature difference can be

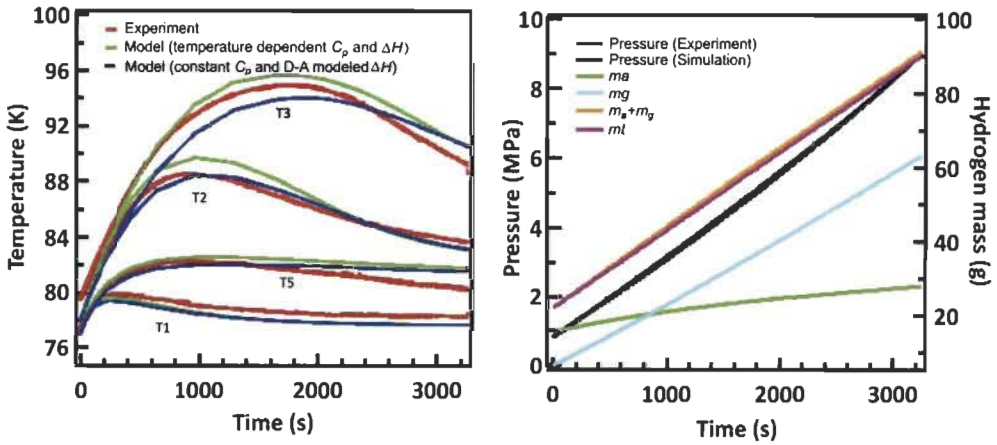

Fig. 3 – Temperature (left), pressure (right) and mass (right) evolution during model validation experiment in which 77 K hydrogen is charged into a 2.5 L cryo-sorptive MOF-5 tank. Model calculations are performed using experimentally measured temperature-dependent specific heats and isosteric heats (green profiles in the left panel) and also assuming a temperature invariant heat capacity (blue profile in the left panel) and isosteric heat derived from modified D-A model. (For interpretation of the references to colour in this figure legend, the reader is referred to the web version of this article.)

caused by non-uniform bulk density of MOF-5. The variation of the powder bulk density within the vessel would affect local heat generation rates, volumetric heat capacity and bed thermal conductivity [7]. Use of a temperature-invariant thermal conductivity in Eq. (11) also may contribute to the observed difference between model and experiment results as the thermal conductivity in the cryogenic regime can vary significantly as a function of temperature.

From Fig. 3 (left) it is seen that the lowest temperature values are recorded at T_1 which is located at the top of the tank. This is anticipated because the top axial points are located near the inlet where the influence of incoming cold hydrogen is predominant. As a result of this temperature lowering, there will be significant adsorption which releases heat into the bed. This heat gets conductively transferred to the central part of the bed, towards points T_2 and T_3. The temperature at the point T_5 is less than that at the central regions due to the poor heat transfer stemming from the lower thermal conductivity of MOF-5 adsorption bed. In one of our previous works [25], we performed simulations assuming a constant specific heat capacity (700 J kg^{-1} K^{-1}) over all temperature range and isosteric heat of hydrogen adsorption estimated from the modified D-A model (Fig. 3, left, blue profile) [36]. On the other hand, here we employed experimentally measured specific heat and isosteric heat. However, this renders no considerable difference in the model predictions at points T_1 and T_5, where the temperatures are lower than 80 K. The most significant difference is observed at the point T_3 where a maximum temperature of 94 K is noted. The higher discrepancy at T_3 can be attributed to slightly higher temperature conductivity of the bed at higher temperature while it is assumed to be constant in the model. The simulated pressure shows good agreement with the experimentally measured one (Fig. 3 (right)). Using the total inflow hydrogen mass (m_t) from the experiment (continuous red line in the right panel) and that from the model ($m_a + m_g$, broken red line in the right panel) adsorbed (m_a) and gas phase masses (m_g), the mass balance of the storage system is verified (Fig. 3, right).

To understand the contributions of various heat source terms on the observed temperature evolution in the tank, we modelled the system's temperature and heats by considering the adsorption heat and the heat due to pressure-volume work separately. The heat sources and the corresponding temperature evolutions displayed in Fig. 4 show that at the beginning of charging that adsorption heat (red profile) is the main contributor to the temperature evolution while as charging progresses, the work due to compression (black profile) crosses over that due to adsorption. As adsorption progresses, the heat released into the bed raises the average bed temperature. This eventually reduces adsorption, and the adsorptive heat is reduced consequently. The pressure work heat source increases in the beginning and stays almost

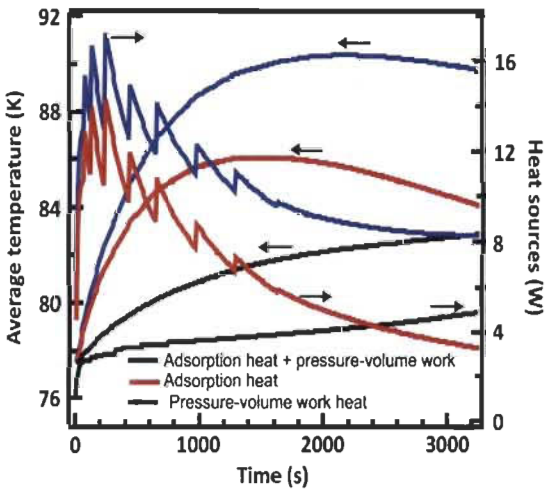

Fig. 4 – Heat source contributions and their influence on bed temperature evolutions as 77 K hydrogen is charged at a rate of 15 SLPM into 2.5 L cryo-sorptive tank filled with MOF-5. Arrows point towards the axis corresponding to the data.

uniform throughout the charging stage. The oscillating behaviour of the heat sources seen in the Fig. 4 is an artefact probably caused by large time steps between the model iterations.

Flowthrough cooling in 2.5 L MOF-5 tank: comparison of experiments and simulation

In order to perform flowthrough tests, 77 K pre-cooled hydrogen is charged into the tank which is initially equilibrated at 77 K and evacuated to 0.065 MPa. Hydrogen is continuously admitted into the tank at a flow rate of 20 SLPM, until a pressure 1.15 MPa is reached. When pressure is stabilized at 1.1 MPa, the BPV#2 is adjusted so that any pressure rise due to further charging is prevented by releasing hydrogen out of the tank by means of the flowthrough manifold (Fig. 1.) As mentioned earlier, the excess hydrogen is vented and charging is continued using fresh cold hydrogen instead of recirculating it after passing through any external heat exchangers. This is continued till the average temperature of the bed reached to maximum possible lowest temperature, 80 K. Even though the test bench has the capability to perform the flowthrough experiment at high operating pressure, we limited the experiment at low pressure. This is because at high operating pressure, larger amount of hydrogen and longer time period are required for cooling the storage system during the flowthrough stage when low mass flow rate, 20 SLPM is used in the experiment. For validating the model, this is avoided by letting the maximum pressure only to be 1.1 MPa.

Fig. 5 compares pressure and temperature histories of tank obtained from experiments and simulations at different tank monitoring points. Due to adsorption/pressure work heat, the bed temperature increases to a maximum of 123 K during the charging stage and then decreases to around 80 K during the flowthrough stage as the heat is transported by flowing hydrogen Fig. 5 (right). At the instant of opening of BPV for releasing the excess pressure causes the sudden short rise and fall of pressure, which can be seen as a characteristic peak in Fig. 5 (left). While overall behaviour of pressure and temperatures are reproduced, the model results are slightly overestimated with respect to the experiments. To understand how flowthrough cooling affects storage capacity and reduction in cooling time, we performed simulation of charging to the same pressure as flowthrough runs but using only external cooling with LN_2 bath, while keeping the inlet hydrogen temperature and charging rate same as that for the flowthrough tests. After the tank pressure and the average bed temperature reached 1.4 MPa and 110 K respectively in 590 s, the charging is stopped and the storage tank is allowed to cool down to 77 K Fig. 6 (left) compares average bed temperature of the tank for flowthrough cooling and LN_2 cooling scenarios. The average bed temperature (blue profile in Fig. 6, left) decreased to ~79 K while the tank pressure decreased to ~0.7 MPa (LN_2). The temperature profile indicates that in the cooling time considered (0.7 h) there is no considerable reduction in the temperature due to flowthrough approach. This is because the flow rate used for charging hydrogen is only 20 SLPM. Faster flow rates are required for flowthrough cooling to be efficient for heat removal [7]. In the right panel of Fig. 6, total amount of hydrogen stored in the system is calculated by summing the masses of hydrogen in the gas-phase and adsorbed phase. This is in very good agreement with the experimentally measured amount of hydrogen. The latter is determined from the difference between in- and out-flow mass flow meters during the experimental flowthrough runs. Gas phase mass increases as charging progresses and it increases slightly throughout the flowthrough stage. Masses of hydrogen, m_a and m_g in the storage system are obtained by the volume integration of adsorbed- and gas-phase hydrogen densities. A significant increase in the adsorbed-phase mass is seen during the flowthrough stage, which is attributed to decreasing tank temperature during the flowthrough stage. In the case of storage system with only LN_2 as a coolant, gas phase mass decreases and adsorbed mass increases, but net storage mass remains same in the both cases.

Flowthrough cooling in MOF-5 cyro-adsorptive hydrogen reservoir for bulk storage applications

For simulating large-scale bulk reservoir filling, we modelled charging 77 K hydrogen into a 20 m^3 reservoir completely filled with MOF-5 until a maximum pressure of 4 MPa is reached. An

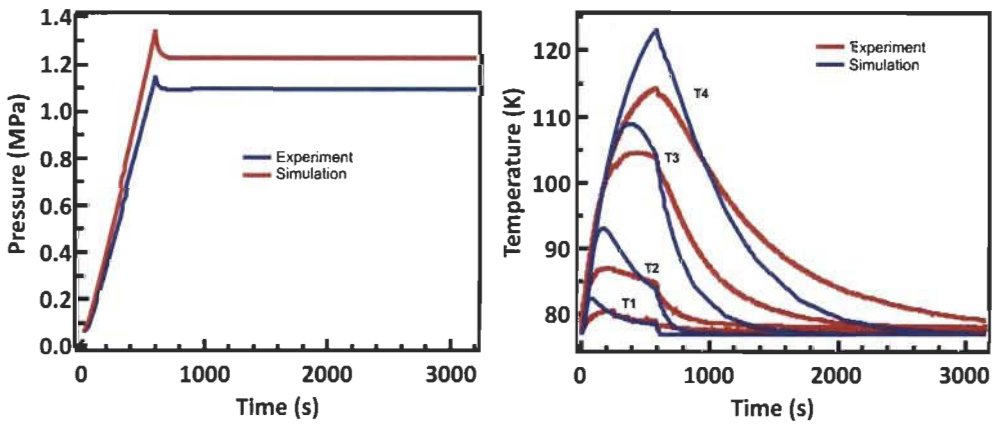

Fig. 5 – (Left). Comparison of experimental pressure with that obtained from the simulation during flowthrough run. (right) Temperatures at various thermocouple points obtained from flowthrough experiments and simulation. Heat removal in these experiments is through combined flowthrough and external LN_2 bath.

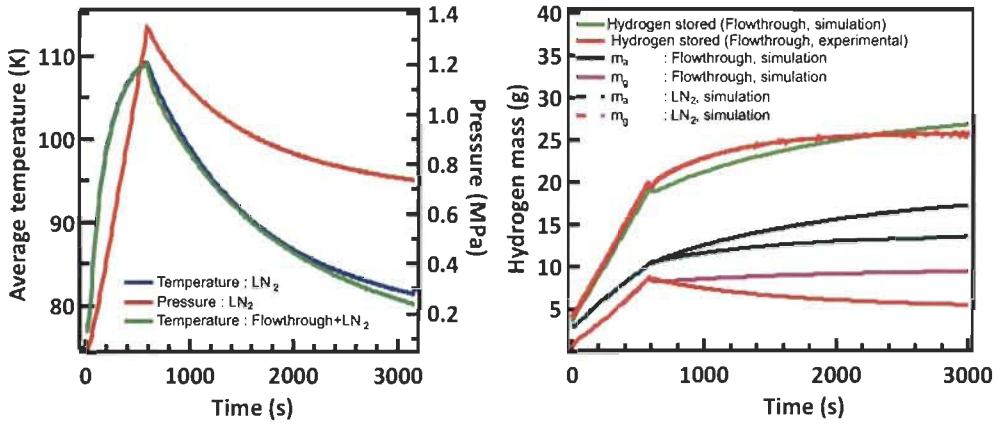

Fig. 6 – Comparison of average bed temperatures (left) and amount of hydrogen stored in the system (right) obtained from flowthrough simulations with those obtained when on LN_2 cooling bath was used. In the right panel, the amount of hydrogen stored during flowthrough experiments are also compared with that obtained from the simulation.

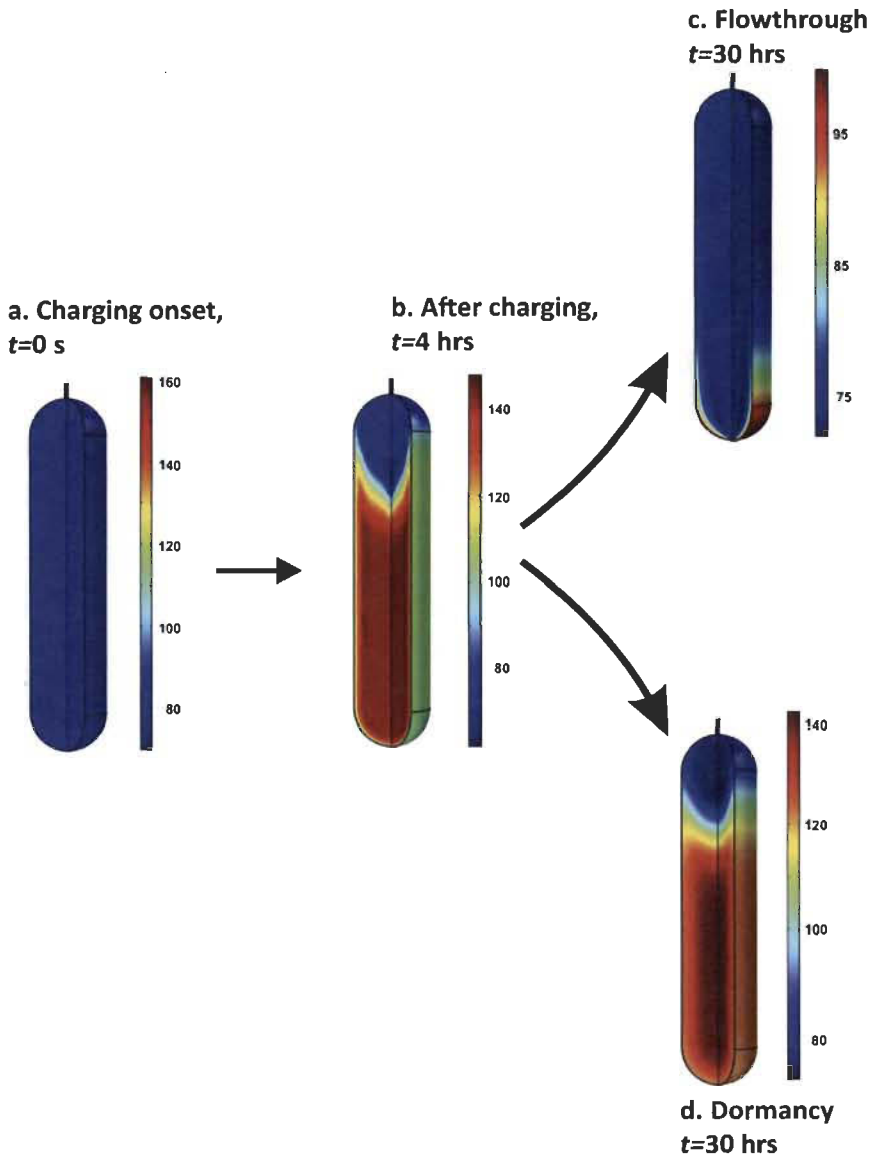

Fig. 7 – Evolution of temperature in 20 m^3 bulk storage tank containing MOF-5. (a) at the onset of charging, (b) after charging hydrogen at a rate of 10000 SLPM, (c) during flowthrough for 30 h and (d) during idling for 30 h (without the flowthrough).

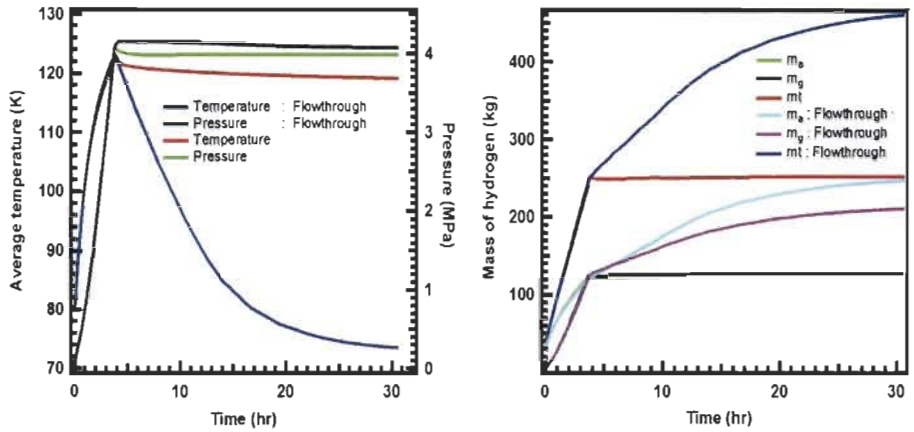

Fig. 8 – (Left) shows average bed temperature and pressure of the storage tank as function of time. (right) Mass of hydrogen stored in the tank with and without flowthrough.

axisymmetric geometry of the 20 m^3 reservoir is used in the simulation. The details of general 2D axisymmetric model and its validation are discussed in the previous sections. An adiabatic well insulated tank is assumed for which the heat leakage rate estimated from daily evaporation rate (%) data of oxygen-filled tank is implemented as a heat flux.[23] Initial pressure and temperature of the reservoir are set to 0.1 MPa and 80 K, respectively and charging is performed at a rate of 10000 SLPM until the maximum pressure (4 MPa) of the reservoir is reached in ~4 h. After reaching the maximum capacity of tank pressure the outlet boundary condition of the tank is set to flowthrough at a constant tank pressure of 4 MPa while the average temperature falls back to almost 77 K in 30 h.

In Fig. 7, snapshots of temperature gradients inside the tank during the flowthrough heat removal is compared with that would happen in the absence of flowthrough. At the onset of charging (Fig. 7a), the system is equilibrated at 77 K with no hydrogen present. As hydrogen is charged into the system, the temperature rises to 121 K. Until the end of charging (Fig. 7b and 4 hr), adsorption enthalpy/pressure work enthalpy enhances the temperature in the bed and the heat front (red hue) conductively transported to the centre of the tank. During the flowthrough (Fig. 7c), the heat is transported out of the vessel by the hydrogen leaving the vessel, indicated by the cold front (blue hue) advancing down. It is noted that the temperature at the top of the tank reduces to less than liquid nitrogen temperature. This is because of the cooling effects contributed by the positive Joule-Thomson effect as hydrogen gas expands while it enters the tank and the cooling effect produced by partial desorption of hydrogen that was initially adsorbed. A tentative scenario if no flowthrough cooling is active is shown in Fig. 7d. Here, after 4 h of hydrogen charging, the system is allowed to be dormancy for 30 h. Poor thermal conduction of MOF-5 bed will cause the system to remain hot at ~121 K as indicated by red hue in Fig. 7d.

At the end of charging, the average pressure and average bed temperature of the tank reach 4 MPa and ~121 K, respectively (Fig. 8, left). During the flowthrough the tank pressure remains stable due to the continuous filling of hydrogen whereas temperature decreases to 77 K. In Fig. 8 (right), the effect of flowthrough cooling on the system storage capacity obtained using mass analysis is shown. The gas-phase mass increases linearly during the charging stage, however the rate decreases during the flowthrough as addition of hydrogen is compensated by simultaneous outflow. Adsorbed phase mass increases throughout the charging and flowthrough regimes. The calculated total mass (m_t) of hydrogen when flowthrough is operational is 460 kg (in 30 h, Fig. 8, right; dark blue). When there is no flowthrough cooling in MOF-5 reservoir, heat of adsorption and heat due to pressure work raise the temperature inside the tank to ~121 K. The maximum amount of hydrogen stored is only ~255 kg as the storage pressure reaches a maximum of 4 MPa when no further storage is possible (Fig. 8, right; red). Within ~5.5 h, a break-even point is reached when the total stored amount of hydrogen in flowthrough system, ~275 kg becomes equal to net storage amount in a cryo-compressed tank with hydrogen maintained at 77 K and 4 MPa. Simulations also show that additional storage capacity of flowthrough cooled system arises because of the increased gas phase density. Above 5.5 h flowthrough cooled cryo-sorptive MOF-5 tank stores significantly more hydrogen than a cryo-compressed storage tank maintained at 77 K and 4 MPa. This suggests that flowthrough cooling is an efficient heat removal strategy suitable for bulk hydrogen reservoirs filled adsorbents, such as MOF-5 provided fast filling rates are applied and the storage system is allowed to completely cool down to its pre-filling temperature.

Conclusions

We have performed a computational fluid dynamics simulation study of hydrogen flowthrough cooling in a 20 m^3 MOF-5 cryo-adsorptive bulk hydrogen reservoir to understand the effects of flowthrough on adsorptive heat removal and system-level storage performance. The relevant computational model makes use of experimentally measured thermophysical and physicochemical properties of MOF-5 and is

validated by experimental measurements of flowthrough cooling using a 2.5 L storage tank filled with MOF-5.

We establish that adsorption heat is the most significant contributor to the heat evolved during hydrogen filling into MOF-5 cryo-sorptive reservoirs, especially at early filling stage. As hydrogen is charged into the tank equilibrated at 77 K, adsorption heat as well as the heat due to pressure-volume work raise the average temperature of tank from 77 to 121 K. By performing the flowthrough cooling for ~30 h, the average temperature of the adsorbent bed can be brought down to 77 K; this results in a hydrogen storage capacity of 460 kg at tanks maximum pressure of 4 MPa, which is even higher than the storage capacity of a cryo-compressed hydrogen tank equilibrated at 77 K and 4 MPa (275 kg). On the other hand, in the absence of flowthrough cooling, poor thermal conductivity of MOF-5 causes the bed to remain at 121 K as the bed idles for 30 h. This results in a much reduced hydrogen storage capacity of 255 kg. Our work suggests that flowthrough cooling is an efficient heat removal approach for bulk hydrogen reservoirs containing with MOF-5 adsorbent, especially when fast filling rates are applied and the storage system is allowed to completely cool down to its pre-filling temperature.

Acknowledgement

The authors acknowledge the Natural Science and Engineering Research Council (NSERC) of Canada, Air Liquide, and the H2Can network for providing the financial support for this work. Authors gratefully acknowledge K.A. Follivi (Institut de recherche sur l'hydrogène, Université du Québec à Trois-Rivières) for providing specific heat capacity and isosteric heat data of MOF-5.

REFERENCES

[1] Berry GD, Aceves SM. Onboard storage alternatives for hydrogen vehicles. Energy Fuels 1998;12:49–55.
[2] Cummings DL, Powers GJ. The storage of hydrogen as metal hydrides. Ind Eng Chem Process Des Dev 1974;13:182–92.
[3] Dinga GP. Hydrogen: the ultimate fuel and energy carrier. J Chem Educ 1988;65:688–91.
[4] Fu J, Sun H. An ab initio force field for predicting hydrogen storage in IRMOF materials. J Phys Chem C 2009;113:21815–24.
[5] Suh MP, Park HJ, Prasad TK, Lim DW. Hydrogen storage in metal-organic frameworks. Chem Rev 2012;112:782–835.
[6] Frost H, Snurr RQ. Design requirements for metal-organic frameworks as hydrogen storage materials. J Phys Chem C 2007;111:18794–803.
[7] Hardy B, Corgnale C, Chahine R, Richard MA, Garrison S, Tamburello D, et al. Modeling of adsorbent based hydrogen storage systems. Int J Hydrogen Energy 2012;37:5691–705.
[8] Purewal J, Liu D, Sudik A, Veenstra M, Yang J, Maurer S, et al. Improved hydrogen storage and thermal conductivity in high-density MOF-5 composites. J Phys Chem C 2012;116:20199–212.
[9] Liu D, Purewal JJ, Yang J, Sudik A, Maurer S, Mueller U, et al. MOF-5 composites exhibiting improved thermal conductivity. Int J Hydrogen energy 2012;37:6109–17.
[10] Chakraborty A, Kumar S. Thermal management and desorption modeling of a cryo-adsorbent hydrogen storage system. Int J Hydrogen Energy 2013;38:3973–86.
[11] Ahluwalia RK, Peng JK. Automotive hydrogen storage system using cryo-adsorption on activated carbon. Int J Hydrogen Energy 2009;34:5476–87.
[12] Karelle C, Joppich F, Wörner A, Tamme R. Tank design for on-board hydrogen storage in metal hydrides. In: Proceedings of ES2008 and energy sustainability 2008; August 10—14. Jacksonville, Florida, USA; 2008.
[13] Golz D, Keller C, Polifke W, Schmidt-Ihn E, Wenger D. Hydrogen reservoir and process for filling a hydrogen reservoir. US patent. US 2009/0127137 A1, May 21, 2009.
[14] Schuetz W, Michl F, Polifke W, Paggiaro R. Storage system for storing a medium and method for loading a storage system with a storage medium and emptying the same therefrom. US patent. US 2008/0020250 A1, Jan. 24, 2008.
[15] Paggiaro R, Michl F, Bénard P, Polifke W. Cryo-adsorptive hydrogen storage on activated carbon. II: Investigation of the thermal effects during filling at cryogenic temperatures. Int J Hydrogen Energy 2010;35:648–59.
[16] Corgnale C, Hardy B, Chahine R, Cossement D, Tamburello D, Anton D. Simulation of hydrogen adsorption systems adopting the flowthrough cooling concept. Int J Hydrogen Energy 2014;39:17083–91.
[17] Kumar VS, Raghunathan K, Kumar SA. Lumped-parameter model for cryo-adsorber hydrogen storage tank. Int J Hydrogen Energy 2009;34:5466–545.
[18] Pyda M, Bartkowiak M, Wunderlich B. Computation of heat capacities of solids using a general Tarasov equation. J Therm Anal 1998;52:631–56.
[19] Follivi KA, Zacharia R, Cossement D, Chahine R. Specific heat capacities of MOF-5, Cu-BTC, Fe-BTC, MOF-177 and MIL-53 over wide temperature ranges: measurements and application of empirical group contribution method. Microporous Mater 2015. http://dx.doi.org/10.1016/j.micromeso.2015.05.047. in press.
[20] Follivi KA, Zacharia R, Cossement D, Chahine R, Balderas-Xicohténcatl R, Oh H, Streppel B, Schlichtenmayer M, Hirscher M. Heats of adsorption on MOFs and Maxsorb: Comparison between adsorption calorimetry, isosteric method and analytical models. 2015. To be submitted for publication.
[21] The volume of the tank can be downloaded from, http://www.cryolor.com/en/notre-offre/cryogenic-storage-vessels/tanks-for-lin-lox-and-lar.html [accessed 10.02.14].
[22] Wang G, Zhou J, Hu S, Dong S, Wei P. Investigations of filling mass with the dependence of heat transfer during fast filling of hydrogen cylinders. Int J Hydrogen Energy 2014;39:4380–8.
[23] W E, Lemmon MLH, McLinden MO. NIST standard reference database 23: reference fluid thermodynamic and transport properties-REFPROP. Gaithersburg: National Institute of Standards and Technology; 2007. Standard Reference Data Program, version 8.0.
[24] Marquardt ED, Le JP, Radebaugh R. Cryogenic material properties database. In: 11th International cryo cooler conference, Keystone, US; June 20–22, 2000.
[25] Ubaid S, Xiao J, Zacharia R, Chahine R, Bénard P. Effect of para-ortho conversion on hydrogen storage system performance. Int J Hydrogen Energy 2014;39:11651–60.
[26] Ahluwalia RK, Hua TQ, Peng JK, Roh HS, Bailey J, Kumar R. System level analysis of hydrogen storage options. In: Presentation for DOE hydrogen program review; may 14—18, 2012. Washington, DC, USA; 2012.
[27] Dundar E, Zacharia R, Chahine R, Bénard P. Performance comparison of adsorption isotherm models for supercritical hydrogen sorption on MOFs. Fluid Phase Equilib 2014;363:74–85.

[28] Xiao J, Tong L, Deng C, Bénard P, Chahine R. Simulation of heat and mass transfer in activated carbon tank for hydrogen storage. Int J Hydrogen Energy 2010;35:8106–16.
[29] Purewal JJ, Liu D, Yang J, Sudik A, Siegel DJ, Maurer S, et al. Increased volumetric hydrogen uptake of MOF-5 by powder densification. Int J Hydrogen Energy 2012;37:2723–7.
[30] Richard MA, Cossement D, Chandonia PA, Chahine R, Mori D, Hirose K. Preliminary evaluation of the performance of an adsorption-based hydrogen storage system. AIChE J 2009;55:2985–96.
[31] Zhou W, Wu H, Hartman RM, Yildirim T. Hydrogen and methane adsorption in metal-organic frameworks: a high-pressure volumetric study. J Phys Chem C 2007;111:16131–7.
[32] Xiao J, Wang J, Cossement D, Bénard P, Chahine R. Finite element model for charge and discharge cycle of activated carbon hydrogen storage. Int J Hydrogen Energy 2012;37:802–10.
[33] Comsol Multiphysics 4.4 version 4.3.1.161 Copyright1998—2012. Comsol AB.
[34] Jin T, Hong JP, Zheng H, Tang K, Zh Gan. Measurement of boiling heat transfer coefficient in liquid nitrogen bath by inverse heat conduction method. J Zhejiang Univ Sci A 2009;10:691–6.
[35] Schmitz B, Müller U, Trukhan N, Schubert M, Férey G, Hirscher M. Heat of adsorption for hydrogen in microporous high-surface-area materials. Chem Phys Chem 2008;9:2181–4.
[36] Richard MA, Bénard P, Chahine R. Gas adsorption process in activated carbon over a wide temperature range above the critical point. part 2: conservation of mass and energy. Adsorption 2009;15:53–63.

Nomenclature

C_{pg}: specific heat capacity of hydrogen gas, J kg^{-1} K^{-1}
C_{ps}: specific heat capacity of adsorbent, J kg^{-1} K^{-1}
D_P: particle diameter, mm
k: permeability, m^2
k_{eq}: equivalent thermal conductivity, W $m^{-1}K^{-1}$
k_s: thermal conductivity of adsorbent, W m^{-1} K^{-1}
k_g: thermal conductivity of hydrogen gas, W m^{-1} K^{-1}
M_{H_2}: molecular mass of hydrogen, kg mol^{-1}
m_a: mass of adsorbed phase, kg
m_g: mass of gas phase, kg
m_t: total mass, kg
n_a: absolute adsorption amount/unit adsorbent, mol kg^{-1}
n_{max}: limit adsorption amount per unit adsorbent, mol kg^{-1}
P: pressure, Pa
P_0: saturation pressure (D-A model), Pa
Q: heat source term, W m^{-3}
Q_a: adsorption heat, W m^{-3}
Q_p: heat produced due to pressure work, W m^{-3}
q_{st}: isosteric heat of adsorption, J mol^{-1}
R: universal gas constant, J mol^{-1} K^{-1}
S_m: mass source term, kg s^{-1} m^{-3}
T: temperature, K
u: darcy velocity, m s^{-1}
α: enthalpic factor, J mol^{-1}
β: entropic factor, J mol^{-1} K^{-1}
μ: dynamic viscosity, Pa s
ρ_g: density of hydrogen gas, kg m^{-3}
ρ_s: particle density of adsorbent, kg m^{-3}
ε_b: bed porosity

Article – 3

Charge-discharge cycling, flowthrough cooling and *para-ortho* conversion for cooling bulk hydrogen storage tank filled with MOF-5

Siyad Ubaid[*a], Renju Zacharia[*a,**], Jinsheng Xiao[a], Richard Chahine[a], Pierre Bénard[a], and Pascal Tessier[b]

[a] Institut de recherche sur l'hydrogène, Université du Québec à Trois-Rivières, P.O. Box 500, Trois-Rivières, Québec G9A 5H7, Canada

[b]Air Liquide Research and Development, Delaware Research and Technology Center, 200 GBC Drive, Newark, DE 19702, USA

Abstract

We numerically studied the thermal and storage performance of the 20 m^3 bulk hydrogen storage reservoir filled with MOF-5. In this study, at first, we present two methods such as charge-discharge cycles and flowthrough cooling for cooling the 20 m^3 bulk hydrogen storage reservoir filled with MOF-5. The results show that cooling of room temperature maintained bulk storage reservoir to 80 K is a time and energy consuming process when flowthrough cooling alone is considered as a cooling option compared to charge-discharge cycles. Further, the effect of mass flow rate on heat removal from the system during the flowthrough stage is investigated. The result shows that high mass flow rate accelerates the heat removal and cool the tank in a short period of time. Also, the effect of *para-ortho* conversion together with flowthrough cooling on temperature reduction in the tank is studied. The results shows that instantaneous *para-ortho* conversion together with flowthrough cooling enhances not only the heat removal from the system but the storage capacity also. The hydrogen mass loss during the 10 days dormancy stage is calculated and found that 28 kg of hydrogen is lost during the dormancy stage.

INTERNATIONAL JOURNAL OF HYDROGEN ENERGY XXX (2015) 1–9

Available online at www.sciencedirect.com

ScienceDirect

journal homepage: www.elsevier.com/locate/he

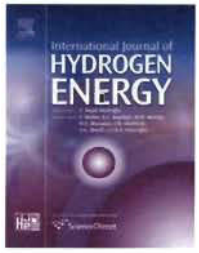

Charge–discharge cycling, flowthrough cooling and *para-ortho* conversion for cooling bulk hydrogen storage tank filled with MOF-5

Siyad Ubaid [a,*], *Renju Zacharia* [a,**], *Jinsheng Xiao* [a], *Richard Chahine* [a], *Pierre Bénard* [a], *Pascal Tessier* [b]

[a] *Institut de recherche sur l'hydrogène, Université du Québec à Trois-Rivières, P.O. Box 500, Trois-Rivières, Québec G9A 5H7, Canada*

[b] *Air Liquide Research and Development, Delaware Research and Technology Center, 200 GBC Drive, Newark, DE 19702, USA*

ARTICLE INFO

Article history:
Received 17 July 2015
Received in revised form
13 October 2015
Accepted 14 October 2015
Available online xxx

Keywords:
Hydrogen storage
Bulk storage reservoir
Charge–discharge cycles
Effect of mass flow rate on flow-through cooling
Para-ortho conversion
Dormancy

ABSTRACT

We numerically studied the thermal and storage performance of the 20 m^3 bulk hydrogen storage reservoir filled with MOF-5. In this study, at first, we present two methods such as charge–discharge cycles and flowthrough cooling for cooling the 20 m^3 bulk hydrogen storage reservoir filled with MOF-5. The results show that cooling of room temperature maintained bulk storage reservoir to 80 K is a time and energy consuming process when flowthrough cooling alone is considered as a cooling option compared to charge–discharge cycles. Further, the effect of mass flow rate on heat removal from the system during the flowthrough stage is investigated. The result shows that high mass flow rate accelerates the heat removal and cool the tank in a short period of time. Also, the effect of *para-ortho* conversion together with flowthrough cooling on temperature reduction in the tank is studied. The results shows that instantaneous *para-ortho* conversion together with flow-through cooling enhances not only the heat removal from the system but the storage capacity also. The hydrogen mass loss during the 10 days dormancy stage is calculated and found that 28 kg of hydrogen is lost during the dormancy stage.

Introduction

Energy is a basic requirement for economic development. Every sector of economy, i.e. agriculture, industry, transport, commercial, and domestic, needs inputs of energy. The growing consumption of energy has resulted in the world becoming increasingly dependent on non-renewable fossil fuels that causes emission of harmful and greenhouse gases [1,2]. Hydrogen has been identified as a potential energy carrier for the future mainly due to its renewability and non-polluting nature [3,4]. However, there are many technical challenges that remain to be solved before hydrogen-based energy economy can become a reality [5,6]. Among them, hydrogen storage is a key challenge in developing hydrogen

* *Corresponding author*. Tel.: +1 819 376 5011x4463; fax: +1 819 376 5164.
** *Corresponding author*. Current address: Gas Processing Center, College of Engineering, Qatar University, P.O. Box 2713 Doha, Qatar. Tel.: +974 7055 4315; fax: +974 4403 4131.
E-mail addresses: siyad.ubaid@uqtr.ca (S. Ubaid), renju.zacharia@qu.edu.qa (R. Zacharia).

http://dx.doi.org/10.1016/j.ijhydene.2015.10.056

Please cite this article in press as: Ubaid S, et al., Charge–discharge cycling, flowthrough cooling and *para-ortho* conversion for cooling bulk hydrogen storage tank filled with MOF-5, International Journal of Hydrogen Energy (2015), http://dx.doi.org/10.1016/j.ijhydene.2015.10.056

economy [7]. In recent years, adsorptive hydrogen storage in microporous material MOF-5 has evolved as one of the most promising adsorptive hydrogen storage materials for on-board applications [8,9]. Even though adsorptive hydrogen storage research focuses primarily on developing the vehicular storage systems, similar approaches may also be useful for developing bulk hydrogen storage tanks, which are typically used at central hydrogen production facilities, transport terminals and end-use locations [10]. These facilities presently use conventional hydrogen storage methods, such as liquid and compressed gas hydrogen, which are inefficient in terms of product loss due to boil-off and low volumetric density [11]. In this juncture, extending the MOF-5 based adsorptive storage approach to bulk hydrogen storage could overcome the aforementioned limitations of conventional methods. However the hydrogen adsorption on MOF-5 causes significant heat release into the adsorbent bed which should be removed in order for not to adversely affect the net capacity of the tank [12]. Even though generation of adsorption heat is relatively low, removing even small amount of heat during refuelling is difficult at cryogenic temperatures. This is because the thermal conductivity of MOF-5 is low, which is less than 0.1 W m^{-1} K at cryogenic temperature [13].

Since desorption of hydrogen from MOF-5 is an endothermic process which removes heat from the bed, adsorption-desorption or charging–discharging cycle is an attractive option for cooling the storage bulk hydrogen storage tank [14,15]. Other cooling options are the flowthrough cooling and endothermic *para-ortho* conversion [16,17]. In our previous studies, we found that no additional cooling system is required when flowthrough cooling and *para-ortho* conversion approaches are implemented in bulk tank (20 m^3) or small tank (2.5 L) storage systems, both maintained at 80 K [18,19]. In the present work, we investigate the cooling performance of the 20 m^3 bulk hydrogen storage reservoir filled with the MOF-5 when charge–discharge cycle, flowthrough cooling and flowthrough together with *para-ortho* conversion are considered as cooling options. The tank is initially maintained at room temperature. To cool the tank to 80 K, we use charge–discharge cycle and flowthrough cooling methods. The effect of mass flow rate on cooling time during the flowthrough stage and the effect of instantaneous *para-ortho* conversion together with flowthrough cooling are investigated. Finally, hydrogen loss rate during the 10 days dormancy stage is calculated. Pilot-level experimentation of bulk-hydrogen storage tank filled with MOF-5 to evaluate its thermal and storage performance is cumbersome, expensive and practically difficult. A convenient alternative approach is to predict such bulk tank's thermal and storage performance using a validated numerical model that accounts the heat and mass transfer and the adsorption model. The study is performed using computational fluid dynamics platform COMSOL multiphysics [20].

Mathematical model

The general mass and energy balance models used to simulate the storage system's performance are given by Refs. [21–23]:

$$\frac{\partial}{\partial t}(\rho\varepsilon_b) + \nabla\cdot(\rho\vec{u}) = S_m. \tag{1}$$

$$(\rho C_p)_{eq}\frac{\partial T}{\partial t} + \rho C_p\vec{u}\cdot\nabla T = \nabla\cdot(k_{eq}\nabla T) + Q. \tag{2}$$

where ρ, ε_b and u are the density of the hydrogen gas, the adsorbent bed porosity of gas flow through the adsorbent and the Darcy velocity, respectively. The Darcy velocity is related to Darcy permeability κ, gas viscosity μ, particle diameter D_p, and pressure gradient ∇p (Darcy law). Darcy velocity and permeability can be written as [21,14]:

$$\vec{u} = -\frac{\kappa}{\mu}\nabla p. \tag{3}$$

$$\kappa = \frac{1}{150}\frac{D_p^2\varepsilon_b^3}{(1-\varepsilon_b)^2}, \tag{4}$$

In Eq. (2) ρC_{peq} and k_{eq} are the equivalent volumetric heat capacity and thermal conductivity of the adsorbent-gas system, respectively, it can be written as [14]:

$$(\rho C_p)_{eq} = \varepsilon_b\rho_g C_{pg} + (1-\varepsilon_b)\rho_s C_{ps}, \tag{5}$$

$$k_{eq} = \varepsilon_b k_g + (1-\varepsilon_b)k_s. \tag{6}$$

where ρ_g, ρ_s, C_{pg}, C_{ps}, k_g and k_s are the densities, specific heat capacities and thermal conductivities of the hydrogen gas and adsorbent, respectively. In eqs. (1) and (2), Sm and Q are the mass and heat source terms. The heat source term Q, consist of adsorption, pressure-work and the conversion heat sources. If no *para-ortho* conversion is taken into account, the heat source term consists only of the adsorption heat and the pressure-work heat sources. The mass, adsorption, pressure work and conversion heat sources can be written as [14,18]:

$$S_m = -\rho_b M_{H2}\frac{\partial n_a}{\partial t}, \tag{7}$$

$$Q_a = \rho_b M_{H2}\frac{\partial n_a}{\partial t}\Delta H, \tag{8}$$

$$Q_p = \varepsilon_b\frac{\partial p}{\partial t} + u_r\frac{\partial p}{\partial r} + u_z\frac{\partial p}{\partial z}, \tag{9}$$

$$Q_c = \frac{d}{dt}\left[(n_a M_{H2}\rho_b(1-f_{PH2})h^{po})\right]. \tag{10}$$

In eqs.(7)–(10), ρ_b, M_{H2}, ΔH, u_r and u_z represent the bed density, molar mass of hydrogen gas, isosteric heat of adsorption and the components of velocity field along the radial and axial directions, respectively. The modified Dubinin–Astakhov (D–A) adsorption model is used to calculate the absolute adsorption n_a in Eq. (7) [23].

$$n_a = n_{max}exp\left[-\left(\frac{RT}{\alpha+\beta T}\right)^m ln^m\left(\frac{P_0}{P}\right)\right], \tag{11}$$

where R = 8.314 J mol^{-1} kg^{-1}, $m = 9$, n_{max} = 67.5 mol kg^{-1}, $P_0 = 2.75\times10^{10}$ MPa, α = 3481 J mol^{-1} and β = 153.6 J mol^{-1} K^{-1} are universal gas constant, heterogeneity parameter, the limiting absolute adsorption corresponding to the limit $p\rightarrow p_0$, where p_0 is the pseudo saturation pressure, enthalpic and entropic contributions to the free energy of adsorption [24]. The

Please cite this article in press as: Ubaid S, et al., Charge–discharge cycling, flowthrough cooling and *para-ortho* conversion for cooling bulk hydrogen storage tank filled with MOF-5, International Journal of Hydrogen Energy (2015), http://dx.doi.org/10.1016/

fraction of *ortho* hydrogen in the equilibrium hydrogen is estimated from the temperature-induced evolution of equilibrium mass fraction of *para* hydrogen using an empirical relation [25]:

$$f_{PH2} = 0.1\left[\exp\left(\frac{-175}{T}\right) + 0.1\right]^{-1} - 7.06 \times 10^{-9}T^3 + 3.42 \times 10^{-6}T^2 - 6.2 \times 10^{-5}T - 0.00227 \quad (12)$$

In Eq. (10), h^{po} is the endothermic conversion enthalpy. Even though REFPROP standard reference database has the enthalpies of ortho and *para* hydrogen, these are defined with the reference states of ortho or *para* hydrogen at the normal boiling point (20.4 K) with zero enthalpy assigned in REFPROP [26]. In order to properly calculate this conversion enthalpy, a common reference state is required. Therefore, the enthalpies of ortho and *para* hydrogen given by the REFPROP are adjusted using a common reference state which is the *p*-hydrogen at 0 K for which the internal energy is at its lowest quantized value. Accordingly, the enthalpy of conversion h^{po} can be written as the sum of the enthalpy from REFPROP, $h^{po}_{(refprop)}$ and the enthalpy with respect to the new reference state, $\Delta h^{po}_{(0\ K)}$:

$$h^{po} = h^{po}_{(refprop)} + \Delta h^{po}_{(0\ K)} \quad (13)$$

$$h^{po} = h^{o}_{(refprop)} - h^{p}_{(refprop)} \quad (14)$$

The enthalpy with respect to new reference state is further expressed as:

$$\Delta h^{po} = \Delta h^{o}_{(0\ K)} - \Delta h^{p}_{(0\ K)} \quad (15)$$

where, Δh^{p}, and Δh^{o} are the enthalpies of *para* and *ortho* at the new reference state (0 K), respectively. The values of Δh^{p}, and Δh^{o} at 0 K are −256.06 kJ kg^{-1} and 444.695 kJ kg^{-1}, respectively [27]. $h^{o}_{(refprop)}$ and $h^{p}_{(refprop)}$ are the enthalpies of *para* and *ortho* hydrogen defined in NIST REFPROP.

Parameters used in the simulation

The modified Benedict–Webb–Rubin real gas equation of state, as implemented in REFPROP is used to calculate the thermodynamics properties such as specific heat capacity, density, viscosity and thermal conductivity of *ortho*, *para* and normal hydrogen [26]. The properties of normal hydrogen are used in the simulation when there is no *ortho-para* conversion is taken into account. The following correlations are used in the model when the effect of *ortho-para* conversion is taken into account [18,27].

$$\rho_g = \left(\frac{f_{oh2}}{\rho_{oh2}} + \frac{f_{ph2}}{\rho_{ph2}}\right)^{-1} \quad (16)$$

$$C_p = f_{oh2}\, C_p^{oh2} + f_{ph2}\, C_p^{ph2} \quad (17)$$

$$k = f_{oh2}\, k_{nh2} + f_{ph2}\ k_{ph2} \quad (18)$$

$$\mu = f_{oh2}\, \mu_{nh2} + f_{ph2}\ \mu_{ph2} \quad (19)$$

$$\gamma = f_{oh2}\, \gamma_{nh2} + f_{ph2}\ \gamma_{ph2} \quad (20)$$

where ρ_g, C_p, k, μ and γ are the density, specific heat capacity, thermal conductivity, viscosity and the ratio of specific heat capacities at constant pressure and constant volume of the hydrogen gas, respectively. As no data of the thermal conductivity, viscosity and the ratio of specific heat capacitates of *ortho* hydrogen in the range of 20–300 K are available in NIST REFPOROP, we used normal hydrogen's equivalent properties. Experimentally measured specific heat capacity of MOF-5 and isosteric heat of adsorption at cryogenic temperatures are used for solving the energy balance equation in model [28,29]. For thermal conductivity of MOF-5 at cryogenic temperatures, we use the reported 0.088 W m^{-1} K^{-1} [17]. Measured bulk density (155.60 kg m^{-3}) and reported skeleton density (2000 kg m^{-3}) are used to calculate total porosity ($\varepsilon_t = 0.92$) of the adsorbent bed [19,30]. Total porosity and adsorption volume V_a obtained from the modified D–A model are used to estimate the bed porosity [19,24]. Material properties, such as thermal conductivity and specific heat capacity of the stainless steel tank are obtained from published correlations: $Y = \sum_{i=0}^{8} a_i (\log T)^i$ [31]. Density of stainless steel used is 7830 kg m^{-3} [14].

We have used the details of Celine 3 type tank from the reference [32] for performing the simulation. The inner and outer radii at the entrance and middle of the 20 m^3 tank are 0.04 m, 0.046 m, 0.907 m and 0.918 m respectively. The internal and external heights of the tank are 8.58 m and 8.98 m, respectively. The maximum allowed pressure of the bulk tank is assumed to be 4 MPa. In the simulation, an adiabatic insulated tank is assumed and the estimated heat leakage rate is calculated and applied in the form of heat flux (0.8287 W m^{-2}) at the outer wall of the tank [19]. For calculating the heat leakage of the storage tank, we use the data of daily evaporation rate (%) of liquid oxygen filled tank. The initial pressure, initial temperature and the mass flow rate are set to 0.1 MPa, 300 K and 10,000 SLPM, respectively.

Results and discussion

Model validation

For model validation, we used storage and flowthrough experimental data obtained from an experimental test bench. The details of model validation and its discussion, technical aspects of test bench, geometry and boundary conditions are available elsewhere [19]. In brief, the adsorption test bench consists of a 2.5 L stainless steel tank, filled with 358 g of MOF-5 and submerged into liquid nitrogen Dewar. For cryogenic charging tests, hydrogen gas is precooled to ~80 K before feeding into the storage tank. This is done by means of a helical cooling loop which is immersed inside a liquid nitrogen Dewar. Helium expansion method is used to estimate the dead volume of the manifold and adsorption tank. Temperature evolution in the tank is monitored using k-type thermocouples distributed along the tank's axial direction. Mass flow controllers and metres are used to quantify the amount of gas flowing in and out of the tank [19].

Please cite this article in press as: Ubaid S, et al., Charge–discharge cycling, flowthrough cooling and *para-ortho* conversion for cooling bulk hydrogen storage tank filled with MOF-5, International Journal of Hydrogen Energy (2015), http://dx.doi.org/10.1016/

Cooling of 20 m^3 hydrogen storage reservoir filled with MOF-5

At first, the model is used to test the effect of charge–discharge cycles to cool the room temperature maintained reservoir to cryogenic condition (80 K). To this end, hydrogen cooled to 77 K is filled into the tank until the maximum pressure of 4 MPa is reached. Immediately, 3 MPa is released from the tank into the ambient. In order to release the gas from the reservoir, the outflow velocity of 1.5 m s^{-1} boundary condition is applied at outlet of the tank. Even though the model can accommodate high outflow gas velocity value as a boundary condition at the outlet of the tank, we used low outflow gas velocity value (1.5 m s^{-1}). This is because the convergence during the simulation is complex when high value is considered. The result (Fig. 1, right) shows that, at the end of the filling stage, the temperature of the system increases due to the adsorption and pressure work heat. The maximum temperature is observed at the bottom region of the tank followed by middle and top regions (Fig. 1, right). The temperatures at the bottom, middle and top regions of the tank shows 341 K, 321 K and 77 K, respectively. During the discharging stage, the heat inside the tank is transported out with the outflowing hydrogen, subsequently the temperatures at the bottom, middle and top regions of the tank are reduced to 300 K, 122 K and 60 K, respectively. Once the tank pressure is decreased to 1 MPa from 4 MPa, filling is carried out again using 77 K hydrogen to reach 4 MPa (Fig. 1, left). Like in the first cycle, due to the increased heat during the filling time, the temperature at the top point of the tank is increased to 73 K from 66 K (Fig. 1, right). The increased heat from the top region of the tank is transferred to the middle region, which leads to desorption of hydrogen from the middle region that results further temperature reduction to 103 K from 122 K at the middle point (Fig. 1, right). Due to the decreased temperature at the middle region, adsorption occurs and the resulted adsorption heat is transferred to the bottom part of the tank, there temperature is increased to 321 K. In order to remove the heat, again outlet of the tank is opened and released 3 MPa pressure. This charge–discharge cycle is repeated until the whole bed in the tank reaches to 80 K.

Fig. 2 shows the pictorial representation of the tank's temperature variations during the charging–discharging cycles. At 0 s, the temperature of the whole system is 300 K, which is represented by red colour. The red colour at the top region of the tank disappears when the first filling stage is finished. At the top region, the red colour is replaced by blue colour, which means that the heating effect at that part is diminished due to the influence of incoming cold hydrogen. After releasing 3 MPa hydrogen from the reservoir, the blue colour enlarges from the top to the middle region, which means that the tank's temperature is further reduced due to the convective heat transfer during the hydrogen releasing time. At the end of three charging–discharging cycles, the red colour is completely disappeared and it is replaced by blue colour, which suggests that the temperature of the whole bed in the tank is reduced to 80 K from 300 K.

In the next part, we focused to study the effect of flowthrough cooling technique to cool the storage reservoir which is initially maintained at 300 K. To this end, charging is carried out using 77 K hydrogen at the rate of 10,000 SLPM for reaching the maximum allowable storage pressure of 4 MPa. At the end of the charging stage, the model is set to flowthrough. The result in Fig. 3, left shows that tank reaches 4 MPa pressure in 2.1 h; while the tank stored 106 kg of hydrogen. From Fig. 3 (right), it is seen that the average tank temperature decreased to 268 K from 300 K during the charging stage. This is because cooling effect due to the incoming cold hydrogen is dominant at the top region of the tank (Fig. 1, right and Fig. 2) and the resulting adsorption heat from the top region is transferred to the bottom region of the tank that leads to increase in temperature at the bottom region (Fig. 3, right). The average temperature of the whole tank from the cold and hot regions is 268 K.

During the flowthrough cooling stage, the average bed temperature is reduced to 80 K from 268 K. In order to reduce the tank temperature, around 1537 kg of hydrogen is used in 28 h. Out of 1537 kg of hydrogen, 281 Kg of hydrogen is stored and the remaining hydrogen is eventually recovered. The total amount of used hydrogen during the flowthrough cooling stage is calculated integrating the inlet mass flow rate. We assumed here that the excess hydrogen is vented and that the

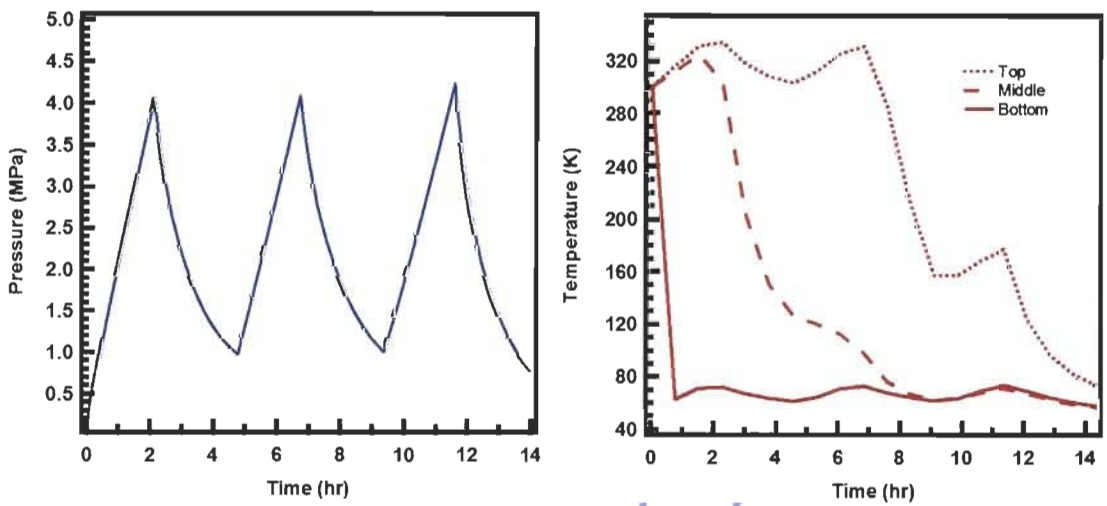

Fig. 1 – Pressure (left) and temperature (right) of the tank during the charging/discharging cycles.

Please cite this article in press as: Ubaid S, et al., Charge–discharge cycling, flowthrough cooling and *para-ortho* conversion for cooling bulk hydrogen storage tank filled with MOF-5, International Journal of Hydrogen Energy (2015), http://dx.doi.org/10.1016/

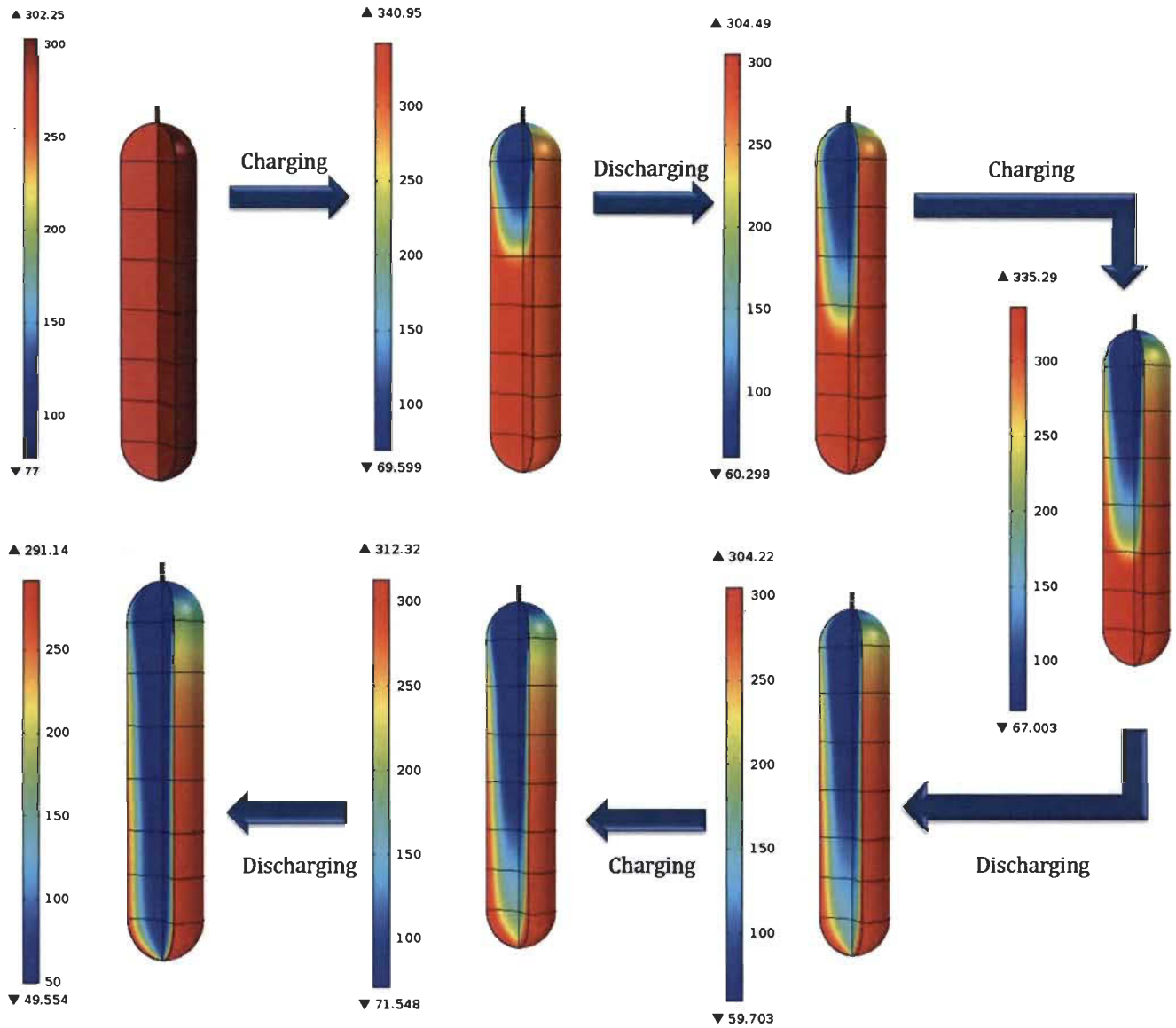

Fig. 2 – Pictorial representation of heating and cooling of the tank during the charging–discharging cycle.

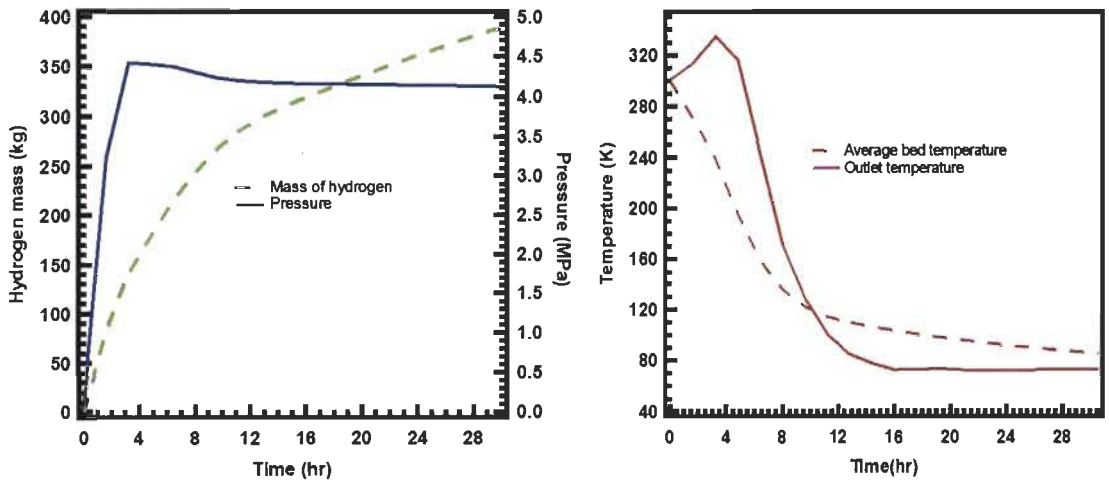

Fig. 3 – Pressure and total mass of hydrogen (left) and temperatures (right) of the tank during the charging/flowthrough stage.

Please cite this article in press as: Ubaid S, et al., Charge–discharge cycling, flowthrough cooling and *para-ortho* conversion for cooling bulk hydrogen storage tank filled with MOF-5, International Journal of Hydrogen Energy (2015), http://dx.doi.org/10.1016/

charging is continued using fresh cold hydrogen instead of recirculating it after passing through any external heat exchangers. The simulation results from the two methods: flowthrough cooling and charging–discharging cycle show that the cooling of room temperature maintained large storage reservoir to 80 K is a time and energy consuming process when flowthrough cooling alone is considered as a cooling option compared to charging–discharging cycles.

Even though we assumed here that the excess hydrogen is not re-circulated, the model is further used to study the temperature of the exhaust hydrogen gas during the flowthrough cooling stage. The estimation of exhaust hydrogen temperature profile is useful for calculating the required energy for cooling the exhaust hydrogen when the re-circulation is taken into account. The point located at the outlet of the tank is selected for monitoring the temperature of the outgoing gas. The result (Fig. 3, right) shows that the temperature rises during the charging time and decreases during the flowthrough stage. The energy required for cooling the exhaust hydrogen gas can be reduced when the flowthrough cooling is active.

Effect of mass flow rate on cooling time reduction during flowthrough cooling stage

To understand the effect of mass flow rates on cooling time reduction during flowthrough cooling stage, 77 K hydrogen at the rate of 10,000 SLPM is charged into the 80 K temperature maintained storage reservoir to reach maximum allowable pressure, 4 MPa. At the end of the charging stage, the model tested different mass flow rates such as 10,000 SLPM, 15,000 SLPM and 20,000 SLPM during the flowthrough regime. Fig. 4 compares the average bed temperatures of the system when different mass flow rates are taken into account. The results shows that the time taken for cooling the storage system from ~125 K to 80 K is 6 h when 20,000 SLPM flow rate is considered, which is less compared to 8 h for 15,000 SLPM and 12.8 h for 10,000 SLPM. The higher the flow rate, higher is the velocity of the hydrogen gas inside the tank during the flowthrough cooling stage; this results faster convective heat removal compared to that during low flow rate flowthrough cooling.

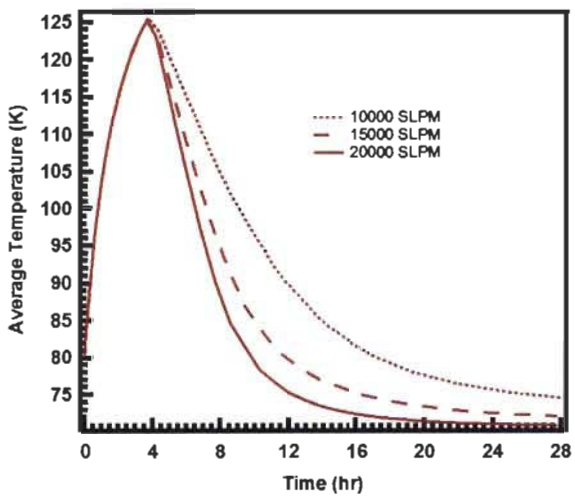

Fig. 4 – Effect of mass flow rate on temperature reduction during the flowthrough stage.

Effect of flowthrough cooling together with para-ortho conversion on the storage tank performance

In a previous work, we presented the maximum possible effect of an instantaneous *para* to *ortho* conversion on the total heat in the 2.5 L storage system and reported that the endothermic *para* to *ortho* conversion in the equilibrium hydrogen reduces the system storage temperature [18]. Here, the model is applied to a 20 m^3 storage reservoir and the simulation is performed to understand the effect of *para* to *ortho* conversion together with the flowthrough cooling technique. To perform the simulation, hydrogen gas at 77 K is filled in the tank until 4 MPa reached. At the end of the charging stage, flowthrough cooling is accommodated in the model and continued the simulation. In order to implement the *para-ortho* conversion effect in the storage system, the heat source term due to *para-ortho* conversion is included in the energy balance equation of the adsorptive system model. Also, we assumed here that equilibrium hydrogen at 77 K consists of ~49 of ortho hydrogen and ~51% of para hydrogen is used for filling the storage tank.

Fig. 5 compares the average bed temperature and pressure of the tank for flowthrough cooling is used with and without *para-ortho* conversion heats. It shows that if no conversion heat is considered, the allowable maximum pressure of the tank 4 MPa reaches in ~4 h. If the *para-ortho* conversion is taken into account, the maximum pressure reaches in 4.17 h. The average temperature of the tank at the end of the charging stage is ~119 K when *para-ortho* conversion takes place, which is lower compared to the system has no *para-ortho* conversion, there the final average temperature at the end of the charging stage is ~125 K. During the flowthrough stage, the generated heat is convectively transferred out of

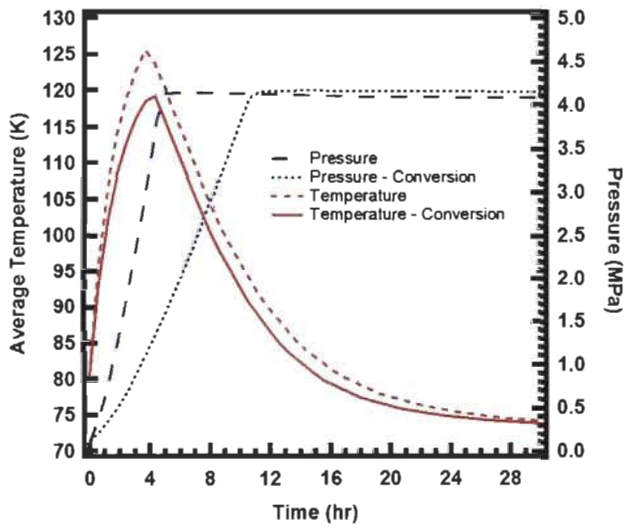

Fig. 5 – Average temperature and pressure in the system when *para-ortho* conversion together with flowthrough cooling and flowthrough cooling alone scenario.

Please cite this article in press as: Ubaid S, et al., Charge–discharge cycling, flowthrough cooling and *para-ortho* conversion for cooling bulk hydrogen storage tank filled with MOF-5, International Journal of Hydrogen Energy (2015), http://dx.doi.org/10.1016/

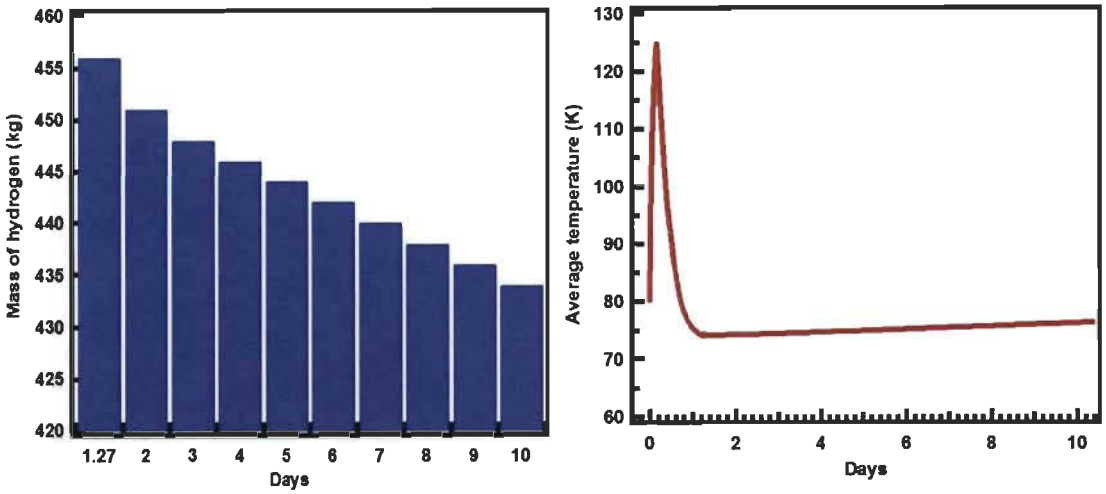

Fig. 6 – Hydrogen mass loss rate (left) and average bed temperature (right) during the dormancy stage.

the reservoir with outflowing hydrogen. If *para-ortho* conversion together with flowthrough cooling exists, temperature reduction due to the conversion helps to charge more hydrogen into the system during the charging stage and the storage capacity can be increased during the flowthrough cooling stage.

Performance of the bulk tank during the dormancy stage

It is important to understand the hydrogen loss rate of large storage reservoir during the long term dormancy stage. The hydrogen loss during the dormancy stage depends highly on the tank insulation. If the tank is not well insulated, the possible heat leak of the tank causes the heating of the storage system. This leads to build up excess pressure inside the tank, which is required to be vented for the safety reasons. Here, an adiabatic insulated tank is assumed and the estimated heat leakage rate is applied in the form of heat flux (0.8287 W m^{-2}) at the outer wall of the tank. In order to understand the storage and thermal performance of the tank during the dormancy stage, the 80 K maintained reservoir is charged with 77 K hydrogen to reach maximum storage pressure, 4 MPa. At the end of the charging stage, the tank is allowed to cool down using flowthrough cooling method. Once the system reaches to 80 K, the 4 MPa pressure tank inlet is closed and pressure boundary condition is set to 4 MPa at the inlet of the tank. The simulation is continued to understand the performance of the tank during the 10 days dormancy period. The result presented in Fig. 6 (left) shows that 28 kg of hydrogen is lost during the 10 days dormancy stage. Except the first day, each day ~2.4 kg of hydrogen is necessary to be vent out to comply with the maximum pressure of the tank. Between 0.8 and 1 day, around ~4 kg of hydrogen needs to be exhausted. This may be due to the sudden temperature increment in the reservoir immediately after the flowthrough cooling is stopped. Fig. 6 (right) shows that the temperature increases during the filling time and decreases during the flowthrough stage. During the dormancy period, temperature increases slightly due to the heat transfer from the ambient to reservoir.

Conclusion

To conclude, a validated CFD model is used to perform the simulation for studying the thermal and storage performance of a 20 m^3 storage reservoir filled with MOF-5. The tank is originally maintained at 300 K and the tank is cooled to 80 K using methods, such as charge–discharge cycles and flowthrough cooling. The simulation results shows that the cooling of room temperature large storage reservoir to 80 K is a time and energy consuming process when flowthrough cooling alone is considered as a cooling option as compared with charging–discharging process. Even though, time can be reduced if high flow rate is used during the charging and flowthrough stage, charging and discharging cycle is still a better option for reducing the temperature of the large storage reservoir. The temperature of the exhaust hydrogen gas during the flowthrough cooling time shows that the required energy for cooling the exhaust hydrogen can be reduced when the flowthrough cooling is on progress. The simulation continued for studying the effect of mass flow rate on heat removal from the system during the flowthrough stage. The higher mass flow rate during flowthrough cooling accelerates the heat removal from the storage tank and cool the tank in a short period of time. Further, the effect of *para-ortho* conversion together with flowthrough cooling shows that instantaneous *para-ortho* conversion helps to charge more hydrogen during the charging stage compared to the system has no *para-ortho* conversion. This storage capacity together with cooling efficiency of the reservoir is enhanced during the flowthrough cooling stage. Finally, the hydrogen mass loss during the 10 days dormancy stage is calculated and observed that each day ~2.4 kg of hydrogen is necessary to remove from the reservoir for complying with the maximum allowed pressure in the tank. The heat removal methods such as

Please cite this article in press as: Ubaid S, et al., Charge–discharge cycling, flowthrough cooling and *para-ortho* conversion for cooling bulk hydrogen storage tank filled with MOF-5, International Journal of Hydrogen Energy (2015), http://dx.doi.org/10.1016/

charge–discharge cycles, flowthrough cooling and *para-ortho* conversion are suitable for the system contains not only MOF-5 but these methods are applicable in the storage system with other porous materials, such as other MOFs, COFs, ACs. Nevertheless, the overall advantage in cooling the system depends on the parameters, such as adsorption heat, catalytic activity of the material etc.

Acknowledgement

The authors acknowledge the Natural Science and Engineering Research Council (NSERC) of Canada, Air Liquide, and the H2Can network for providing the financial support for this work.

REFERENCES

[1] Bockris JÓM. Hydrogen no longer a high cost solution to global warming: new ideas. Int J Hydrogen Energy 2008;33:2129–31.
[2] Suleman F, Dincer I, Agelin-Chaab M. Environmental impact assessment and comparison of some hydrogen production options. Int J Hydrogen Energy 2015;40:6976–87.
[3] Dutta S. A review on production, storage of hydrogen and its utilization as an energy resource. J Ind Eng Chem 2014;20:1148–56.
[4] Nicoletti G. The hydrogen option for energy: a review of technical, environmental and economic aspects. Int J Hydrogen Energy 1995;20:759–65.
[5] Satyapal S, Petrovic J, Read C, Thomas G, Ordaz G. The U.S. department of energy's national hydrogen storage project: progress towards meeting hydrogen-powered vehicle requirements. Catal Today 2007;120:246–56.
[6] Stern AG. Design of an efficient, high purity hydrogen generation apparatus and method for a sustainable, closed clean energy cycle. Int J Hydrogen energy 2015;40:9885–906.
[7] Mori D, Hirose K. Recent challenges of hydrogen storage technologies for fuel cell vehicles. Int J Hydrogen Energy 2009;34:4569–74.
[8] Ren J, Musyoka NM, Annamalai P, Langmi HW, North BC, Mathe M. Electrospun MOF nanofibers as hydrogen storage media. Int J Hydrogen Energy 2015;40:9382–7.
[9] Suh MP, Park HJ, Prasad TK, Lim DW. Hydrogen storage in metal-organic frameworks. Chem Rev 2012;112:782–835.
[10] Alesaadi SJ, Sabzi F. Hydrogen storage in a series of Zn-based MOFs studied by Sanchez-Lacombe equation of state. Int J Hydrogen Energy 2015;40:1651–6.
[11] Sarkar A, Banerjee R. Net energy analysis of hydrogen storage options. Int J Hydrogen Energy 2005;30:867–77.
[12] Marco-Lozar JP, Juan-Juan J, Suárez-García F, Cazorla-Amorós D, Linares-Solano A. MOF-5 and activated carbons as adsorbents for gas storage. Int J Hydrogen Energy 2012;37:2370–81.
[13] Liu D, Purewal JJ, Yang J, Sudik A, Maurer S, Mueller U, et al. MOF-5 composites exhibiting improved thermal conductivity. Int J Hydrogen energy 2012;37:6109–17.
[14] Xiao JS, Hu M, Cossement D, Bénard P, Chahine R. Finite element simulation for charge-discharge cycle of cryo-adsorptive hydrogen storage on activated carbon. Int J Hydrogen Energy 2012;37:12947–59.
[15] Xiao JS, Wang J, Cossement D, Bénard P, Chahine R. Finite element model for charge and discharge cycle of activated carbon hydrogen storage. Int J Hydrogen energy 2012;37:802–10.
[16] Schuetz W, Michl F, Polifke W, Paggiaro R. Storage system for storing a medium and method for loading a storage system with a storage medium and emptying the same therefrom. US patent. US 2008/0020250 A1, Jan. 24, 2008.
[17] Ahluwalia RK, Hua TQ, Peng JK, Roh HS, Bailey J, Kumar R. System level analysis of hydrogen storage options. Presentation for DOE hydrogen program review. May 14–18, 2012 [Washington, DC, USA].
[18] Ubaid S, Xiao J, Zacharia R, Chahine R, Bénard P. Effect of *para-ortho* conversion on hydrogen storage system performance. Int J Hydrogen Energy 2014;39:11651–60.
[19] Ubaid S, Zacharia R, Xiao JS, Chahine R, Bénard P, Tessier P. Effect of flowthrough cooling heat removal on the performances of MOF-5 cryo-adsorptive hydrogen reservoir for bulk storage applications. Int J Hydrogen Energy 2015;40:9314–25.
[20] Comsol Multiphysics 4.4 version 4.3.1.161 Copyright1998–2012. Comsol AB.
[21] Xiao J, Tong L, Deng C, Bénard P, Chahine R. Simulation of heat and mass transfer in activated carbon tank for hydrogen storage. Int J Hydrogen Energy 2010;35:8106–16.
[22] Hardy B, Corgnale C, Chahine R, Richard M-A, Garrison S, Tamburello D, et al. Modeling of adsorbent based hydrogen storage systems. Int J Hydrogen Energy 2012;37:5691–705.
[23] Richard M-A, Bénard P, Chahine R. Gas adsorption process in activated carbon over a wide temperature range above the critical point. Part 1: modified Dubinin-Astakhov model. Adsorption 2009;15:43–51.
[24] Dundar E, Zacharia R, Chahine R, Benard P. Performance comparison of adsorption isotherm models for supercritical hydrogen sorption on MOFs. Fluid Phase Equilib 2014;363:74–85.
[25] James Patrick Meagher. Modeling of hydrogen liquefiers with kinetic conversion of *ortho* to *para* hydrogen in plate-fin heat exchangers. Thesis. Department of Chemical and Biological Engineering, University at Buffalo; April 22–2008 [State University of New York, USA].
[26] Lemmon EW, Huber ML, McLinden MO. NIST standard reference database 23: reference fluid thermodynamic and transport properties-REFPROP. Standard Reference Data Program. Gaithersburg: National Institute of Standards and Technology; 2007. Version 8.0.
[27] Peng JK, Ahluwalia RK. Enhanced dormancy due to *para*-to-*ortho* hydrogen conversion in insulated cryogenic pressure vessels for automotive applications. Int J Hydrogen Energy 2013;38:13664–72.
[28] Kloutse FA, Zacharia R, Cossement D, Chahine R, Balderas-Xicohténcatl R, Oh H, et al. Heats of adsorption on MOFs and Maxsorb: comparison between adsorption calorimetry, isosteric method and analytical models. July 2015. Submitted for publication.
[29] Kloutse FA, Zacharia R, Cossement D, Chahine R. Specific heat capacities of MOF-5, Cu-BTC, Fe-BTC, MOF-177 and MIL-53 (Al) over wide temperature ranges: measurements and application of empirical group contribution method. Micropor Mesopor Mat 2015;217:1–5.
[30] Purewal JJ, Liu D, Yang J, Sudik A, Siegel DJ, Maurer S, et al. Increased volumetric hydrogen uptake of MOF-5 by powder densification. Int J hydrogen energy 2012;37:2723–7.
[31] Marquardt ED, Le JP, Radebaugh R. Cryogenic material properties database. In: 11th international cryo cooler conference, Keystone, US; June 20–22; 2000.
[32] The volume of the tank can be downloaded from, http://www.cryolor.com/en/notre-offre/cryogenic-storage-vessels/tanks-for-lin-lox-and-lar.html [accessed 10.02.14].

Please cite this article in press as: Ubaid S, et al., Charge–discharge cycling, flowthrough cooling and *para-ortho* conversion for cooling bulk hydrogen storage tank filled with MOF-5, International Journal of Hydrogen Energy (2015), http://dx.doi.org/10.1016/

Nomenclatures

C: Conversion
C_{peq}: Equivalent specific heat capacity adsorbent-gas, J $kg^{-1}K^{-1}$
D_P: Particle diameter, mm
k: Permeability, m^2
k_{eq}: Equivalent thermal conductivity of adsorbent-gas, W $m^{-1}K^{-1}$
M_{H2}: Molecular mass of hydrogen, kg mol^{-1}
m_a: Mass of adsorbed phase, kg
m_g: Mass of gas phase, kg
m_t: Total mass, kg
n_a: Absolute adsorption amount/unit adsorbent, mol kg^{-1}
n_{max}: Limit adsorption amount per unit adsorbent, mol kg^{-1}
P: Pressure, Pa
P_0: Pseudo-saturation pressure (D–A model), Pa
Q: Heat source term, W m^{-3}
Q_a: Adsorption heat, W m^{-3}
Q_p: Heat produced due to pressure work, W m^{-3}
q_{st}: Isosteric heat of adsorption, J mol^{-1}
R: Universal gas constant, J mol^{-1} K^{-1}
S_m: Mass source term, kg s^{-1} m^{-3}
T: Temperature, K
u: Darcy velocity, m s^{-1}
α: Enthalpic factor, J mol^{-1}
β: Entropic factor, J mol^{-1} K^{-1}
μ: Dynamic viscosity, Pa s
ρ_g: Density of hydrogen gas, kg m^{-3}
ρ_s: Particle density of adsorbent, kg m^{-3}
ε_b: Bed porosity

Please cite this article in press as: Ubaid S, et al., Charge–discharge cycling, flowthrough cooling and *para-ortho* conversion for cooling bulk hydrogen storage tank filled with MOF-5, International Journal of Hydrogen Energy (2015), http://dx.doi.org/10.1016/

Section C

Annexure

Adsorptive hydrogen storage system model implimentation in COMSOL Multiphysics® platform

❖ Paramters

Name	Expression	Value	Description
bedporosity	0.73	0.73000	Bed porosity
alpha	3481[J/mol]	3481.0 J/mol	Enthalpic contribution to the charecteristic free energy of adsorption
beta	153.6[J/mol/K]	153.60 J/(mol·K)	Entropic contribution to the charecteristic free energy of adsorption
R	8.314[J/mol/K]	8.3140 J/(mol·K)	universal gas constant
n_max	67.54[mol/kg]	67.540 mol/kg	Limiting adsorption (per unit mass of adsorbent).
P_0	2.753e10[MPa]	2.7530E16 Pa	Saturation pressure of the vapour at temperature
Dp	0.0035[mm]	3.5000E-6 m	Particle diameter
rho_p	576[kg/m^3]	576.00 kg/m³	Particle density
M_H2	0.002016[kg/mol]	0.0020160 kg/mol	Molicular mass of hydrogen
T_amp	77[K]	77.000 K	Ampient temperature
rho_b	155.6[kg/m^3]	155.60 kg/m³	Bulk density
heattransfercoefficient	0[W/m^2/K]	0 W/(m²·K)	Heat transfer coefficient
m1	-1.4087	-1.4087	Coefficient - Thermal conductivity - Stainless steel
m2	1.3982	1.3982	Coefficient - Thermal conductivity - Stainless steel
m3	0.2543	0.25430	Coefficient - Thermal conductivity - Stainless steel
m4	-0.6260	-0.62600	Coefficient - Thermal conductivity - Stainless steel
m5	0.2334	0.23340	Coefficient - Thermal conductivity - Stainless steel
m6	0.4256	0.42560	Coefficient - Thermal conductivity - Stainless steel
m7	-0.4658	-0.46580	Coefficient - Thermal conductivity - Stainless steel
m8	0.1650	0.16500	Coefficient - Thermal conductivity - Stainless steel
m9	-0.0199	-0.019900	Coefficient - Thermal conductivity - Stainless steel
m11	22.0061	22.006	Coefficient - Specific heat capacity - Stainless steel
m22	-127.5528	-127.55	Coefficient - Specific heat capacity - Stainless steel
m33	303.6470	303.65	Coefficient - Specific heat capacity - Stainless steel
m44	-381.0098	-381.01	Coefficient - Specific heat capacity - Stainless steel
m55	274.0328	274.03	Coefficient - Specific heat capacity - Stainless steel
m66	-112.9212	-112.92	Coefficient - Specific heat capacity - Stainless steel
m77	24.7593	24.759	Coefficient - Specific heat capacity - Stainless steel
m88	-2.239153	-2.2392	Coefficient - Specific heat capacity - Stainless steel
m99	0	0	Coefficient - Specific heat capacity - Stainless steel

❖ Variables

Name	Expression	Unit	Description
n_a	n_max*exp(-(R*T_sr/(alpha+beta*T_sr))^9.045*(log(P_0/p_sr))^9.045)	mol/kg	Absolute adsorption
permiabilty	(Dp^2/150)*(bedporosity^3/(1-bedporosity)^2)	m²	Permeability of bed
Qa_DA	(-(mass_source*Iso_MOF5_DA)/M_H2)	W/m³	Adsorption heat source - using modified D-A modeled isosteric heat of adsorption
mass_source	(-M_H2*rho_p*(1-bedporosity)*d(n_a,t))	kg/(m³·s)	Mass source term
density_H2	int1(T_sr,p_sr/1000000)		Density of hydrogen - NIST
visocity_H2	int2(T_sr,p_sr/1000000)		Viscosity of hydrogen - NIST
thermalconductivity_H2	int3(T_sr,p_sr/1000000)		Thermal conductivity of hydrogen - NIST
Cp_H2	int4(T_sr,p_sr/1000000)		Specific heat capacity of hydrogen - NIST
CpCv_H2	int5(T_sr,p_sr/1000000)		Ratio of heat specific capacitites - NIST
Qp	(bedporosity*d(p_sr,t))+(dl.u*(d(p_sr,r))+dl.w*(d(p_sr,z)))	Pa/s	Pressure work - Heat source
k_steel	10^((m1+(m2*(log10(T_sr)))+(m3*((log10(T_sr)))^2)+(m4*((log10(...		Thermal conductivity of stainless steel
Cp_steel	10^((m11+(m22*(log10(T_sr)))+(m33*((log10(T_sr)))^2)+(m44*((lo...		Specific heat capacity of stainless steel
Cp_MOF5	int27(T_sr)		Specific heat capacity of MOF-5
Iso_MOF5	int26(n_a)		Isosteric heat of adsoprtion - Exp
Qa_Exp	-(mass_source*Iso_MOF5)/M_H2		Adsorption heat source - using exp. isosteric heat of adsorption
Iso_MOF5_DA	alpha*(sqrt(log(n_max/n_a)))	J/mol	Isosteric heat of adsorption - modified D-A model

❖ **Darcy law interface is used for solving mass and momentum balance equations**

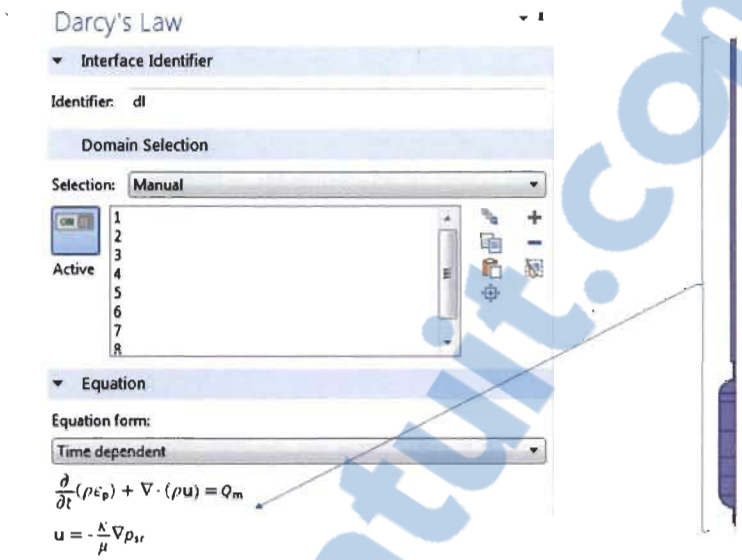

❖ **Hydrogen and MOF-5 properties are applied to the domain where MOF-5 and hydrogen are present**

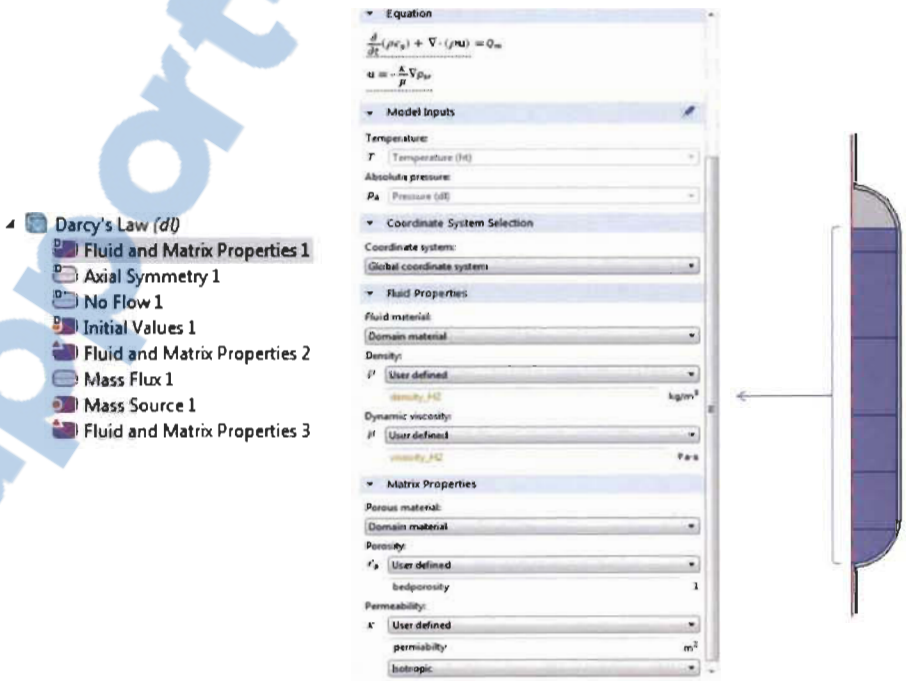

❖ **Hydrogen gas properties are applied to the upper manifold domain where only hydrogen is present, bed porosity = 1**

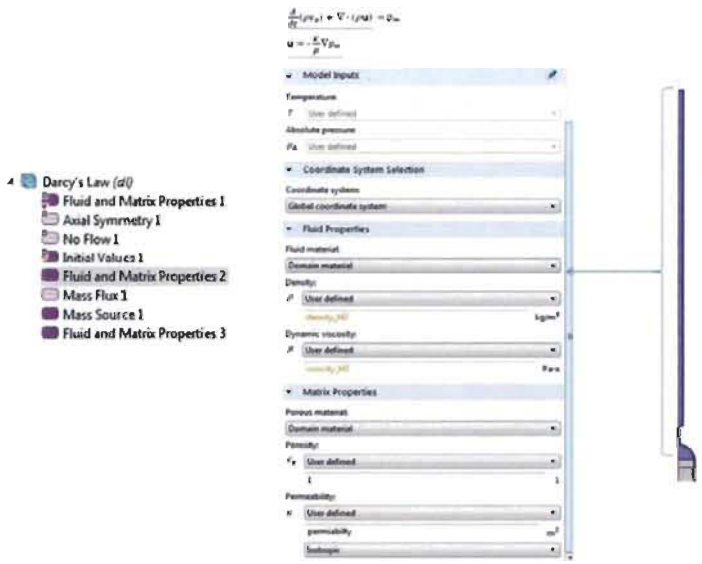

❖ **Hydrogen gas properties are applied to the lower manifold domain where only hydrogen is present, bed porosity = 1**

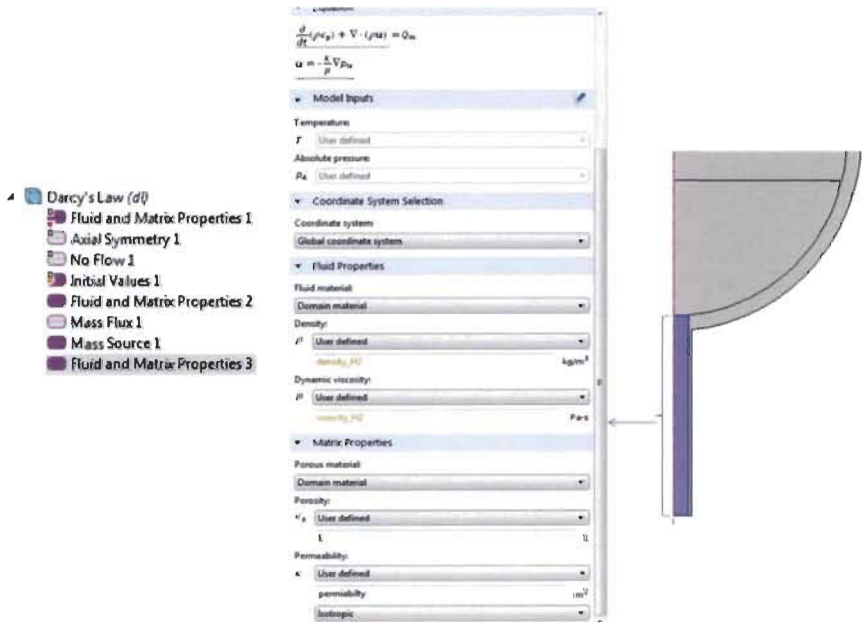

❖ **Mass source term is applied to the domain where MOF-5 and hydrogen is present**

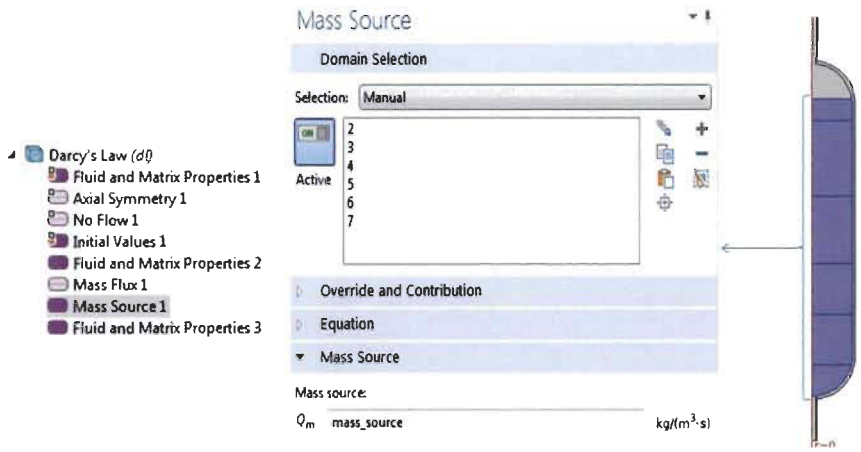

❖ **Two dimensional axisymmetry is used for simulation. The inner wall, no flow boundary condition is applied. The inlet of the tank is located at the top of the upper manifold where hydrogen gas at room temperature is charged into the tank.**

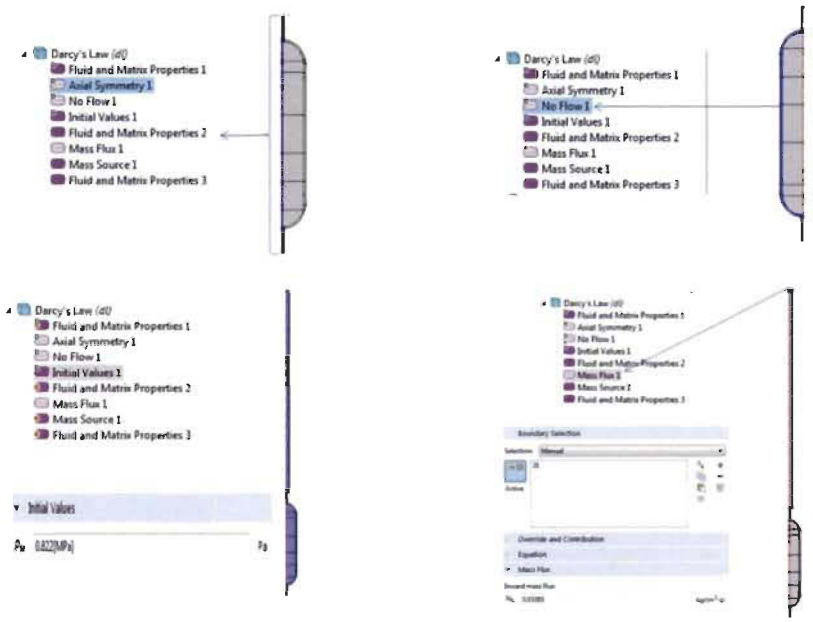

❖ **Standard energy balance equation is applied in all the domains.**

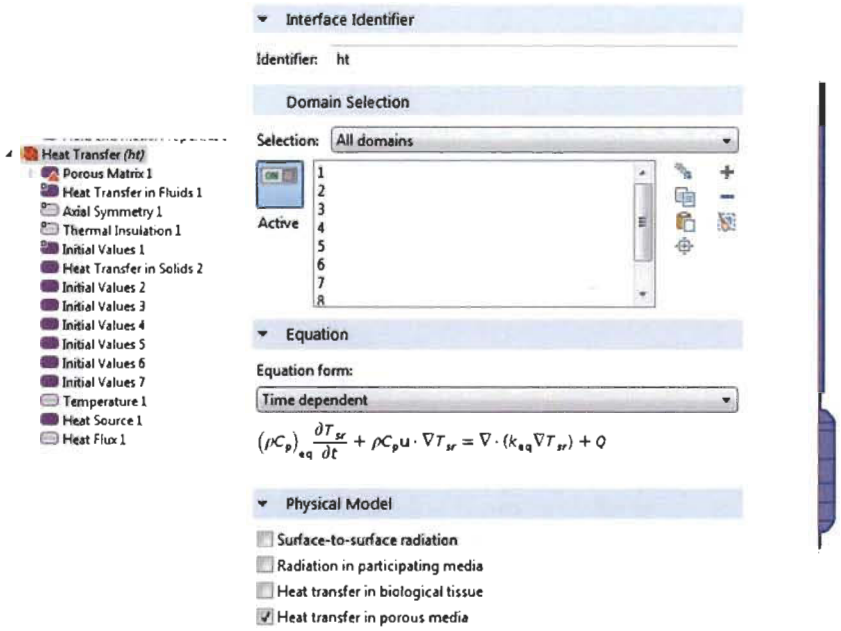

❖ **Properties of porous matrix is applied to the domain where MOF-5 is present**

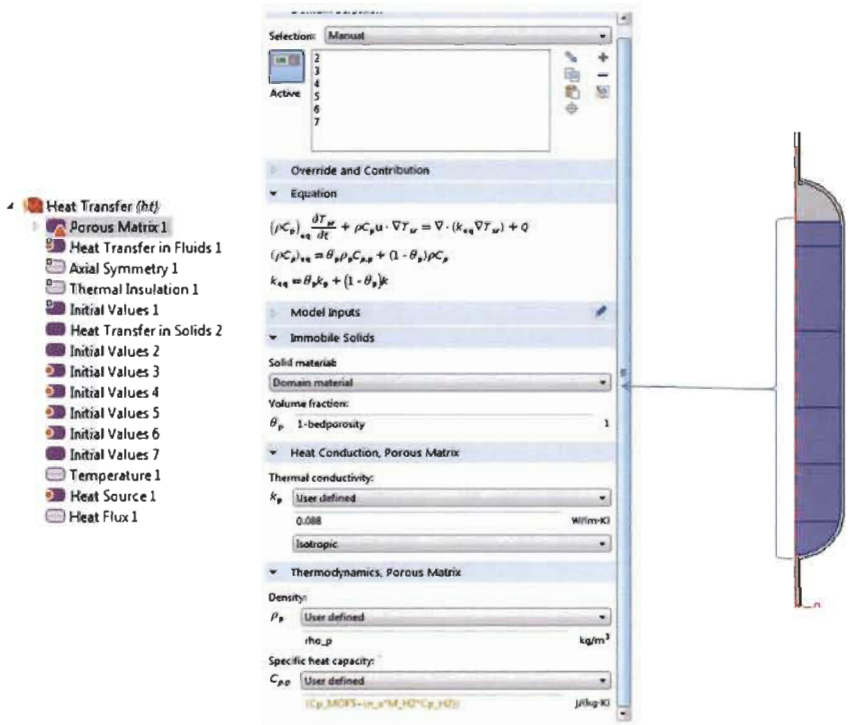

❖ **Equation for solving heat transfer in fluid (hydrogen) is applied to the domain where hydrogen gas is present**

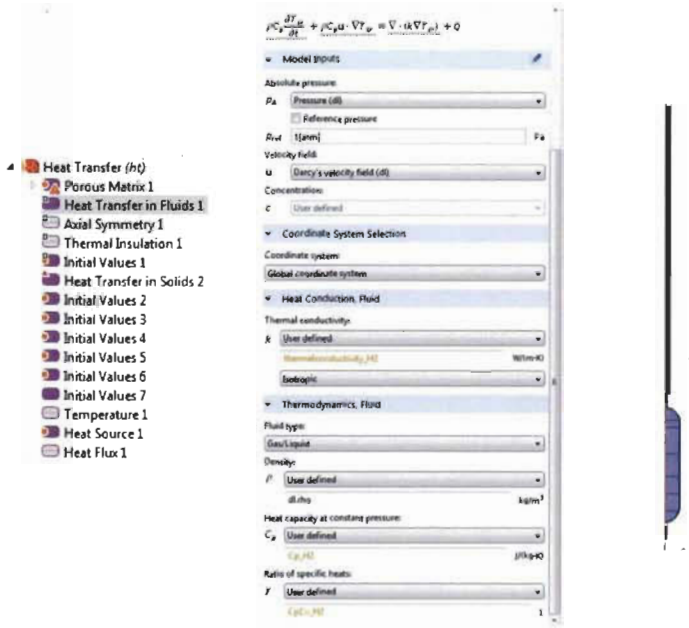

❖ **Equation for solving heat transfer in solid is applied to the tank wall domain (stainless steel)**

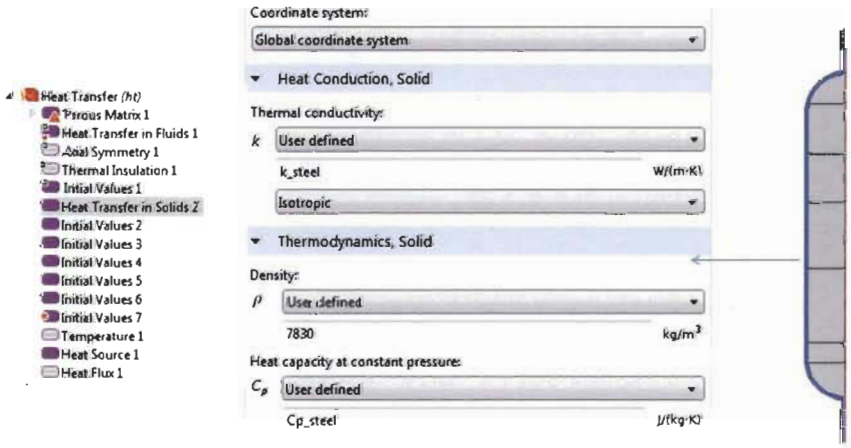

❖ **Heat flux boundary condition is applied to outer wall of the tank**

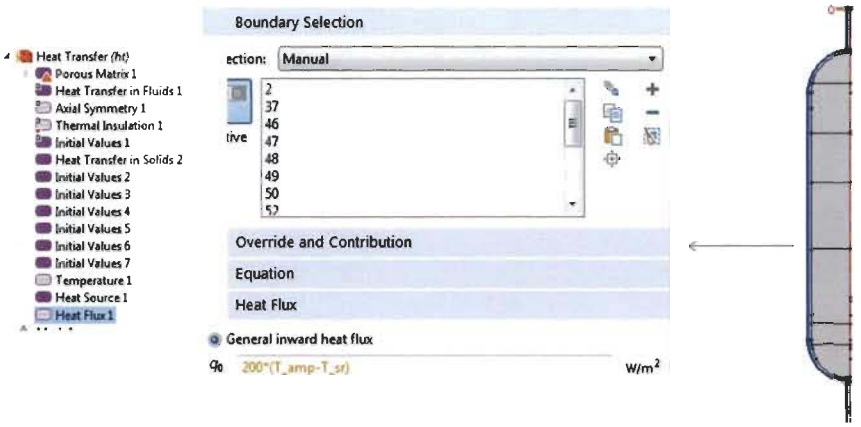

❖ **The inlet of the tank is located at the top of the upper manifold where hydrogen gas at room temperature is charged into the tank. Heat source term applied the domain where MOF-5 is and hydrogen gas are present**

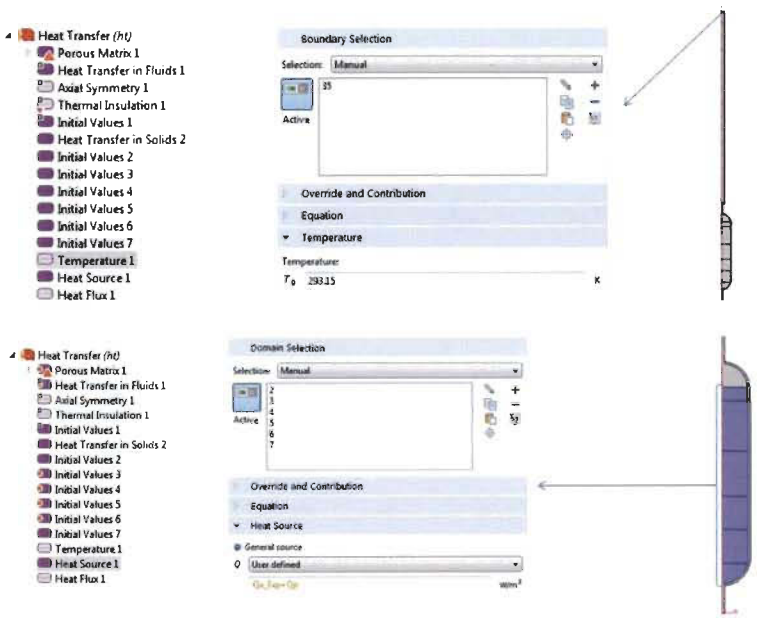

❖ Mesh

Geometric Entity Selection

Geometric entity level: Entire geometry

ON

Active

Statistics

Complete mesh

Element type: All elements

Triangular elements:	4004
Edge elements:	1349
Vertex elements:	65

Domain element statistics

Number of elements:	4004
Minimum element quality:	1.464E-4
Average element quality:	0.7472
Element area ratio:	9.027E-6
Mesh area:	0.03472 m^2
Maximum growth rate:	15.06
Average growth rate:	1.384

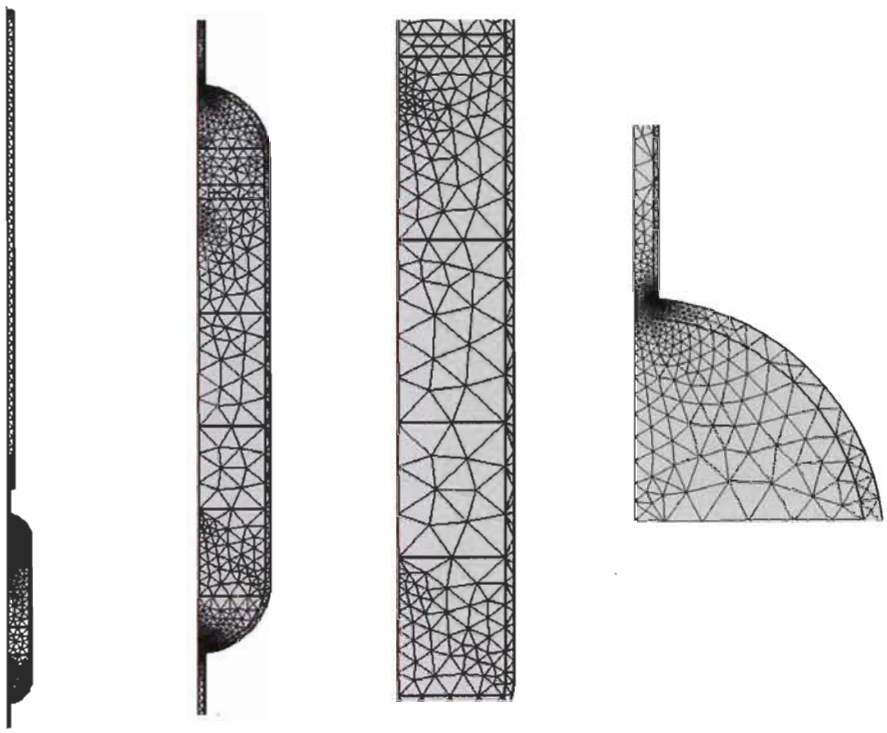

Supplementary results

❖ **Hydrogen gas density vs temperature and pressure**

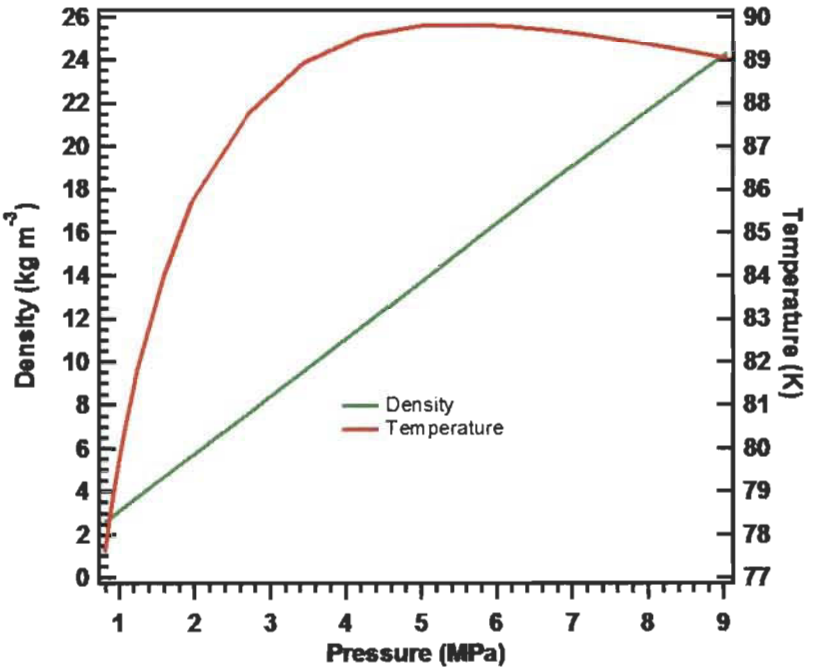

❖ **Hydrogen gas viscosity vs temperature and pressure**

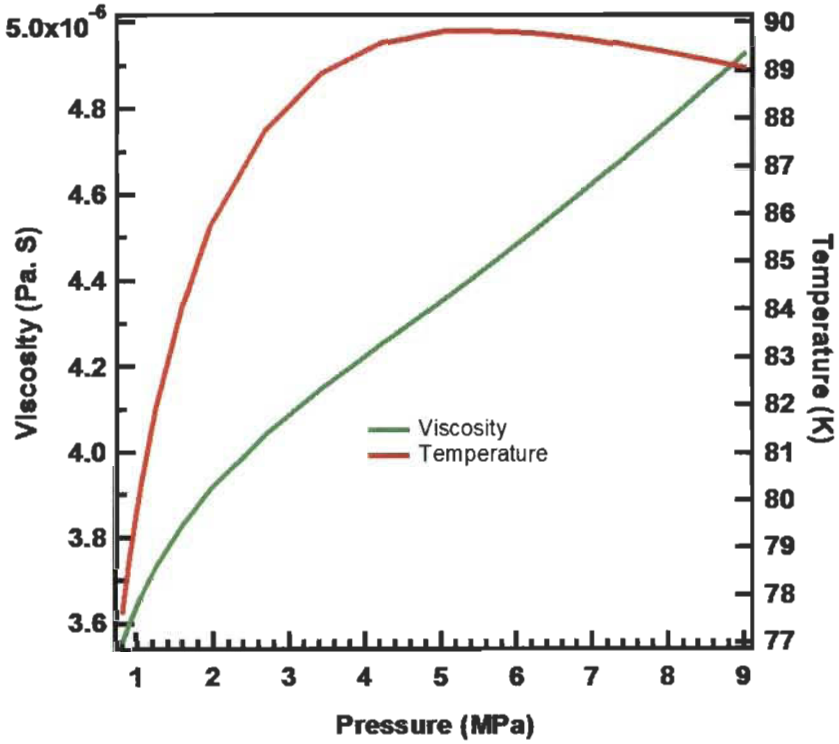

❖ **Hydrogen gas thermal conductivity vs temperature and pressure**

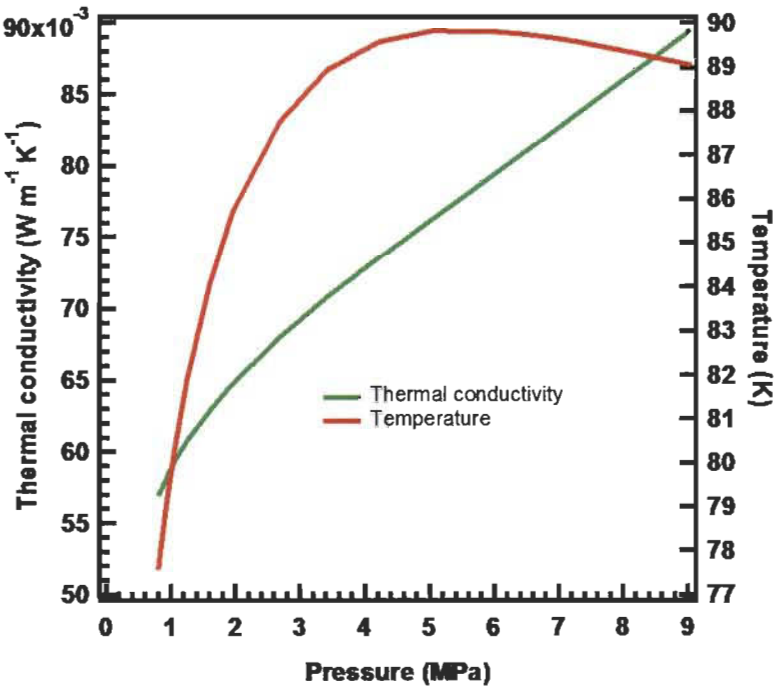

❖ **Hydrogen gas specific heat capacity vs temperature and pressure**

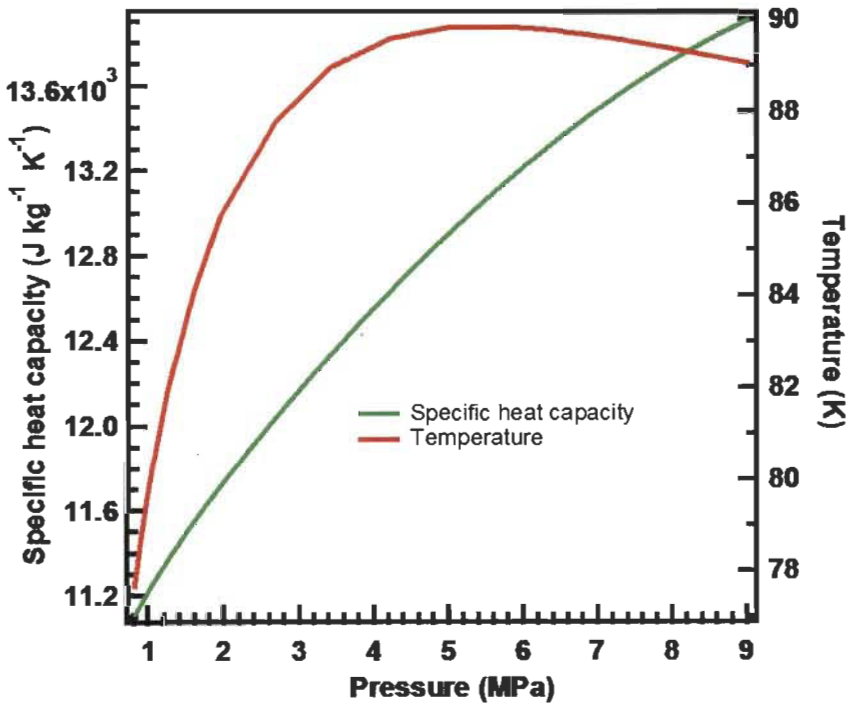

❖ **Hydrogen gas's ratio of specific heat capacities vs temperature and pressure**

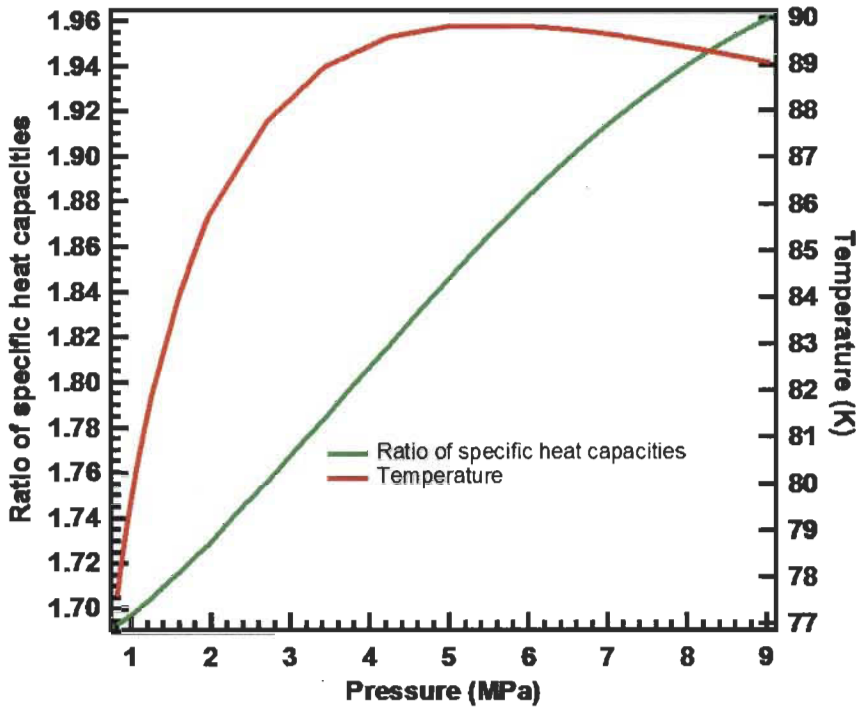

❖ **Thermal conductivity of stainless steel vs temperature**

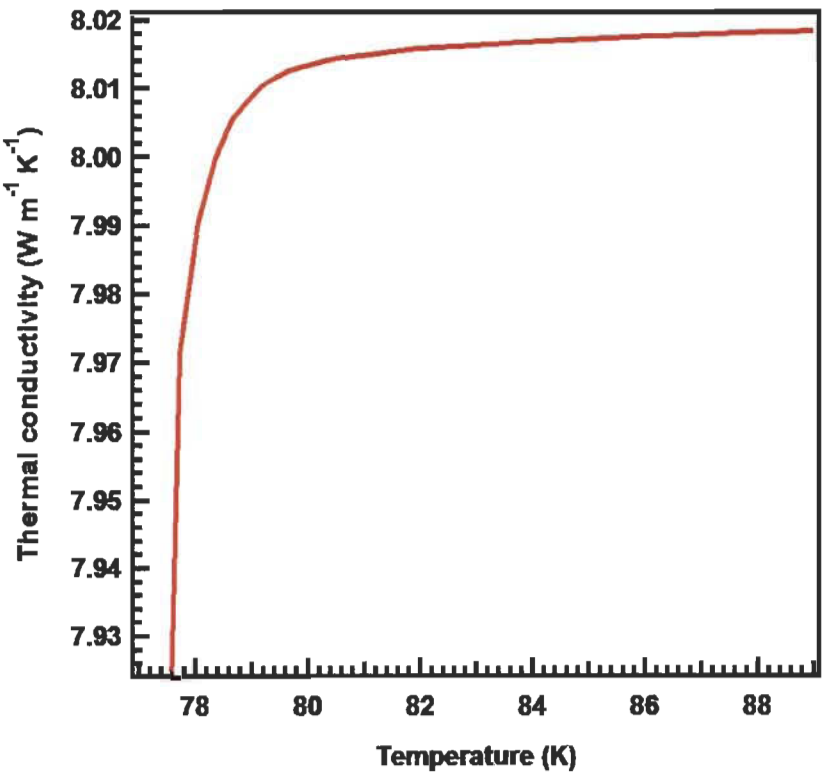

❖ **Specific heat capacity of stainless steel vs temperature**

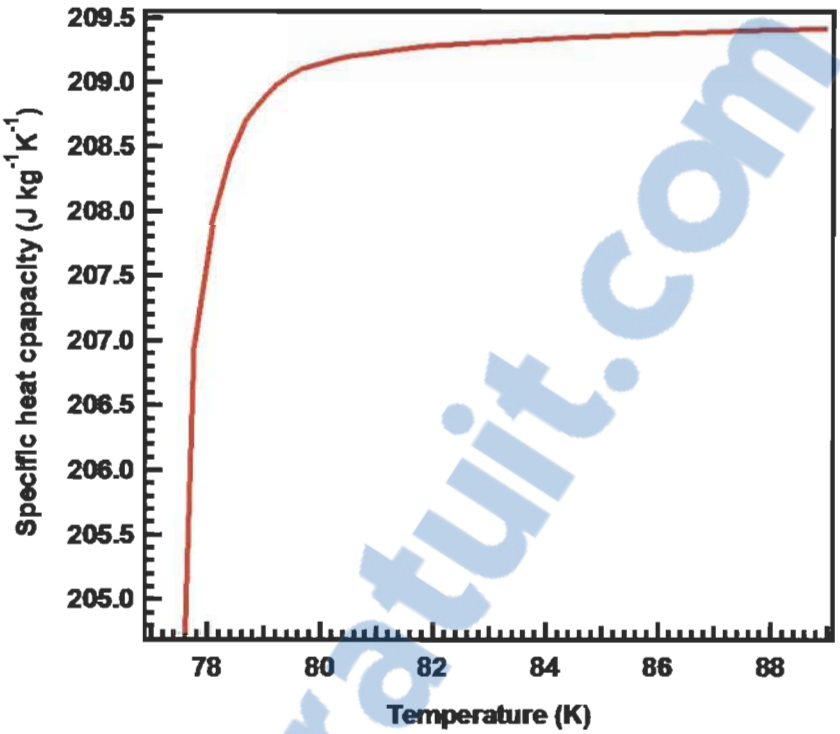

❖

❖ **Specific heat capacity of MOF-5 vs temperature**

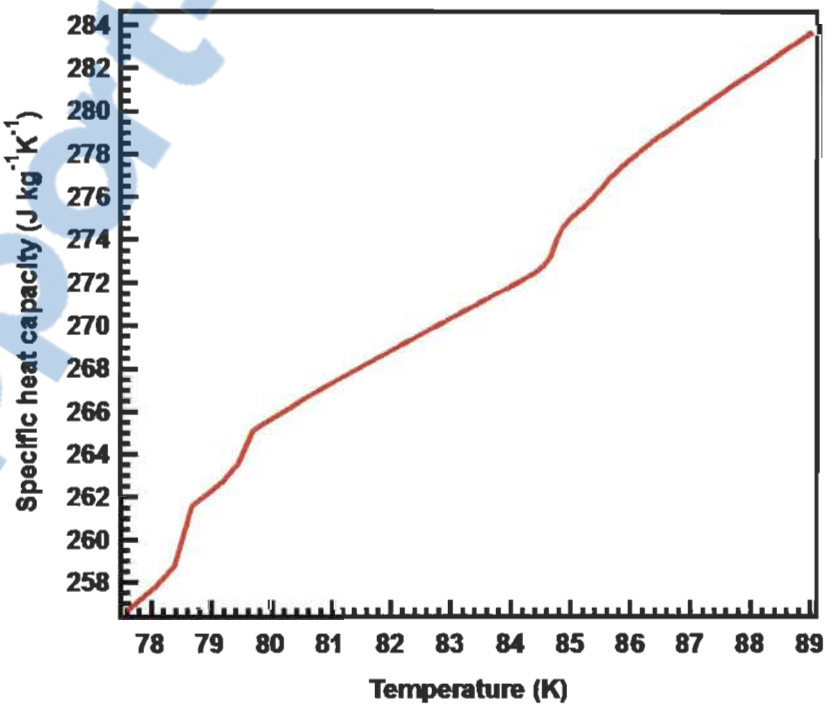

❖ **Isosteric heat vs absolute adsorption**